DEPARTMENT OF THE AIR FORCE

AIR UNIVERSITY

AIR FORCE INSTITUTE OF TECHNOLOGY

Wright-Patterson Air Force Base, Ohio

AFIT/GAE/AA/88S-1

APPLICATION OF THE BOUNDARY ELEMENT METHOD TO FATIGUE CRACK GROWTH ANALYSIS

THESIS

Timothy C. Kelley

AFIT/GAE/AA/88S-1

AFIT/GAE/AA/88S-1

APPLICATION OF THE BOUNDARY ELEMENT METHOD TO FATIGUE CRACK GROWTH ANALYSIS

THESIS

Presented to the Faculty of the School of Engineering
of the Air Force Institute of Technology
Air University
In Partial Fulfillment of the
Requirements for a Degree of
Master of Science in Aeronautical Engineering

Timothy C. Kelley, B.S.

September 1988

Preface

The purpose of this study was to apply the boundary element method (BEM) to two dimensional fracture mechanics problems, and to use the BEM to analyze the interference effects of holes on cracks through a parametric study of a two hole tension strip. The study analyzed the effect of hole diameter, pitch and crack length. The results of the study were to be applied to a sample crack growth analysis to display the use of the boundary element method in conventional aircraft damage tolerance analysis.

The analysis of classical fracture problems showed excellent results, and the comparisons to different finite element methods were also very good.

I could not have performed this study without the assistance, guidance and "long term" support of my faculty advisor Dr. Anthony N. Palazotto. I would also like to thank the department chairman Dr. Peter J. Torvik for his support in enabling me to complete this thesis.

I wish to especially thank my wife, Teri, and my two children, Matthew and Kevin, for their love and support during the evenings and weekends that this thesis was completed in.

Timothy C. Kelley

VAX 8800:All-IN-ONE/LN03 Laser Printer.

Table of Contents

List of Symbols

a	- crack length
λ	- element inclination angle
β	- normalized stress intensity factor
γ	- relative element inclination $(\lambda_i - \lambda_j)$
${}^{ij}C_{sn}$	- influence coefficient
${}^{ij}A_{ns}$	- boundary coefficient
F_x	- x directon of applied force
G	- shear modulus
E	- Young's modulus
ν	- Poisson's ratio
N	- number of elements
K_I	- Mode I stress intensity factor
$g_{,x}$	- partial derivative of g with respect to x
P_y	- y applied traction stress
$\Sigma^N_{j=1}$	- summation over j from 1 to N
σ_{xx}	- x component of stress
${}^{i}\sigma_n$	- normal stress component at element i
u_y	- y component of displacement
${}^{j}u_s$	- shear displacement at element j

List of Figures

List of Tables

Abstract

This investigation analyzes a crack emanating from one hole, and approaching a second hole, in a two hole tension strip with finite boundaries using the Boundary Element Method. The study included the effects of varying the hole diameter, hole separation and the length of crack. The final results were plotted as a function of the geometric correction factor β, which can be presented as a family of curves. An example damage tolerance analysis is presented with the β curves being incorporated into a β look-up table as used in the NASA/FLAGRO fatigue crack growth program. This technique is acceptable in most fatigue crack growth programs now used in the aircraft industry to ensure aircraft structural integrity.

Several classic fracture mechanics problems are analyzed, and computational efficiency as compared to conventional finite element techniques is investigated. Agreement with analytic solutions as well as other numerical methods (finite element) is excellent. The computation efficiency was shown to an improvement over existing methods.

I. Introduction

The present day acceptance of a fracture mechanics based aircraft damage tolerance criteria is based on the work done in the late sixties and early seventies, credited to Mr Charles Tiffany and Dr John Lincoln [16]. Dr Lincoln gives an excellant review of the Air Force Damage Tolerance experience in reference [25]. Within the last decade, the Air Force has placed increased emphasis on the fracture mechanics life-cycle structural integrity of its' manned aircraft systems [6]. The original implementation of an Aircraft Structural Integrity Program (ASIP) was in 1959 and the catastrophic events leading up to it are well documented [2]. The most significant event being the B-47 fatigue failures which crippled the Strategic Air Command at a time of extreme world tension. The B-47 showed that modern aircraft could no longer be designed solely for static strength. This 1959 ASIP involved the "Safe-Life" concept revolving around classical "Fatigue" analysis. To account for the significant "scatter factor" associated with fatigue testing, a scatter factor of "four" was established whereby an aircraft designed for a 4000 hour service life must be analyzed and tested for 16000 hours of service life. The F-111 was such an aircraft and was tested successfully for 16000 hours. However, in December of

1969 an F-111 with approximately 100 flight hours crashed at Nellis AFB, Utah.

The cause of this crash was a manufacturing defect in the wing pivot fitting that was undetected by inspections. Also, the KC-135 aircraft was judged to have a Safe-Life of 13000 hours, yet service experience had detected fourteen cases of unstable cracking in the lower wing skins at flight times ranging from 1800 to 5000 hours. An F-5 which was judged to have a Safe-Life of 4000 hours was lost at Williams AFB, Arizona, with approximately 1900 hours. From these and other cases it was apparent that the Safe-Life methodology had not precluded the use of "brittle" materials and "rogue" manufacturing or service induced defects that could lead to premature failure. The result was the implementation of a "Fracture Mechanics" based "Damage Tolerance" approach to structural integrity [5].

The Damage Tolerance approach relies on fatigue crack growth calculations to establish the time interval required to grow a crack from an initial size (usually the maximum flaw undetectable with current NDI techniques) to the critical crack length which denotes the onset of unstable crack growth. The crack growth equations are a function of the local change in Stress Intensity, K, as a stress cycle is applied. All of the current fatigue crack growth codes in use by industry have "canned" subroutines to calculate K for classical crack configurations. However, the practicing

engineer is frequently faced with design details which are not represented by the conventional solutions. In this case the solution for K must be analyzed independently of the crack growth code, with the results placed in a look-up table as a function of crack length.

The most common method of independent analysis of Stress Intensity Factors is the finite element method. This numerical technique is extremely flexible in its' ability to analyze a wide range of problems. However, finite element models require the descretization of the body being studied, with a gradual refinement towards the crack tip. This is very expensive in both computer time and man hours. Alternative solution techniques are always being sought to increase the efficiency of these Stress Intensity Factor analyses, and this thesis will investigate the possible advantages of using the Boundary Element Technique.

The Boundary Element Method is based on a singular solution which represents the analysis of a segment of the boundary of the body being analyzed. The values of the boundary conditions are known, and the solution calculates the results for the rest of the body. The singular solution will satisfy the governing differential equations exactly, and the user will approximate the boundary conditions.

Some of the earliest uses of BEM were in 1963 by Jaswon and Ponter [10], Jaswon [9], and Symm [22] concerning potential problems. The first elasticity application was in

1967 by Rizzo [17]. Since then the method has been used in a wide variety of applications as documented by Mackerle and Andersson [12]. Examples of the BEM applied to fracture mechanics can be found in papers by Snyder and Cruse [20] and Rizzo and Shippy [18].

The purpose of this research is to investigate a crack emanating from a hole towards another hole in a two hole tension strip with finite boundaries. The basic BEM technique will be verified on similar problems, either classical or by finite element methods. A parametric case study of the two hole tension strip was conducted varying the hole diameter, hole separation and crack length to create a family of Stress Intensity Factor data curves suitable for fatigue crack growth analysis. A sample damage tolerance analysis using the results of the parametric stress intensity study is shown.

After a theoretical development of the Fictitious Stress BEM technique, comparison solutions to a few classic fracture problems are presented, as well as a comparison to finite element solutions. The solutions to the two hole tension strip parametric study are presented, followed by the example damage tolerance analysis.

II. Theoretical Discussion

The analytical method used for this study was the Boundary Element Method. This method relies on a singular solution representing the analysis of a segment of the boundary of the body being analyzed. The boundary conditions are known, and the solution analyzes the impact on the remainder of the body. The complete solution requires all of the boundary segments be solved simultaneously and include the effects of the boundary segments on each other. The technique used in the analysis performed here is the "Fictitious Stress" method as outlined by Crouch and Starfield [4].

A. Fictitious Stress Method

The Fictitious Stress method utilizes the plane strain version of Kelvin's problem [21] as the basic singular solution. Kelvin's problem is a point load in an infinite domain while the plane strain version is a line of concentrated force.

As shown in Figure 1, the plane strain version of Kelvin's problem will involve a line of force F along the z direction. The components F_x and F_y have units of force per unit depth. Kelvin showed that a harmonic function g(x,y) was a solution to the biharmonic equation ($\nabla^2\nabla^2=0$) such that

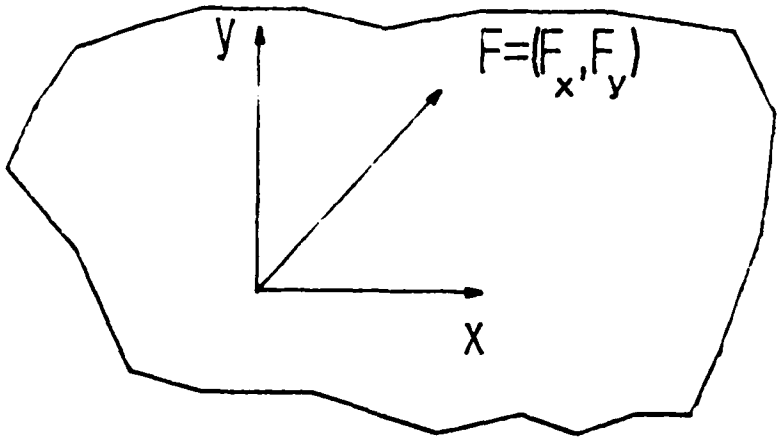

$$g(x,y)=-1/(4\pi(1-\nu))\ln(x^2+y^2)^{1/2}$$

$$g_{,x}=dg/dx \qquad g_{,y}=dg/dy$$

Figure 1. Kelvin's Problem

$$g(x,y) = [-\ln(x^2 + y^2)^{1/2}]/[4\pi(1-\nu)] \quad (1)$$

where ν is Poisson's ratio.

Kelvins solution for displacements components, u_x and u_y, are expressed as

$$u_x = (F_x/2G)[(3-4\nu)g - xg_{,x}] + (F_y/2G)[-yg_{,x}] \quad (2)$$
$$u_y = (F_y/2G)[(3-4\nu)g - yg_{,y}] + (F_x/2G)[-xg_{,y}]$$

where F_x and F_y are the components of the applied point load F, and G is the material shear modulus, and

$$g = g(x,y) \quad (3)$$
$$g_{,x} = [-1/4\pi(1-\nu)][x/(x^2 + y^2)]$$
$$g_{,y} = [-1/4\pi(1-\nu)][y/(x^2 + y^2)]$$
$$g_{,xy} = [1/4\pi(1-\nu)][2xy/(x^2 + y^2)^2]$$
$$g_{,xx} = -g_{,yy} = [1/4\pi(1-\nu)][(x^2 - y^2)/(x^2 + y^2)^2]$$

where $g_{,y}$ denotes the partial differentiation of the function g(x,y) with respect to y ($\partial g/\partial y$) and $g_{,x}$ denotes the partial differentiation of g with respect to x ($\partial g/\partial x$). Using the stress-strain relations produces the stress results as

$$\sigma_{xx} = F_x[2(1-\nu)g_{,x} - xg_{,xx}] + F_y[2\nu g_{,y} - yg_{,xx}] \qquad (4)$$
$$\sigma_{yy} = F_y[2(1-\nu)g_{,y} - yg_{,yy}] + F_x[2\nu g_{,x} - xg_{,yy}]$$
$$\sigma_{xy} = F_x[(1-2\nu)g_{,y} - xg_{,xy}] + F_y[(1-2\nu)g_{,x} - yg_{,xy}]$$

where σ_{xx}, σ_{yy} are the components of stress in the x and y directions and σ_{xy} is the shear stress. The stresses in Eq (4) satisfy the equations of equilibrium, and are singular at the point x=y=0. Timoshenko and Goodier showed that these stresses correspond to a line of concentrated force at the origin [24].

To facilitate the transition of Kelvin's solution into a form usable in a numerical technique, we consider the problem of tractions $t_x = P_x$ and $t_y = P_y$ applied to a line segment $|x| \leq a$, y=0 in an infinite elastic solid. Kelvin's solution is integrated over a line segment of length 2a as shown in Figure 2. If we consider a small segment of the line, dε, the force F becomes

$$F_i(\varepsilon) = P_i d\varepsilon \qquad i=x,y \qquad (5)$$

We will assume a constant traction thus the new harmonic function to satisfy the biharmonic equation, f(x,y), as shown in [4], can be expressed in terms of g(x,y) as

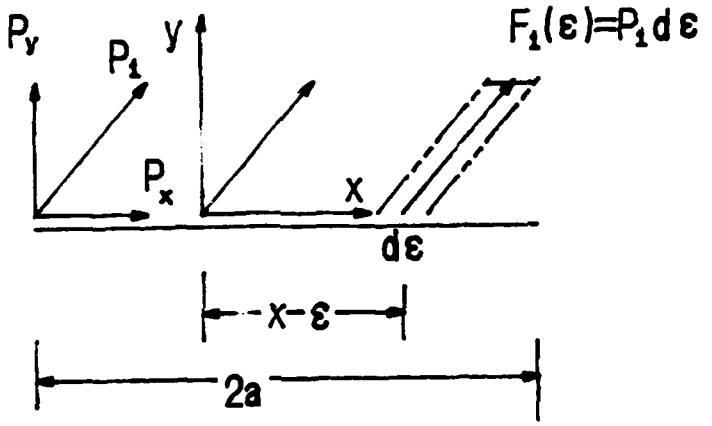

$$f(x,y) = \int_{-a}^{a} g(x-\varepsilon,y)\, d\varepsilon$$

Figure 2. Integration of Kelvin's Problem

$$f(x,y) = {}_{-a}\int^{a} g(x-\varepsilon,y)\,d\varepsilon \tag{6}$$

$$= [-1/4\pi(1-\nu)][y\{\arctan(y/(x-a)) - \arctan(y/x+a)\} + (x+a)\ln\{(x+a)^2 + y^2\}^{1/2} - (x-a)\ln\{(x-a)^2 + y^2\}^{1/2}]$$

Following the procedure outlined previously in the presentation of Kelvin's problem, the displacements due to the line of concentrated force per unit depth, $F_i(\varepsilon)$, are

$$u_x = (P_x/2G)[(3-4\nu)f + yf_{,y}) + (P_y/2G)[-yf_{,x}] \tag{7}$$
$$u_y = (P_y/2G)[(3-4\nu)f + yf_{,y}) + (P_x/2G)[-yf_{,x}]$$

and the stresses become

$$\sigma_{xx} = P_x[(3-2\nu)f_{,x} + yf_{,xy}] + P_y[2\nu f_{,y} + yf_{,yy}] \tag{8}$$
$$\sigma_{yy} = P_x[-1(1-2\nu)f_{,x} - yf_{,xy}] + P_y[2(1-\nu)f_{,y} + yf_{,yy}]$$
$$\sigma_{xy} = P_x[2(1-\nu)f_{,y} + yf_{,yy}] + P_y[(1-2\nu)f_{,x} + yf_{,xy}]$$

The derivatives of f are given as

$$f_{,x} = 1/[4\pi(1-\nu)]\{\ln\{(x-a)^2 + y^2\}^{1/2} - \ln\{(x+a)^2 + y^2\}^{1/2}] \tag{9}$$
$$f_{,y} = -1/[4\pi(1-\nu)][\arctan\{y/(x-a)\} - \arctan\{y/(x+a)\}]$$
$$f_{,xy} = 1/[4\pi(1-\nu)][y/\{(x-a)^2 + y^2\} - y/\{(x+a)^2 + y^2\}]$$

$$f_{,xx} = -f_{,yy}$$
$$= 1/[4\pi(1-\nu)][(x-a)/\{(x-a)^2 + y^2\}$$
$$- (x+a)/\{(x+a)^2 + y^2\}]$$

It is important to note that the stress solutions are not defined for $x=\pm a$, or $y=0$. To investigate this further, it is necessary to consider the the stress tensor along the line $y=0$. Evaluating Eqs (8) and (9) for $y=0$ yields the stresses

$$\sigma_{xx} = -(3-2\nu)/[8\pi(1-\nu)]P_x \ln[(x+a)/(x-a)]^2 \qquad (10)$$
$$- 2\nu/[4\pi(1-\nu)]P_y \lim_{y\to 0\pm}[\arctan\{y/(x-a)\}$$
$$- \arctan\{y/(x+a)\}]$$
$$\sigma_{yy} = (1-2\nu)/[8\pi(1-\nu)]P_x \ln[(x+a)/(x-a)]^2$$
$$- 1/(2\pi)P_y \lim_{y\to 0\pm}[\arctan\{y/(x-a)\}$$
$$- \arctan\{y/(x+a)\}]$$
$$\sigma_{xy} = -1/(2\pi)P_x \lim_{y\to 0\pm}[\arctan\{y/(x-a)\}$$
$$- \arctan\{y/(x+a)\}]$$
$$- (1-2\nu)/[8\pi(1-\nu)]P_y \ln[(x+a)/(x-a)]^2$$

where the limits on y are necessary as the arctan function is multivalued. The arctan functions in Eq (10) are interpreted to represent the angles, θ_1 and θ_2, from the ends of the line segment, to an arbitrary point (x,y), as shown in Figure 3. The values of θ_1 and θ_2 are seen to be

$$\theta_1 = \arctan[y/(x-a)] \qquad (11)$$

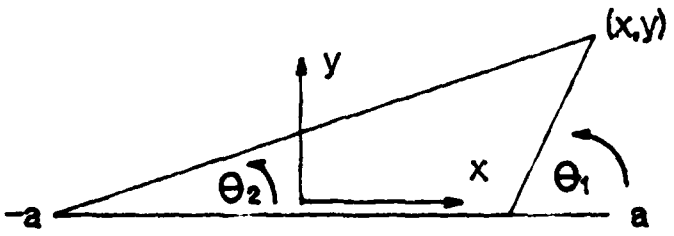

$$\theta_1 = \arctan(y/(x-a))$$

$$\theta_2 = \arctan(y/(x+a))$$

Figure 3. Boundary Element Geometry

$$\theta_2 = \arctan[y/(x+a)]$$

When y=0, it can be seen that θ can be $-\pi$, 0, or $+\pi$. By examining the limit expression in Eq (10), we see that the three possible solutions are

$$\lim_{y\to 0}[\arctan\{y/(x-a)\} - \arctan\{y/(x+a)\}] \qquad (12)$$

$$= 0 \quad |x|>a,\ y=0_+ \text{ or } y=0_-$$
$$= +\pi \quad |x|<a,\ y=0_+$$
$$= -\pi \quad |x|<a,\ y=0_-$$

Examining the last two values of Eq (12), it can be seen the stress tensor is discontinuous across the line segment at y=0. It is instructive to examine the magnitude of the difference in the stress tensor across y=0 for |x|<a. The change in σ_{xx} is

$$\sigma_{xx}(x,0_-) = -(3-2\nu)/[8\pi(1-\nu)]P_x\ln[(x+a)/(x-a)]^2 + P_y\nu/[2(1-\nu)] \qquad (13)$$

$$\sigma_{xx}(x,0_+) = -(3-2\nu)/[8\pi(1-\nu)]P_x\ln[(x+a)/(x-a)]^2 - P_y\nu/[2(1-\nu)] \qquad (13a)$$

$$\sigma_{xx}(x,0_-) - \sigma_{xx}(x,0_+) = P_y\nu/(1-\nu) \qquad (13b)$$

the change in σ_{yy} is

$$\sigma_{yy}(x,0_-) = (1-2\nu)/[8\pi(1-\nu)]P_x \ln[(x+a)/(x-a)]^2 + P_y/2 \qquad (14)$$

$$\sigma_{yy}(x,0_+) = (1-2\nu)/[8\pi(1-\nu)]P_x \ln[(x+a)/(x-a)]^2 - P_y/2 \qquad (14a)$$

$$\sigma_{yy}(x,0_-) - \sigma_{yy}(x,0_+) = P_y \qquad (14b)$$

and the change in σ_{xy} is

$$\sigma_{xy}(x,0_-) = -(1-2\nu)/[8\pi(1-\nu)]P_y \ln[(x+a)/(x-a)]^2 + P_x/2 \qquad (15)$$

$$\sigma_{xy}(x,0_+) = -(1-2\nu)/[8\pi(1-\nu)]P_y \ln[(x+a)/(x-a)]^2 - P_x/2 \qquad (15a)$$

$$\sigma_{xy}(x,0_-) - \sigma_{xy}(x,0_+) = P_x \qquad (15b)$$

It can be seen that Eqs (14b) and (15b) indicate that the stresses P_x and P_y are the constant discontinuities in σ_{xy} and σ_{yy} respectively. Crouch and Starfield [4] showed that the physical significance of the stresses P_x and P_y could be interpreted as imagining the line segment $|x| \leq 0$, $y=0$ as a

crack in an infinite elastic solid. As shown in Figure 4, the outward normal to the positive side of the crack $y=0_+$ has components $n_i=(0,-1)$, and the outward normal to the negative side $y=0_-$ has components $n_i=(0,1)$. With the tractions t_i defined as,

$$t_i = \sigma_{ji} n_j \tag{16}$$

the tractions on the two surfaces become,

$$\begin{aligned} t_x(x,0_+) &= -\sigma_{xy}(x,0_+) \\ t_y(x,0_+) &= -\sigma_{yy}(x,0_+) \\ t_x(x,0_-) &= \sigma_{xy}(x,0_-) \\ t_y(x,0_-) &= \sigma_{yy}(x,0_-) \end{aligned} \tag{17}$$

The resultant stresses obtained by adding the traction components t_i on both sides of the crack. Substituting the values of σ_{yy} from Eq (14b) and σ_{xy} from Eq (15b) into Eq (17) yields,

$$\begin{aligned} t_x(x,0) &= P_x \\ t_y(x,0) &= P_y \end{aligned} \tag{18}$$

Thus, the stresses P_x and P_y represent the constant resultant tractions across the line segment $|x| \leq a$, $y=0$.

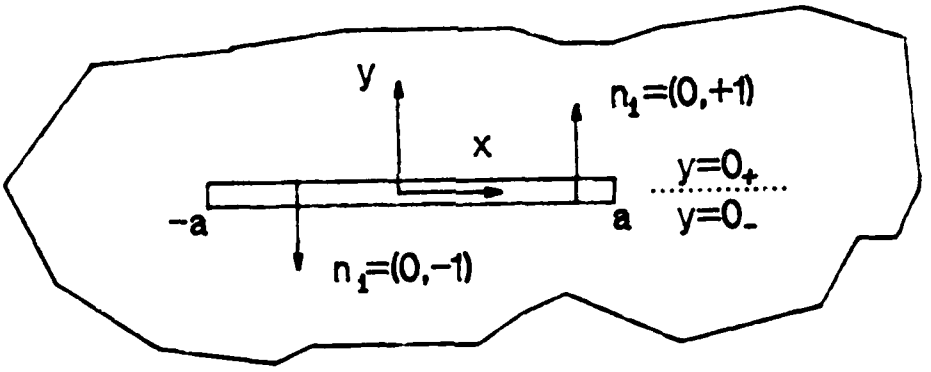

Figure 4. Boundary Element Line Crack

B. Numerical Algorithm

To apply the fictitious stress method to a general problem, it is instructive to consider the case of a hole with a boundary C in an infinite plate. We will let the hole be loaded by an outward pressure (p) load as depicted in Figure 5.(a). As the hole boundary is otherwise traction free, it is assumed the shear stress is zero, therefore, the known boundary conditions relative to the normal (n) tangential or shear (s) directions are

$$\sigma_n = -p \qquad (19)$$
$$\sigma_s = 0$$

We now create a system of N line segments, joined end to end, along a boundary C' as depicted in Figure 5.(b) that represents the boundary C of the hole in Figure 5.(a). Each line segment i is individually formulated with the fictitious stress solution for a stress P_i. Each line segment in this example will be of a uniform length 2a. If the length 2a is small enough the boundary C will be quite closely modeled by C'. The local coordinates n and s as depicted in Figure 5.(a) are relative to C so they will change depending on the location of the point desired. The local coordinates n and s in Figure 5.(b) will be relative to each line segment i. It

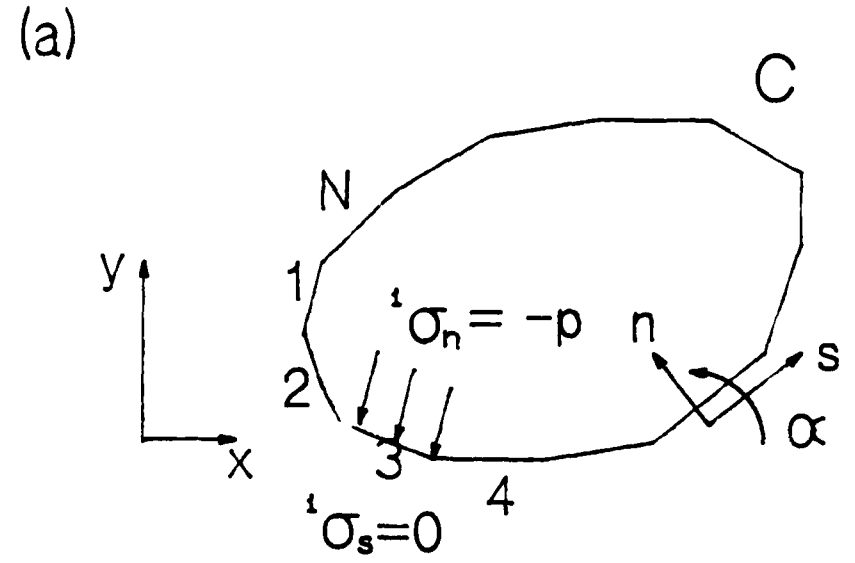

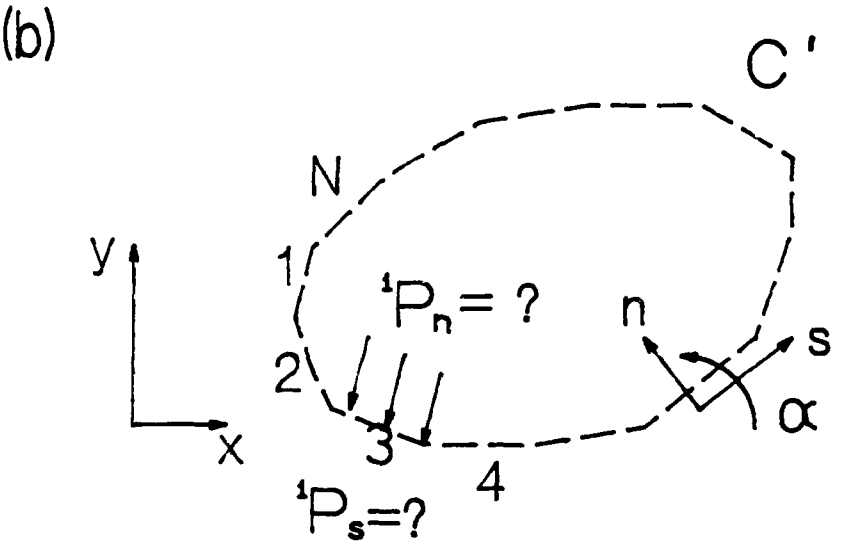

Figure 5. Numerical Method

will then be important to order the line segments such that the local coordinates for C and C′ correspond.

It is now important to remember that the line segments are based on Kelvin's solution for a point load in an infinite solid. So each line segment, or boundary element, is in fact a line of constant local stresses in an infinite elastic body, which happen to coincide with the boundary C. Each element will have its' own applied stress, P_i, but each element will be affected by all of the other elements. Using the theory of superposition, if we were to calculate the stress at a point in the body, we would have to sum all of the solutions for that point due to all of the elements i, each element with an applied stress P_i. So to calculate the final stresses ${}^{i}\sigma_s$ and ${}^{i}\sigma_n$ at each element i, at its' midpoint, requires a summation of the form

$$
\begin{aligned}
{}^{i}\sigma_s &= \Sigma^{N}_{j=1}[{}^{ij}A_{ss}\,{}^{j}P_s] + \Sigma^{N}_{j=1}[{}^{ij}A_{sn}\,{}^{j}P_n] \quad i=1 \text{ to } N \\
{}^{i}\sigma_n &= \Sigma^{N}_{j=1}[{}^{ij}A_{ns}\,{}^{j}P_s] + \Sigma^{N}_{j=1}[{}^{ij}A_{nn}\,{}^{j}P_n] \quad i=1 \text{ to } N
\end{aligned}
\qquad (20)
$$

where ${}^{ij}A_{ss}$, ${}^{ij}A_{sn}$, ${}^{ij}A_{ns}$, and ${}^{ij}A_{nn}$ are the boundary coefficients. As an example, ${}^{ij}A_{nn}$ gives the actual normal stress at the midpoint of element i (${}^{i}\sigma_n$) due to the application of a unit normal stress to element j (${}^{j}P_n=1$).

Since the values of ${}^{i}\sigma_s$ and ${}^{i}\sigma_n$ are known from the boundary conditions of the original problem, it remains for the system of applied stresses ${}^{i}P_s$ and ${}^{i}P_n$ to be solved

for by assembling a system of 2N simultaneously linear algebraic equations in as many unknowns.

$$0 = \Sigma^{N}_{j=1}[{}^{ij}A_{ss}\,{}^{j}P_{s}] + \Sigma^{N}_{j=1}[{}^{ij}A_{sn}\,{}^{j}P_{n}] \quad i=1 \text{ to } N \qquad (21)$$
$$-p = \Sigma^{N}_{j=1}[{}^{ij}A_{ns}\,{}^{j}P_{s}] + \Sigma^{N}_{j=1}[{}^{ij}A_{nn}\,{}^{j}P_{n}] \quad i=1 \text{ to } N$$

As described in [4], it is important to realize that the stresses ${}^{j}P_{s}$ and ${}^{j}P_{n}$ are fictitious, and do not really exist. They are merely the system of stresses applied to each individual element along C' such that the simultaneous system of integrated Kelvin's solutions result in the calculation of the actual boundary conditions of the problem being analyzed.

C. Co-ordinate Transformation

The equations for the transformation of each individual elements local influence coefficients into a common "global" system is described in detail by Crouch and Starfield [4]. By examining Figure 6, we will label the local co-ordinate system for an arbitrary element as x' and y'. The element is defined as $|x'| \leq a$, $y'=0$. The stresses applied to this element are $P_{x'}$, and $P_{y'}$,.

The local co-ordinate system is produced with a translation of c_x in the global x direction, c_y in the global y direction, and a rotation λ about the global z axis (positive direction being counterclockwise). The co-ordinate

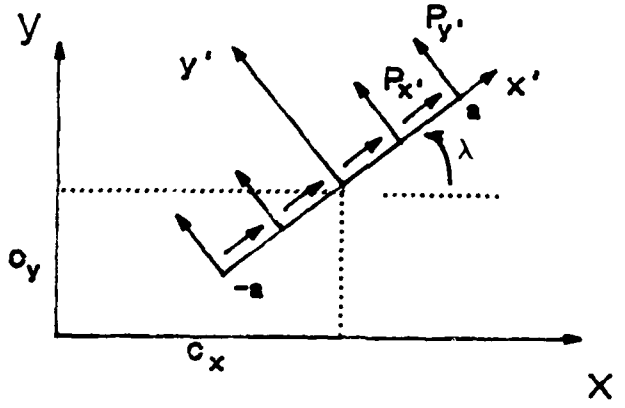

Figure 6. Line Segment of Arbitrary Orientation

transformation is then as follows:

$$x' = (x - c_x)\cos\lambda + (y - c_y)\sin\lambda \qquad (22)$$
$$y' = -(x - c_x)\sin\lambda + (y - c_y)\cos\lambda$$

Substituting (22) and (9) into (7) and (8) produces:

$$u_{x'} = P_{x'}/(2G)[(3-4\nu)F_1 + y'F_3] + P_{y'}/(2G)[-y'F_2] \qquad (23)$$
$$u_{y'} = P_{y'}/(2G)[(3-4\nu)F_1 - y'F_3] + P_{x'}/(2G)[-y'F_2]$$

and

$$\sigma_{x'x'} = P_{x'}[(3-2\nu)F_2 + y'F_4] + P_{y'}[2\nu F_3 - y'F_5] \qquad (24)$$
$$\sigma_{y'y'} = P_{x'}[-(1-2\nu)F_2 - y'F_4] + P_{y'}[2(1-\nu)F_3 + y'F_5]$$
$$\sigma_{x'y'} = P_{x'}[2(1-\nu)F_3 - y'F_5] + P_{y'}[(1-2\nu)F_2 - y'F_4]$$

where the functions $F_1 \ldots F_5$ are defined as:

$$F_1 = f(x',y') \qquad (25)$$
$$= -1/[4\pi(1-\nu)]\{y'[\arctan(y'/[x'-a]) - \arctan(y'/[x'+a])] - (x'-a)\ln\{[(x'-a)^2 + y^2]\}^{1/2} + (x'+a)\ln\{[(x'+a)^2 + y^2]\}^{1/2}\}$$

$$F_2 = f_{,x'}$$
$$= 1/[4\pi(1-\nu)]\{\ln[(x'-a)^2+y'^2]^{1/2} - \ln[(x'+a)^2+y'^2]^{1/2}$$

$$F_3 = f_{,y'}$$
$$= -1/[4\pi(1-\nu)]\{\arctan[y'/(x'-a)] - \arctan[y'/(x'+a)]\}$$

$$F_4 = f_{,x'y'}$$
$$= 1/[4\pi(1-\nu)]\{y'/[(x'-a)^2+y'^2] - y'/[(x'+a)^2+y'^2]\}$$

$$F_5 = f_{,x'x'}$$
$$= -f_{,y'y'}$$
$$= 1/[4\pi(1-\nu)]\{(x'-a)/[(x'-a)^2+y'^2]$$
$$- (x'+a)/[(x'+a)^2+y'^2]\}$$

To calculate the displacements and stresses at a particular element midpoint, it is necessary to calculate x′ and y′ as coordinates relative to the local element location and orientation. The calculated displacements and stresses from Eqs (22) and (23) are also in the local x′y′ system. Since this is not convenient, one more transformation to Eqs (22) and (23) to compute the resulting displacements and stresses in the global xy coordinate system. The relations between the xy global system and the x′y′ local system are

$$u_x = u_x'\cos\lambda - u_y'\sin\lambda \qquad (26)$$
$$u_y = u_y'\cos\lambda - u_y'\sin\lambda$$

$$\sigma_{xx} = \sigma_{x'x'}\cos^2\lambda - 2\sigma_{x'y'}\sin\lambda\cos\lambda + \sigma_{y'y'}\sin^2\lambda \qquad (27)$$
$$\sigma_{yy} = \sigma_{y'y'}\cos^2\lambda - 2\sigma_{x'y'}\sin\lambda\cos\lambda + \sigma_{x'x'}\sin^2\lambda$$

$$\sigma_{xy} = (\sigma_{x'x'} - \sigma_{y'y'})\sin\lambda\cos\lambda + \sigma_{x'y'}(\cos^2\lambda - \sin^2\lambda)$$

Substituting Eqs (26) and (27) into Eqs (22) and (23) yields

$$\begin{aligned} u_x &= P_{x'}/(2G)[(3-4\nu)F1\cos\lambda + y'(F2\sin\lambda + F3\cos\lambda)] \\ &\quad + P_{y'}/(2G)[-(3-4\nu)F1\sin\lambda - y'(F2\cos\lambda - F3\sin\lambda)] \\ u_y &= P_{x'}/(2G)[(3-4\nu)F1\sin\lambda - y'(F2\cos\lambda - F3\sin\lambda)] \\ &\quad + P_{y'}/(2G)[-(3-4\nu)F1\cos\lambda - y'(F2\sin\lambda + F3\cos\lambda)] \end{aligned} \tag{28}$$

$$\begin{aligned} \sigma_{xx} &= P_{x'}[F_2 + 2(1-\nu)(F2\cos 2\lambda - F3\sin 2\lambda) \\ &\quad + y'(F4\cos 2\lambda + F5\sin 2\lambda)] \\ &\quad + P_{y'}[F_3 - (1-2\nu)(F2\sin 2\lambda + F3\cos 2\lambda) \\ &\quad + y'(F4\sin 2\lambda - F5\cos 2\lambda)] \\ \sigma_{yy} &= P_{x'}[F_2 - 2(1-\nu)(F2\cos 2\lambda - F3\sin 2\lambda) \\ &\quad - y'(F4\cos 2\lambda + F5\sin 2\lambda)] \\ &\quad + P_{y'}[F_3 + (1-2\nu)(F2\sin 2\lambda + F3\cos 2\lambda) \\ &\quad - y'(F4\sin 2\lambda - F5\cos 2\lambda)] \\ \sigma_{xy} &= P_{x'}[2(1-\nu)(F2\sin 2\lambda + F3\cos 2\lambda) \\ &\quad + y'(F4\sin 2\lambda - F5\cos 2\lambda)] \\ &\quad + P_{y'}[(1-2\nu)(F2\cos 2\lambda - F3\sin 2\lambda) \\ &\quad - y'(F4\cos 2\lambda + F5\sin 2\lambda)] \end{aligned} \tag{29}$$

As can be seen, Eqs (28) and (29) facilitate the computation of influence coefficients to express displacements and stresses in terms of $P_{x'}$ and $P_{y'}$.

D. Influence Coefficients

To calculate the final influence coefficients, one final transformation of Eqs (28) and (29) are necessary. Eqs (28) and (29) calculate the stresses and displacements at the i'th element in the global coordinate system. We are interested in displacements and stresses at the midpoint of the i'th element in i'th elements local coordinate system, $\bar{x}'$, $\bar{y}'$, as shown in Figure 7. The final transform is

$$\bar{x}' = x'\cos\gamma + y'\sin\gamma \tag{30}$$
$$\bar{y}' = -x'\sin\gamma + y'\cos\gamma$$

where $\gamma=\lambda_i-\lambda_j$. Therefore,

$$^{i}u_{\bar{x}'} = {}^{i}u_{x'}\cos\gamma + {}^{i}u_{y'}\sin\gamma \tag{31}$$
$$^{i}u_{\bar{y}'} = -{}^{i}u_{x'}\sin\gamma + {}^{i}u_{y'}\cos\gamma$$

and

$$^{i}\sigma_{\bar{x}'\bar{x}'} = {}^{i}\sigma_{x'x'}\cos^2\gamma + 2\,{}^{i}\sigma_{x'y'}\sin\gamma\cos\gamma + {}^{i}\sigma_{y'y'}\sin^2\gamma \tag{32}$$
$$^{i}\sigma_{\bar{y}'\bar{y}'} = {}^{i}\sigma_{x'x'}\sin^2\gamma - 2\,{}^{i}\sigma_{x'y'}\sin\gamma\cos\gamma + {}^{i}\sigma_{y'y'}\cos^2\gamma$$
$$^{i}\sigma_{\bar{x}'\bar{y}'} = -({}^{i}\sigma_{x'x'} - {}^{i}\sigma_{y'y'})\sin\gamma\cos\gamma + {}^{i}\sigma_{x'y'}(\cos^2\gamma-\sin^2\gamma)$$

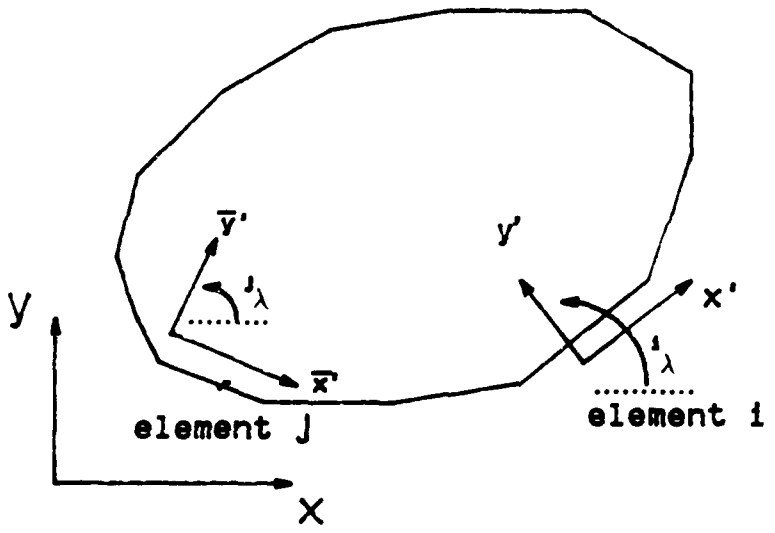

Figure 7. Local Element Co-ordinate Systems

By realizing that

$$j_{P_s} = j_{P_{\bar{x}}}, \qquad (33)$$
$$j_{P_n} = j_{P_{\bar{y}}},$$

$$i_{u_s} = i_{u_{\bar{x}}}, \qquad (34)$$
$$i_{u_n} = i_{u_{\bar{y}}},$$

$$i_{\sigma_s} = i_{\sigma_{\bar{x}},\bar{y}}, \qquad (35)$$
$$i_{\sigma_n} = i_{\sigma_{\bar{y}},\bar{y}},$$

and substituting Eqs (31) and (32) into Eqs (23) and (24) produces

$$\begin{aligned} i_{u_s} &= j_{P_s}/(2G)[(3-4\nu)F1\cos\gamma + y'(F2\sin\gamma - F3\cos\gamma)] \qquad (36) \\ &\quad + j_{P_n}/(2G)[(3-4\nu)F1\sin\gamma - y'(F2\cos\gamma + F3\sin\gamma)] \\ i_{u_n} &= j_{P_s}/(2G)[-(3-4\nu)F1\sin\gamma - y'(F2\cos\gamma + F3\cos\gamma)] \\ &\quad + j_{P_n}/(2G)[(3-4\nu)F1\cos\gamma + y'(F2\sin\gamma - F3\cos\gamma)] \end{aligned}$$

and

$$\begin{aligned} i_{\sigma_s} &= j_{P_s}[-2(1-\nu)(F2\sin 2\gamma - F3\cos 2\gamma) \qquad (37) \\ &\quad - y'(F4\sin 2\gamma + F5\cos 2\gamma)] \\ &\quad + j_{P_n}[(1-2\nu)(F2\cos 2\gamma + F3\sin 2\gamma) \\ &\quad - y'(F4\cos 2\gamma - F5\sin 2\gamma)] \end{aligned}$$

$$
\begin{aligned}
{}^{i}\sigma_n = {}&{}^{j}P_s[F_2-2(1-\nu)(F2\cos 2\gamma + F3\sin 2\gamma) \\
&- y'(F4\cos 2\gamma - F5\sin 2\gamma)] \\
&+ {}^{j}P_n[F_3-(1-2\nu)(F2\sin 2\gamma - F3\cos 2\gamma) \\
&+ y'(F4\sin 2\gamma + F5\cos 2\gamma)]
\end{aligned}
$$

Thus Eqs (35) and (36) can be expressed as

$$
\begin{aligned}
{}^{i}u_s &= \Sigma^{N}_{j=1} {}^{ij}B_{ss}\,{}^{j}P_s + \Sigma^{N}_{j=1} {}^{ij}B_{sn}\,{}^{j}P_n \\
{}^{i}u_n &= \Sigma^{N}_{j=1} {}^{ij}B_{ns}\,{}^{j}P_s + \Sigma^{N}_{j=1} {}^{ij}B_{nn}\,{}^{j}P_n
\end{aligned}
\qquad (38)
$$

and

$$
\begin{aligned}
{}^{i}\sigma_s &= \Sigma^{N}_{j=1} {}^{ij}A_{ss}\,{}^{j}P_s + \Sigma^{N}_{j=1} {}^{ij}A_{sn}\,{}^{j}P_n \\
{}^{i}\sigma_n &= \Sigma^{N}_{j=1} {}^{ij}A_{ns}\,{}^{j}P_s + \Sigma^{N}_{j=1} {}^{ij}A_{nn}\,{}^{j}P_n
\end{aligned}
\qquad (39)
$$

where ${}^{ij}B_{ss}$, ${}^{ij}A_{ss}$, etc., are the final influence coefficients.

The final matrix includes two sets of 2N equations in 2N variables, one for displacements, one for stresses. However, both sets of equations have the fictitious stresses ${}^{j}P_s$ and ${}^{j}P_n$ as the unknowns. Therefore, to create a solvable system of 2N equations, of the four boundary conditions for an element i (${}^{i}u_s$, ${}^{i}u_n$, ${}^{i}\sigma_s$, and ${}^{i}\sigma_n$), only two need be known (one shear, one normal). The final matrix of influence coefficients (2N by 2N) will consist of A's and B's as determined by the type of boundary condition given for each

element. Once the quantities ${}^{j}P_s$ and ${}^{j}P_n$ are known, Eqs (37) and (38) can be used to calculate the remaining unknown boundary conditions, and influence coefficients can be calculated to analyze displacements and stresses at any other point in the body.

It should be noted that the resulting 2N by 2N matrix of influence coefficients is fully populated, as every element effects all other elements as well as itself [4]. This is in contrast to the banded stiffness matrix produced by the finite element method. Though it will be shown in this study that the boundary element method can analyze certain types of problems in far less degrees of freedom than the finite element method, the boundary element method cannot take advantage of a banded matrix so much of the computational advantages are lost.

Another point of interest is each elements "self effects". By examining Eq (6) we see that the value of the integrated Kelvin's solution decreases with increasing distance from the midpoint of an element. Therefore, the maximum value for an influence coefficient must be for an elements influence on itself. Crouch and Starfield [4] show that the values of all elements self effects are

$$ {}^{ii}A_{ss} = {}^{ii}A_{nn} = \pm 0.5 \text{ for } y'=0_{\pm} \tag{40} $$

$$ {}^{ii}B_{ss} = {}^{ii}B_{nn} = -(3-4\nu)/[4\pi G(1-\nu)]({}^{i}a)\ln({}^{i}a) \tag{41} $$

As can be seen from Eqs (14) and (15), the stresses are discontinuous across an element. The convention established by Crouch and Starfield dictates that "the boundary of a finite body is transversed in the clockwise sense, whereas the boundary of a cavity is traversed in the counterclockwise sense". This allows ${}^{ii}A_{ss}$ and ${}^{ii}A_{nn}$ to be equal to 0.5 always.

E. Modeling Considerations

As has historically been the case with the finite element method, an engineers ability to "model" a problem correctly plays as much a role in the value of the final results, as does the accuracy of the method being used. The boundary element method also shares this characteristic. Of particular interest is the fact that the user should not calculate displacements or stresses for a point "too close" to an elements midpoint [4]. The reason is that it has been found empirically that the numerical solution is generally unreliable at points within a circle of radius equal to one element length (2a) centered at the midpoint of a boundary element, except at the midpoint itself. Therefore, to obtain data close to a boundary, the user is forced to refine the lengths of the boundary elements in a gradual fashion as the area of interest is approached. F.R. Harris [8] developed a

modeling technique for a crack of length "a" that can be incorporated into the work done herein. His method can be stated as follows: The crack length is divided into .50a, .25a, .125a and .125a segments. The first segment, or the .50a length segment is divided into three equal length boundary elements (element length = .1667a). The second segment, or the .25a length segment, is divided into three equal length boundary elements, (element length = .0833a). The third segment is divided into three equal length boundary elements (element length = .04167a). The last segment is divided into 25 equal length boundary elements (element length = .005a). By using this method of gradual refinement, stresses can be computed with reasonable accuracy near the area of the singularity at the crack tip.

To model the problems in this study, each body was modeled with a line of symmetry along the line of the crack. The entire line of symmetry was modeled with boundary elements. The crack itself is modeled with the F.R. Harris method of refinement [8] outlined above. The refinement scheme is mirrored at the crack tip both along the crack itself, and along the uncracked material directly in the path of the crack. The elements along the non-cracked boundary utilized enforced displacement conditions (u_n=0) normal to the line of the crack and stress conditions tangential to the crack (σ_s=0). The crack surface itself was modeled as being stress free (σ_n=σ_s=0).

III. Boundary Element vs Finite Element

An initial configuration of a two hole tension strip was analyzed with both the boundary element method described in this study, and with the MSC/NASTRAN finite element code. Both methods were used in order to compare the relative strengths and weaknesses. Both method only modeled the top half of the tension strip using symmetry conditions as enforced through restrained vertical displacement along the line of symmetry.

The geometry and material properties of the problem are illustrated in Figure 8. The tension strip has two holes of 0.25 inch diameter. The holes are separated by one inch. The edge distances to the holes are three diameters for all four sides. The initial crack length is 0.1 inch, and it is emerging from one hole and oriented towards the second hole. The far field tension stress is 46 KSI.

A. Finite Element Method

There were three MSC/NASTRAN models constructed. This was to provide convergence data. The baseline model consisted of 13,858 degrees of freedom. The other two models had respectively 8,610 and 15842 degrees of freedom. Needless to say all of the models were constructed with a graphic pre-processor/model generator (PDA/PATRAN). The baseline

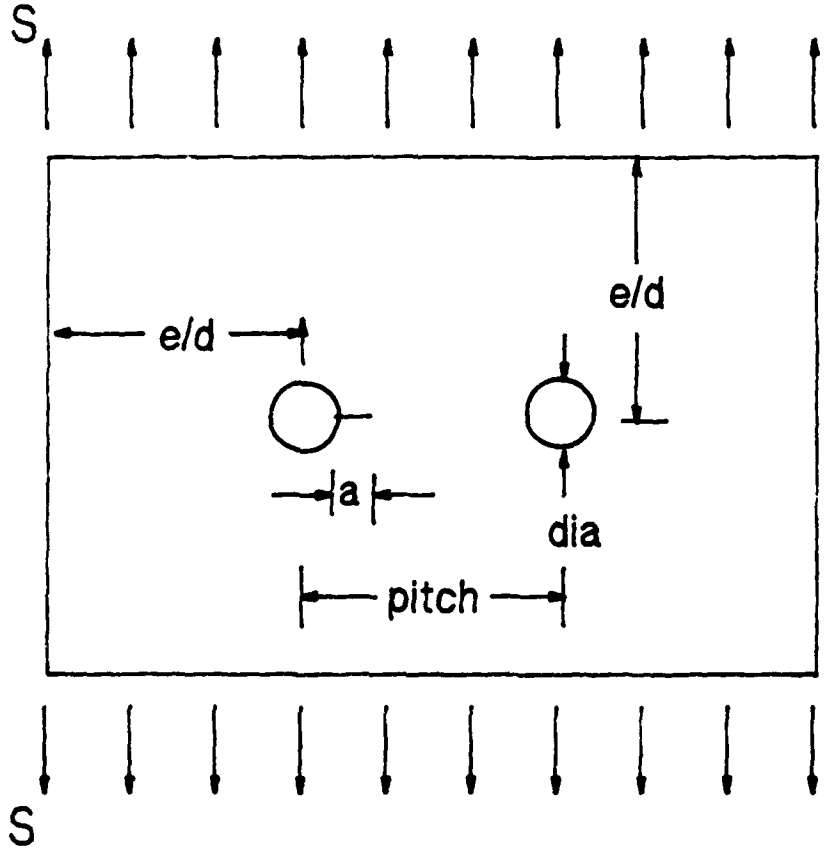

dia = 0.25 in.
pitch = 4d
e/d = 0.10 in.
a = 0.10 in.
S = 46 KSI
E = 10300 KSI
ν = 0.33

Figure 8. Tension Strip Problem

model is shown in Figure 9. The course model (8,610 DOF) and the fine model (15,842 DOF) look identical to the baseline model only differing in the density of the mesh in the immediate vicinity of the crack tip.

All three models consisted of a mesh of eight noded quadratic isoparametric quad elements in the crack area. The eight noded quad (CQUAD8) mesh then transitions into a four noded quad (CQUAD4) element mesh to complete the model. A handful of six noded triangles (CTRIA6) were required in the transition region.

The entire models were declared "Surfaces" as described in the MSC/NASTRAN Users Manual [14] and interpolated stresses were output at all corner grid points. The model used the MSC/NASTRAN "topological" option for grid point stress calculation [14]. This method assumes stresses are continuous across connecting elements. Following the stress intensity factor calculation technique described in the computer implementation section, only those stress grid points along the line of the crack, and at a distance of five to ten percent of the cracks' length ahead of the crack were used in the stress intensity factor determination. The baseline model stress grid points in the crack tip area were only .001 inches apart allowing five grid points in the K_I calculations. The courser finite element model (8,610 DOF) had only two stress points in the calculation zone, while the fine model (15,842 DOF) had nine grids in the calculation of K_I.

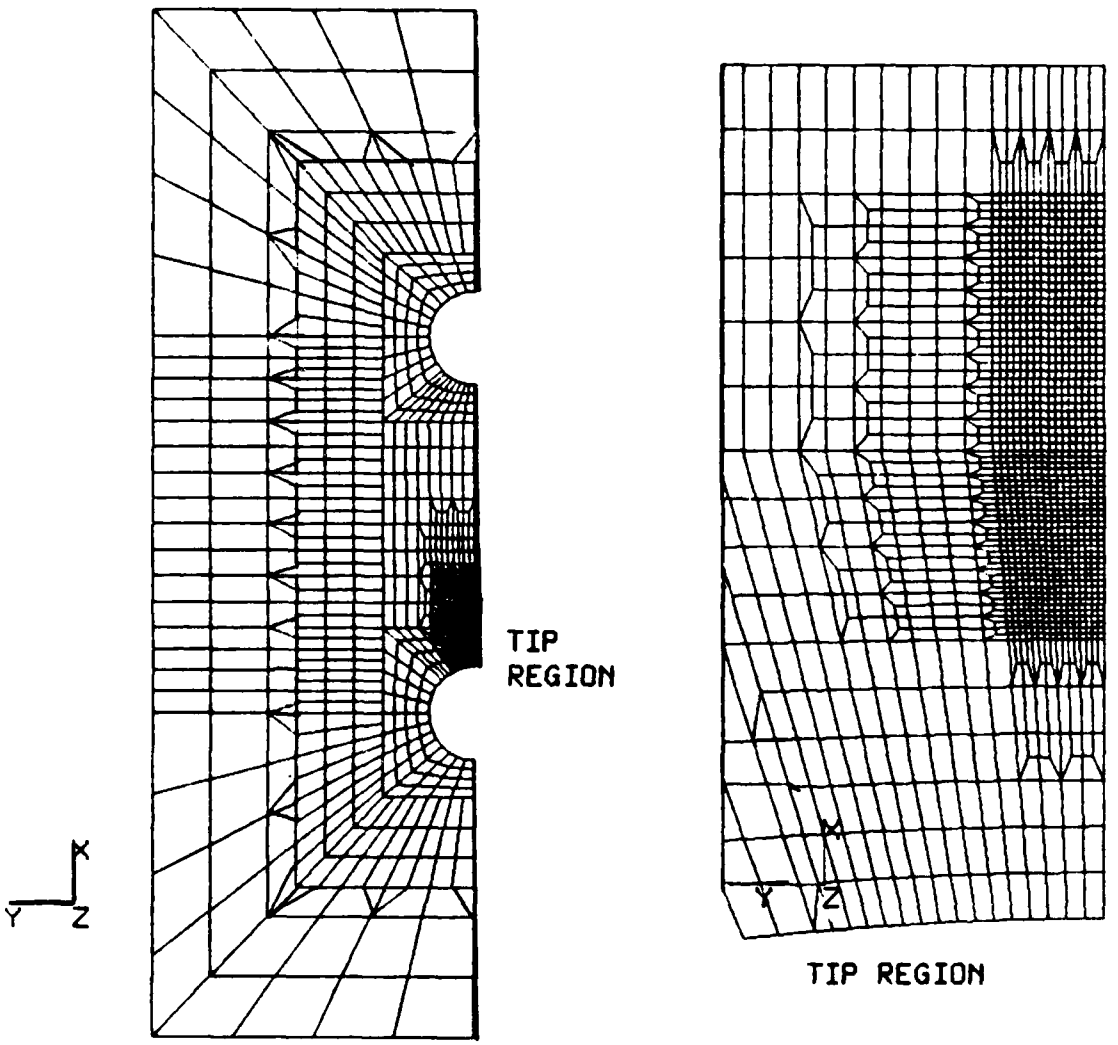

Figure 9. Baseline MSC/NASTRAN Finite Element Model

B. Boundary Element Method

The boundary element model constructed consisted of 287 elements resulting in 574 degrees of freedom. The model is pictured in Figure 10. The crack is descretized with F.R. Harris's refinement technique [8] resulting in elements at the crack tip with a length of 0.0005 inches. The model is restrained from rigid body movement by fixing both displacement boundary conditions for the far right element on the line of symmetry. The boundary element model had five element midpoints in the allowable zone for K_I calculation.

C. Comparisons

Stress Intensity Factor calculations were completed on all three finite element models and the boundary element model using the stress extrapolation method

$$K_I = \text{Lim}_{r \to 0} [\sigma_y \ (2\pi r)^{1/2}] \qquad (43)$$

The values of K_I were plotted against r and r^2 to graphically determine K_I at r=0. Linear regression fits were made for both fits. As was discussed in the computer implementation section (Appendix A), the r^2 method was necessary for cases where the crack length approaches the second hole as the r method yields poor curve fits. For this case, it was not

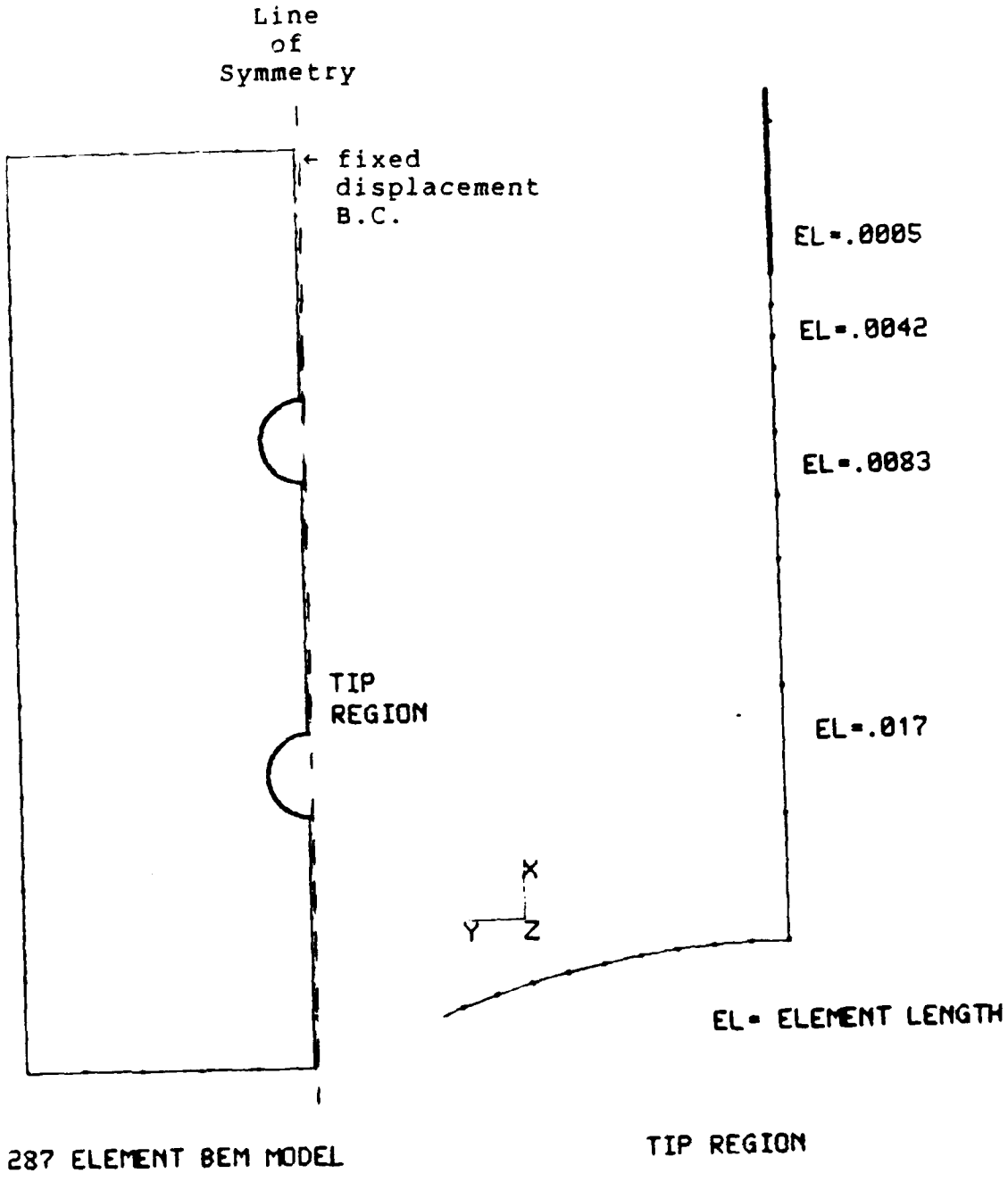

Figure 10. Boundary Element Model

deemed necessary as the crack length is relatively short, but was still done for comparison purposes. Final calculations for K_I for the r fit and the r^2 fit are given in Table I. It can be seen that both fits gave essentially the same answers, as was expected for this case. Also, the boundary element K_I prediction was within two to three percent of the baseline finite element K_I predictions.

The agreement between the boundary element model and the baseline finite element model is encouraging considering the difference in degrees of freedom (13858 to 574). From this simple statement the reader would conclude that the boundary element method is 24 times more efficient. But the user must remember that the boundary element model was a "full" matrix without the banded symmetry common to the finite element method. A highly optimized finite element code, such as MSC/NASTRAN, has a built in nodal resequencer to optimize the stiffness matrix automatically. The VAX computer operates with a "virtual memory" scheme. Matrix storage is handled by writing to scratch files that are erased upon program completion. This makes it difficult to compare storage requirements for both FEM and BEM. Therefore, it is instructive to examine the CPU times required to run all four models as listed in Table 1. All of the CPU times are for a Digital VAX 8350 computer. It can be seen that in comparing the boundary element model to the baseline MSC/NASTRAN model, it ran 2.2 times as long even though the

MSC/NASTRAN model used 24 times as many degrees of freedom. The boundary element model barely ran faster than the 8,610 DOF course MSC/NASTRAN model.

The reason for the CPU time results lie in the relationship between matrix size, fullness and the CPU time to invert and solve it. The MSC/NASTRAN Handbook for Linear Static Analysis [13] outlines a relationship between problem size and computer time. Basically the three elements of computer time are; overhead cost, which is dependent on problem type but not on problem size; initial matrix set up costs, which involve computation of the influence or stiffness matrices; and finally results costs which involve solving the matrices for final computations. The results cost are the one that increases rapidly with an increase in problem size. Reference [13] states that for a finite element model with approximately 100 to 200 grids, all three costs are the same. It is obvious that this study has far more than 200 grids, so will be dominated by the results costs. Reference [13] goes on to give explicit formulas for CPU estimation, but the CPU formulas are proportional to the number of degrees of freedom multiplied by the average (RMS) number of active columns squared. The baseline MSC/NASTRAN output yielded a RMS value for active columns after resequencing of approximately ninety colums. A full BEM matrix of 574 by 574 has a RMS column width of 332.

Therefore:

$$CPU_{BEM} \propto (574 \text{ DOF})(332 \text{ columns RMS})^2 = 63268576 \quad (44)$$
$$CPU_{FEM} \propto (13858 \text{ DOF})(90 \text{ columns RMS})^2 = 112249800$$

The ratio of CPU_{FEM} over CPU_{BEM} is 1.7. This indicates that a preliminary comparison of the boundary element model to the baseline MSC/NASTRAN model should have predicted a run time for the MSC/NASTRAN model of 1.7 times the boundary element model, not 24 times. (Actual CPU time ratio was 2.2) Indeed, the cost of a fully populated matrix is very high.

Table I. MSC/NASTRAN VS BEM Tension Strip Results

Model	DOF	K_I (r fit) $(KSI(in)^{1/2})$	K_I (r^2 fit) $(KSI(in)^{1/2})$	CPU (min)
Coarse FEM	8610	37.9	36.3	96
Baseline FEM	13858	39.6	38.9	183
Fine FEM	15842	39.5	38.9	255
BEM	574	40.4	40.1	83

IV. Boundary Element vs p-Version Finite Element

PROBE is a commercial finite element code sold and promoted by Noetic Technologies. The code was first conceived and implemented at Washington University's Center for Computational Mechanics in St. Louis under Dr. Barna A. Szabo. The theoretical aspects of the p-Version of finite elements are explained by Babuska, Szabo and Katz in reference [2]. The implementation of the p-Version into PROBE is given by Szabo in reference [23]. The innovative aspect of PROBE is that it boasts elements based on variable order polynomials. By doing this, the user can create very rough grids in the creation of finite element models. By varying the polynomial order, or p, increased accuracy in the results is obtained. The second advantage of PROBE is that by running multiple p levels for a given model, the user is given an indication of solution convergence.

Noetic Technologies worked with the Fort Worth Division of General Dynamics (GD) on a research grant to study the application of the p-Version to a stress intensity factor analysis, and compare it to a classical finite element solution. A two hole tension strip, as shown in Figure 11, was analyzed by GD with conventional finite element analysis. Noetic Technologies analyzed the same problem with the p-Version PROBE code and published the results in reference [25]. The GD model, shown in Figure 12, involved

approximately 1500 degrees of freedom. The corresponding PROBE model, as shown in Figure 13, has only 29 nodes. However, by varying the value of p from 1 to 8, the PROBE degrees of freedom varies between 58 and 1623.

A boundary element model was constructed of the problem, as shown in Figure 14, consisting of 220 elements or 440 degrees of freedom. The GD model predicted a K_I of 43.4 KSI(in)$^{1/2}$. The PROBE results for p=1 to p=8 were plotted by K_I versus 1/DOF on a semi-logarithmic scale, and the resulting straight line extrapolated to predict K_I at p=∞. The final PROBE prediction of K_I at p=∞ is 43.1 KSI(in)$^{1/2}$. The final BEM prediction based on a regression fit on r was 42.2 KSI(in)$^{1/2}$. The final BEM prediction for a regression fit on r^2 was 43.2 KSI(in)$^{1/2}$. Both BEM predictions were close to the GD and PROBE predictions, but the r^2 fit was better.

It should be noted that the PROBE analysis gave an indication of convergence to the final answer. The BEM model with an r^2 regression fit was almost exact in its' correlation with the PROBE results.

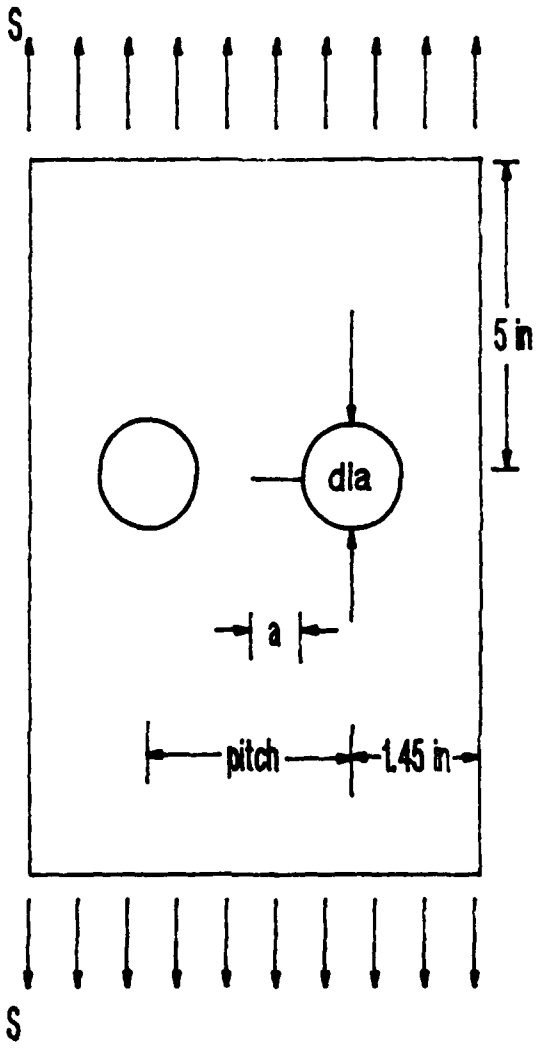

width = 5.0 in
height=10 in
dia = 1.0 in
S = 20 KSI
pitch = 2.1in
a = .55 in

Figure 11. PROBE Two Hole Tension Strip Problem

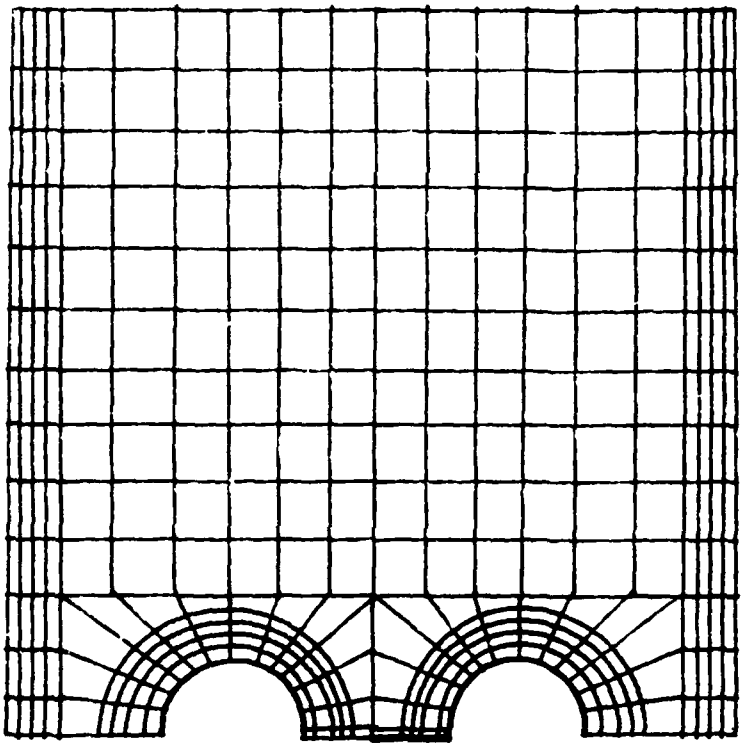

Approximately 1500 degrees of freedom

Figure 12. GD Model of PROBE Problem

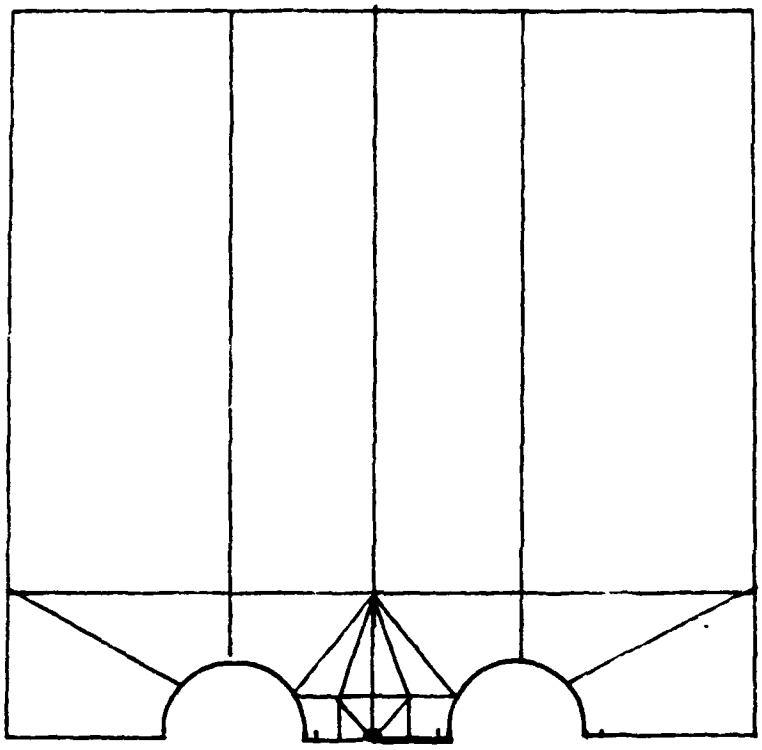

Approximately 29 nodes

Figure 13. PROBE model of PROBE Problem

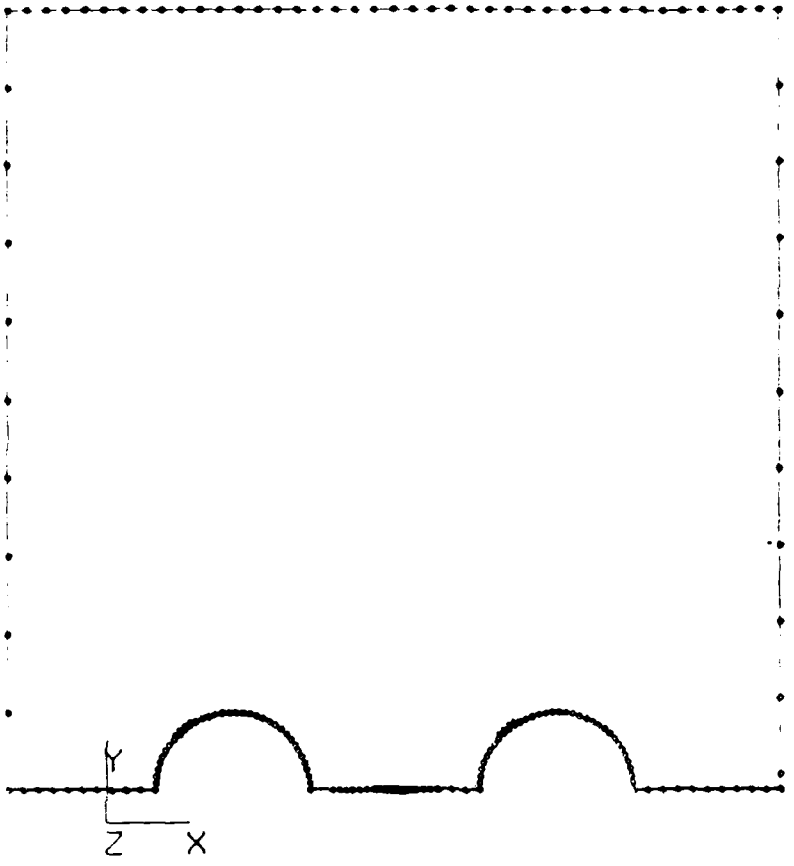

Figure 14. Boundary Element Model of PROBE Problem

V. Boundary Element vs Bowie Solution

Bowie [3] studied the problem of a crack growing from a circular hole in an infinite plate as shown in Figure 15. His solution is well published and can be shown in the form,

$$K = \sigma(\pi a)^{1/2}\beta \qquad (45)$$

where $\beta = f(a/r)$. Other individuals, specifically Grandt, Brussat and Newman [1], have employed various technique to improve on Bowies β term. For the example problem, σ=46 KSI, r=.125 in, and a/r=.5 . Using the value of a/r=0.5, Bowie, Brandt, Brussat and Newman calculate a value of 1.73, 1.735, 1.733 and 1.728 for β respectively [1]. When inserted into Eqn (45), this results in K_I calculations of 35.26, 35.26, 35.32 and 35.22 KSI$(in)^{1/2}$.

A boundary element model was created comprising of 72 elements. To model an infinite domain, a different modeling technique is required than for the finite domains. The model is shown in Figure 16. The model is again a representation of the "upper" half of the geometric boundary. As described in the Computer Implementation section, a line of symmetry is assumed along the x axis. Phantom "image" elements are calculated by the TWOFS99 program for the lower half. One problem is the crack itself. Unlike the finite domain problems, the crack elements cannot be on the line of

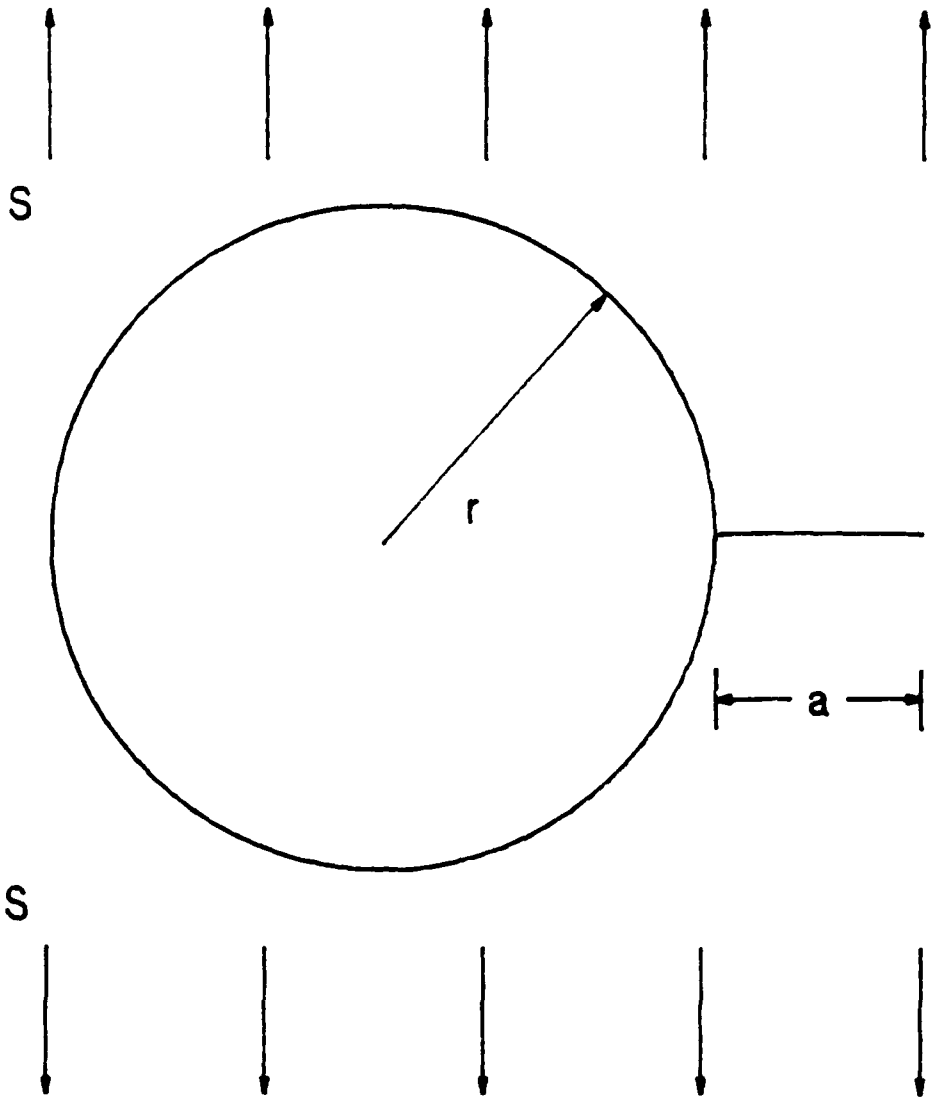

r = hole radius = .125 in.
a = crack length = 0.0625 in.
S = far field tension stress = 46 KSI

Figure 15. Crack from a Hole in an Infinite Plate

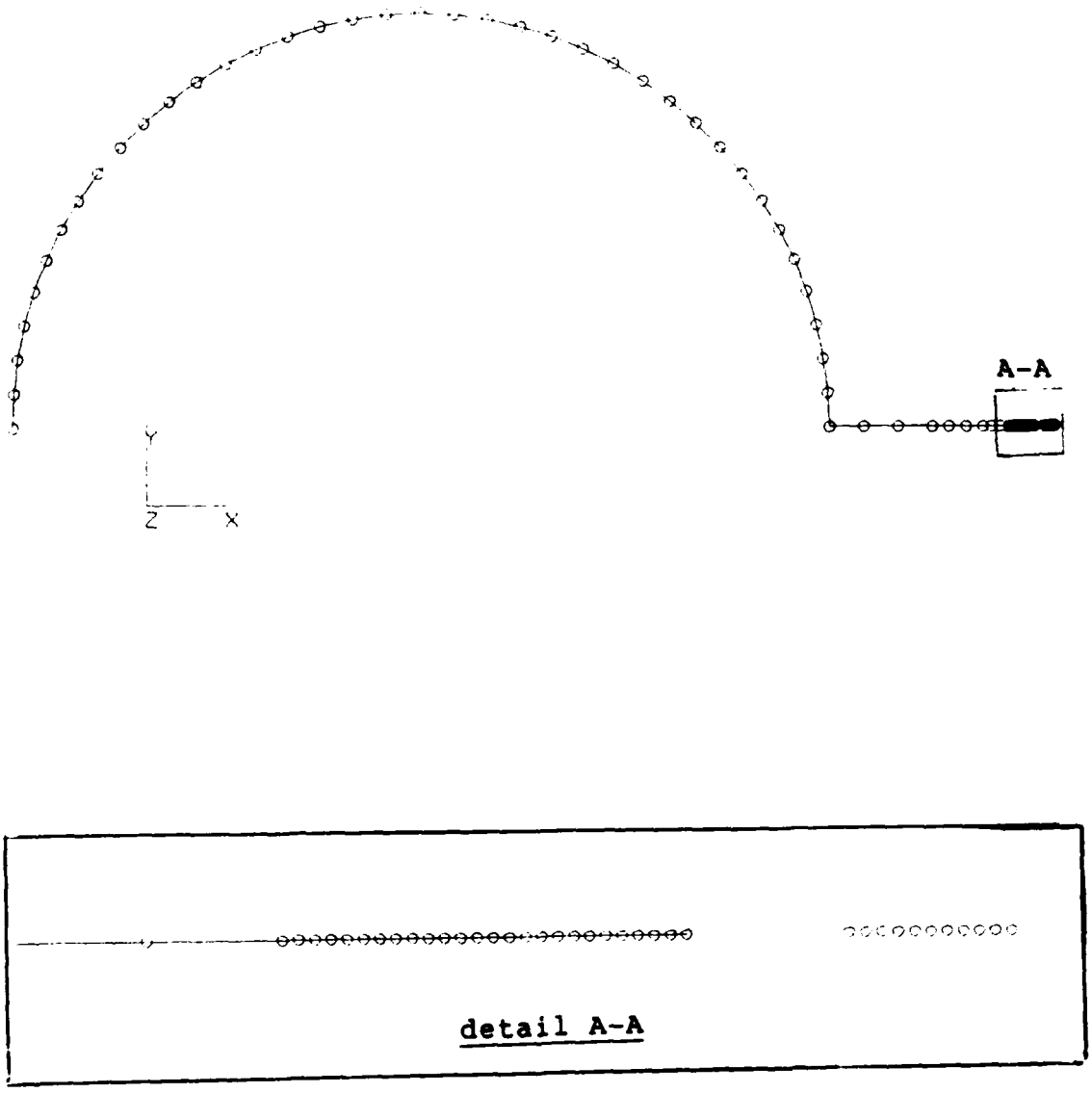

Figure 16. Boundary Element Model of Hole with Crack

symmetry as the program could not distinguish the actual elements representing the "upper" face of the crack, from the "image" elements representing the "lower" face of the crack. Therefore the line of elements representing the "upper" face of the crack are modeled with a small crack opening offset as shown in Figure 17. The elements along the crack are arranged in a straight line between the crack opening offset and the crack tip. The "image" elements are therefore calculated with an equal, but opposite, location below the y=0 line of symmetry. The objective is to model the crack opening offset as small as possible to best represent the actual crack, which has no such offset. But the offset must be large enough for the TWOFS99 program to differentiate between the two faces of the crack. This is usually a function of the accuracy of the computer the program is running on. The Bowie model uses an offset of $5.0(10)^{-6}$ inches from the y=0 line of symmetry, to the intersection of the "upper" face of the crack with the circumference of the hole. This results in an initial offset five orders of magnitude smaller than the actual y displacement at that point. The crack itself is again modeled with the F.R. Harris refinement technique which concentrates 25 elements in the crack tip area. The model is symmetric about the y=0 axis by imposed symmetry, but the element along the circumference of the hole, opposite from the crack, is restrained from x displacements to prevent rigid body translation.

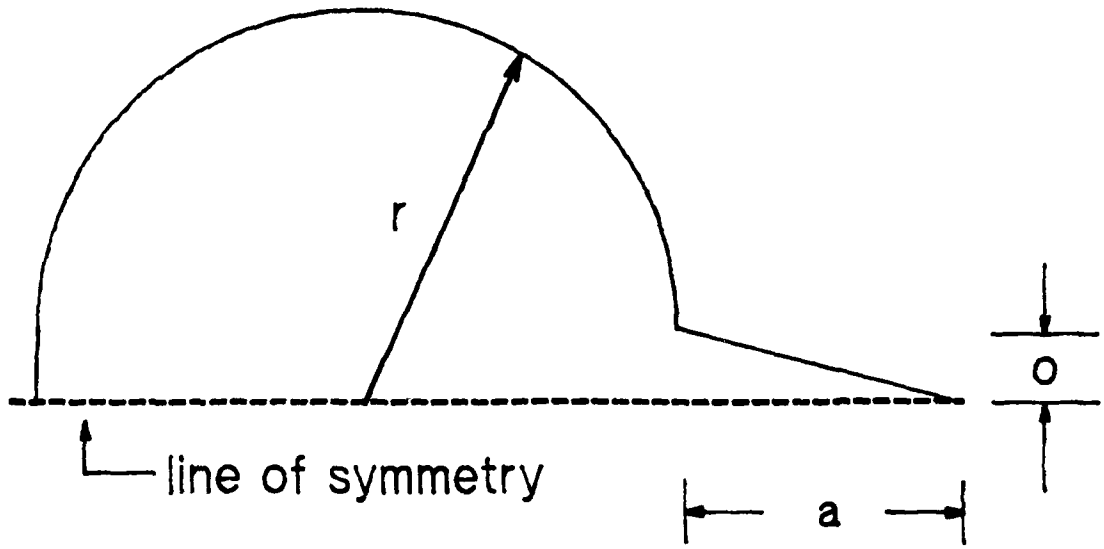

r = radius

a = crack length

o = crack opening (exaggerated)

Figure 17. Infinite Domain BEM Crack Modeling Technique

Since there are no elements in the area of the stress field used for K_I calculations, points of data calculations must be placed there. As can be seen in Figure 16, eleven data points were placed in the line of the crack, at a distance of 1.05a to 1.10a. The y stresses were recovered at these points, and used to create stress extrapolation predictions for K_I. As before, both regression fits on r and r^2 were completed.

Based on the 72 element model, the K_I prediction based on a regression fit on r is 35.0 KSI$(in)^{1/2}$. The same model predicted 35.6 KSI$(in)^{1/2}$ based on a r^2 fit. In this instance the r fit was more accurate than the r^2 fit, but the significant observation is that both methods provided a prediction within one percent of the analytical predictions of Bowie, Grandt, Brussat and Newman [1].

VI. Boundary Element vs Shivakumar Solution

The next problem attempted is an extension of the Bowie problem of Section VI. A second hole is added to the Bowie problem to simulate the two hole tension strip problem of Sections IV and V, only the domain is infinite, not finite. Shivakumar and Foreman solved this problem [19] with a series approach based on the Muskhelishvili formulation. The solution is incorporated into the NASA crack growth computer program NASA/FLAGRO [15]. By selecting a far field stress of 46 KSI, crack length of 0.0625 inches, hole diameter of 0.25 inches and a hole separation of 1.0 inch, the analytical prediction of K_I from the NASA/FLAGRO program is 36.03 KSI(in)$^{1/2}$.

The analytical solution assumes a row of holes in an infinite plate. To properly model the geometry with boundary elements, three holes were included in the analysis. This included one hole on either side of the flawed hole. The modeling techniques were identical to the Bowie solution model in Section VI. The model is depicted in Figure 18. The model consisted of 148 elements, or 296 degrees of freedom. The stress data, as before, was fit to both r and r^2. The K_I prediction for r was 35.3 KSI(in)$^{1/2}$ while the prediction for an r^2 fit was 36.0 KSI(in)$^{1/2}$. In this case the r^2 fit more closely approximated the analytical solution. However, both fits were within two percent of the analytical solution with the r^2 fit being only 0.09 percent different.

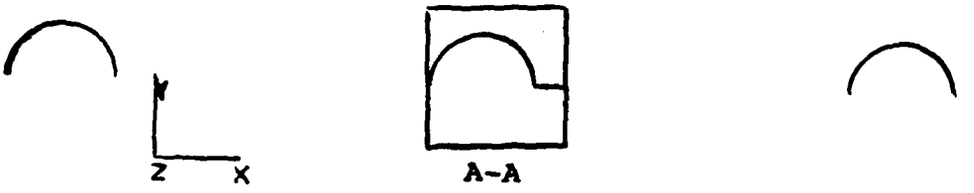

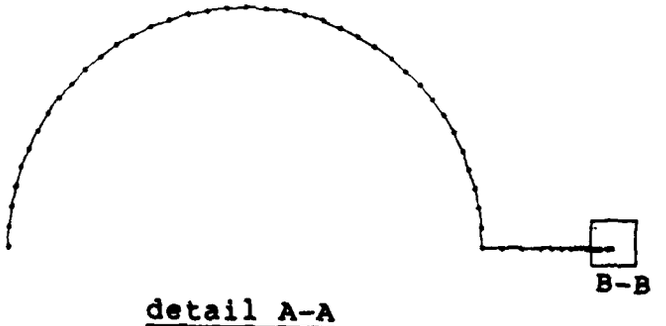

detail A-A

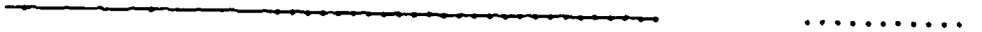

detail B-B

Figure 18. Boundary Element Model of Shivakumar Problem

It is important to observe again that the analytical solution assumes an infinite row of holes. Obviously the three holes nearest to the crack dominated the solution, but additional refinement could be achieved by including more of the remaining holes.

VII. Two Hole Tension Strip Parametric Study

The final analytical task is a parametric study for a two hole tension strip analysis. The comparisons to conventional finite element analysis for this configuration problem was established with MSC/NASTRAN in Section III, and Noetic PROBE in Section IV. Correlation of the boundary element method and modeling techniques employed in this study were shown with the comparison to the infinite domain problems of the Bowie solution in Section V, and the Shivakumar solution in Section VI. This section is an analysis of a two hole tension strip with the geometry and boundary conditions as shown in Figure 19. The edge distance from the center of the holes to the side, top and bottom edges is established as three hole diameters. All cases will be analyzed for a far field tension stress of 46 KSI. The parameters that are varied in this study are hole diameter, d, hole separation (center to center) p (expressed as a ratio of hole diameter), and crack length a. This study expressed crack length as a ratio where

$$\text{crack ratio} = a/(P - D) \qquad (46)$$

where a = crack length (in)

D = hole diameter (in)

P = hole pitch as a ratio of D(D in)

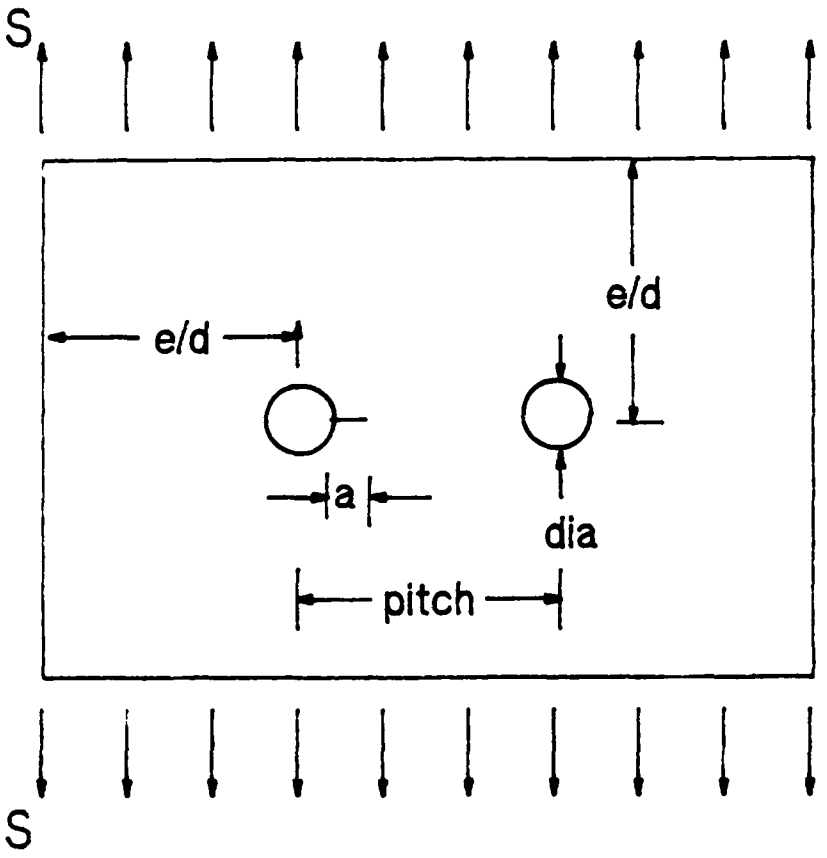

dia = .25, .33, .50 in
pitch = 3, 4, 5 diameters
e/d = 3 dia
Crack Ratio = a/(pitch - dia)
= .1, .2, .3, .4, .5, .6, .7, .8, .9
S = 46 KSI

Figure 19. Two Hole Tension Strip Parametric Study

This enables the crack length to be expressed as a fraction of the distance of material available between the two holes. Therefore a crack ratio of zero corresponds to no crack at all, and a crack ratio of one implies the crack has broken through from the first hole into the second hole.

The study included hole diameters of 0.25, 0.33 and 0.50 inches. The pitch was analyzed for 3D, 4D and 5D, and the crack ratio was analyzed for 0.1, 0.2, 0.3, 0.4, 0.5, 0.6, 0.7, 0.8, and 0.9 . The values for hole diameter, edge distance and hole separation were chosen to represent realistic geometry found in actual applications. The final study involved 81 models of the different configurations listed here, as well as 18 more models for additional work not included in the baseline analysis.

The size of the models varied from 240 to 340 elements. All of the models were created by the same model generator, CHOLE, as documented in Appendix A. The crack tip refinement method was the F.R. Harris technique [8].

The stress field data was collected at a distance five to ten percent of the crack length ahead of the crack tip. This is the same method used throughout this thesis. The stress field is used to predict the mode I crack tip stress intensity factor, K_I, by using the equation

$$K_I = \text{Lim}_{r \to 0} \left[\sigma_y \, (2\pi r)^{1/2} \right] \qquad (43)$$

as documented in Appendix A for the program TWOFS99_EX. TWOFS99_EX extracted the stress field data for all of the boundary element models, computed the values of K_I and r, and fit the data with a linear regression analysis of K_I vs r^2. Throughout this thesis, K_I predictions based on regression fits of r and r^2 have been presented. The results were for the geometry analyzed. There was no significant difference in which fit was chosen, and neither regression fit was consistently more accurate than the other. However, during the course of this study, it was found that for crack ratios approaching 0.9, due to the influence of the approaching second hole, the K_I vs r curve is decidedly non-linear. Therefore, a linear regression fit was non-representative. The K_I vs r^2 curve was much more linear, and the regression fit of that data was representative. For this reason, all K_I predictions presented in this section are based on a K_I vs r^2 regression fit only. Examples of K_I data plotted against r and r^2 are presented in Appendix F.

The K_I calculations for hole diameters of 0.25, 0.33 and 0.50 inches are presented in Figures 20, 21, and 22 respectively. The calculated K_I values are plotted against the crack ratios and are presented as a family of curves varying by the pitch. The figures show the trend is for increasing values of K_I for increasing crack ratios, and for increasing K_I for increasing hole diameter. The K_I also increased for increasing pitch ratios. If the data were plotted on the same graph, the

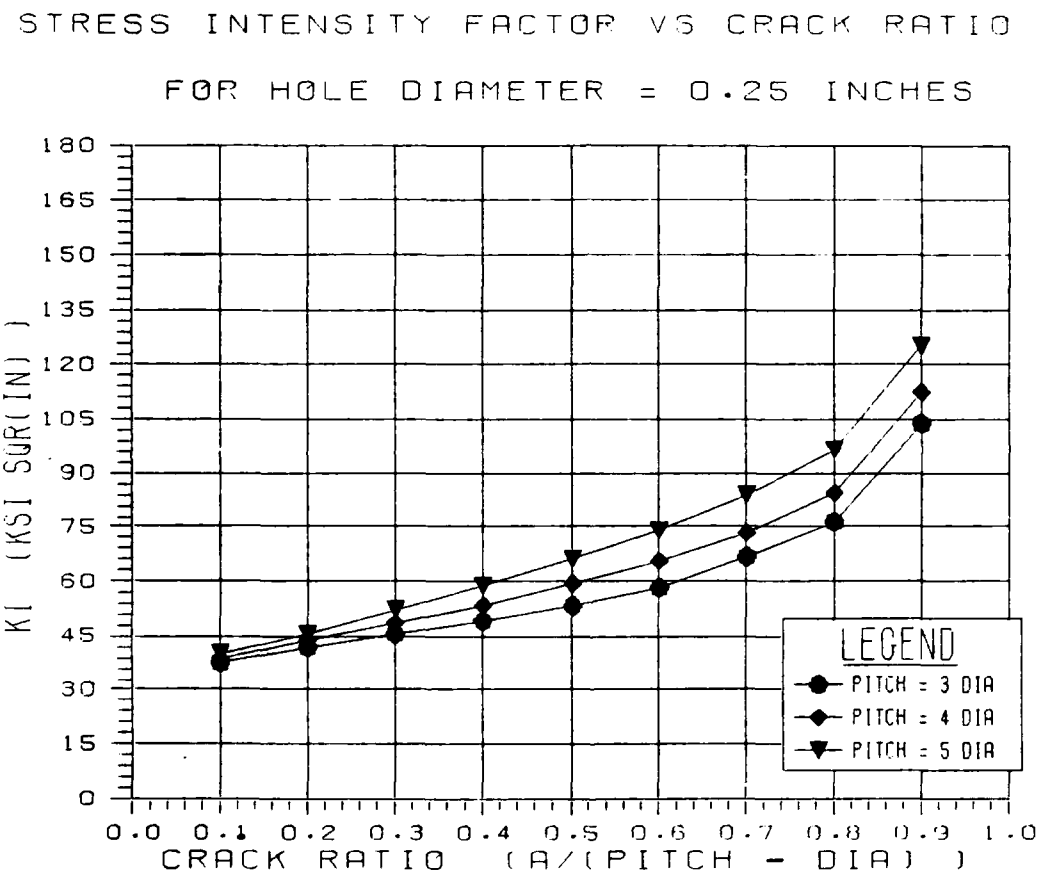

Figure 20. K_I vs Crack Ratio for Hole Diameter = 0.25

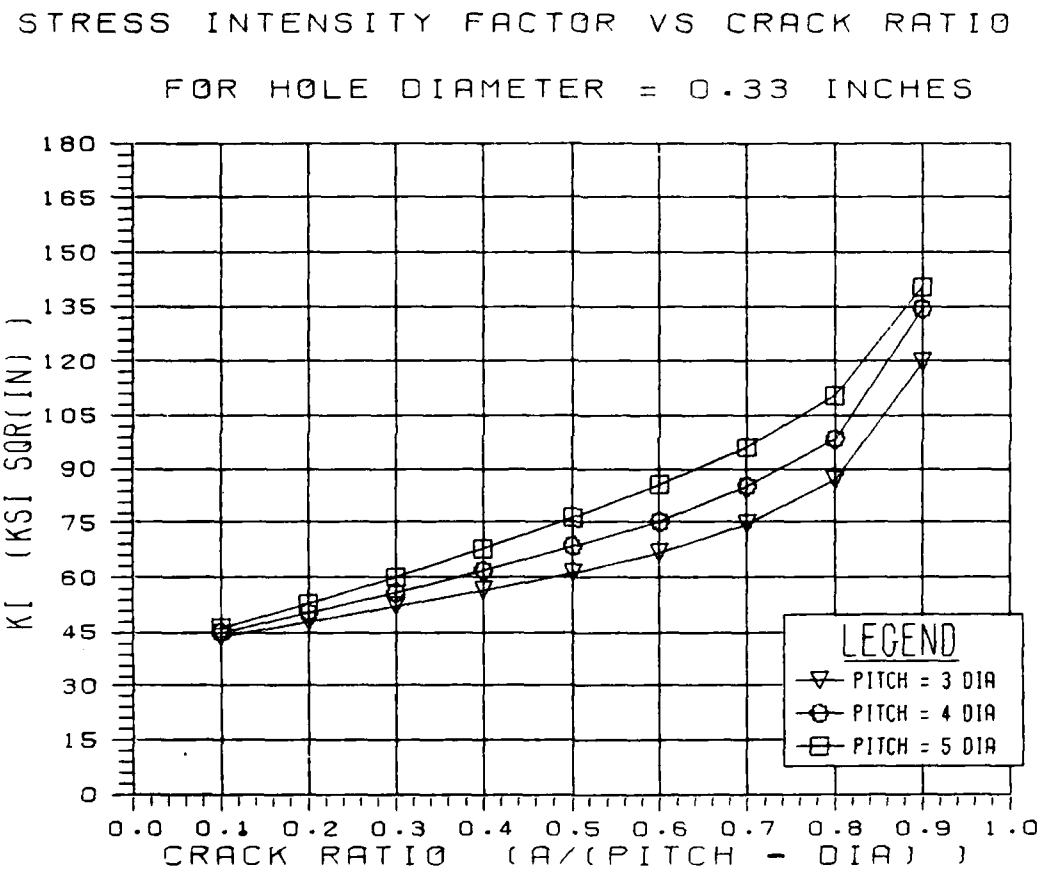

Figure 21. K_I vs Crack Ratio for Hole Diameter = 0.33

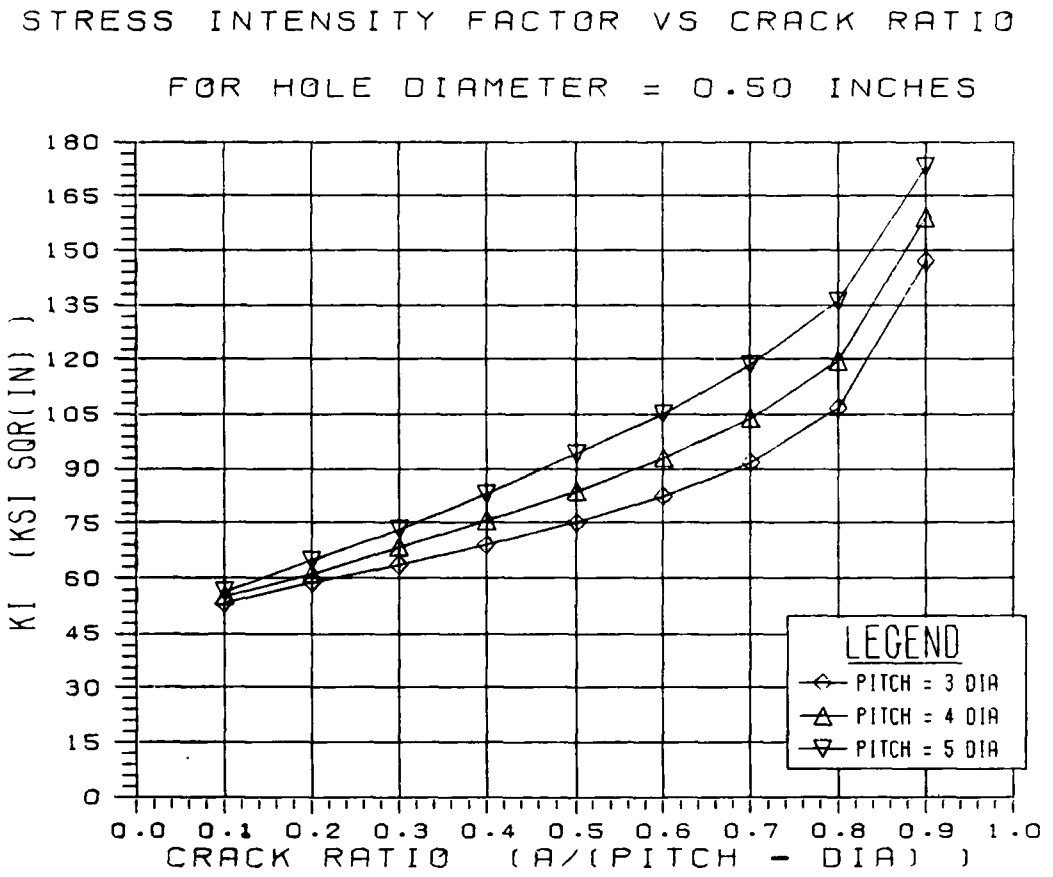

Figure 22. K_I vs Crack Ratio for Hole Diameter = 0.50

presentation would be confusing as the curves would overlap, making interpretation of results difficult. A better way of presenting the data from this study is the Stress Intensity Factor Correction Coefficient, β, as defined by

$$\beta = K_I/\sigma(\pi a)^{1/2} \tag{46}$$

By "normalizing" the stress intensity factor, the influence of far field stress and crack length are removed, allowing for isolation of the geometric Correction Coefficient (β) of the problem being solved. The β factors are presented in Figure 23. It was found that by plotting β versus the crack ratio, a family of curves varying by the pitch ratio could be produced. Once plotted with these parameters, the variation of β with the hole diameter was found to be invariant. Thus, Figure 23 represents a useful tool in the analysis of the two hole tension strip with the edge constraints presented in the beginning of this section. The values of all computed β factors for all of the models run are presented in Tables II, II, and IV.

It is interesting to note the compression of the β curves at the higher pitch ratios, at crack ratios above 0.5. To analyze this phenomena, for a hole diameter of 0.25 inches, two additional curves with a pitch ratio of 3.5 and 4.5 were created. These curves were plotted with the previous β curves to create Figure 24. This shows that there is a

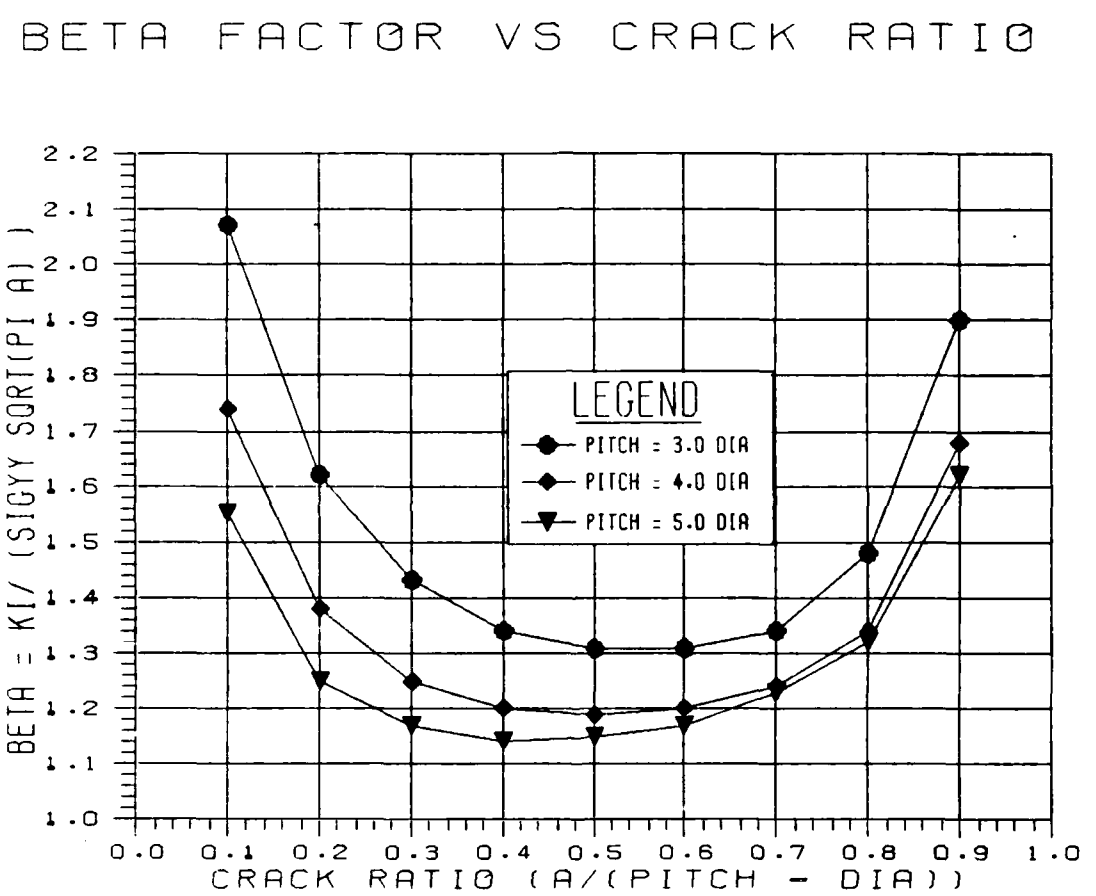

Figure 23. β Factor vs Crack Ratio

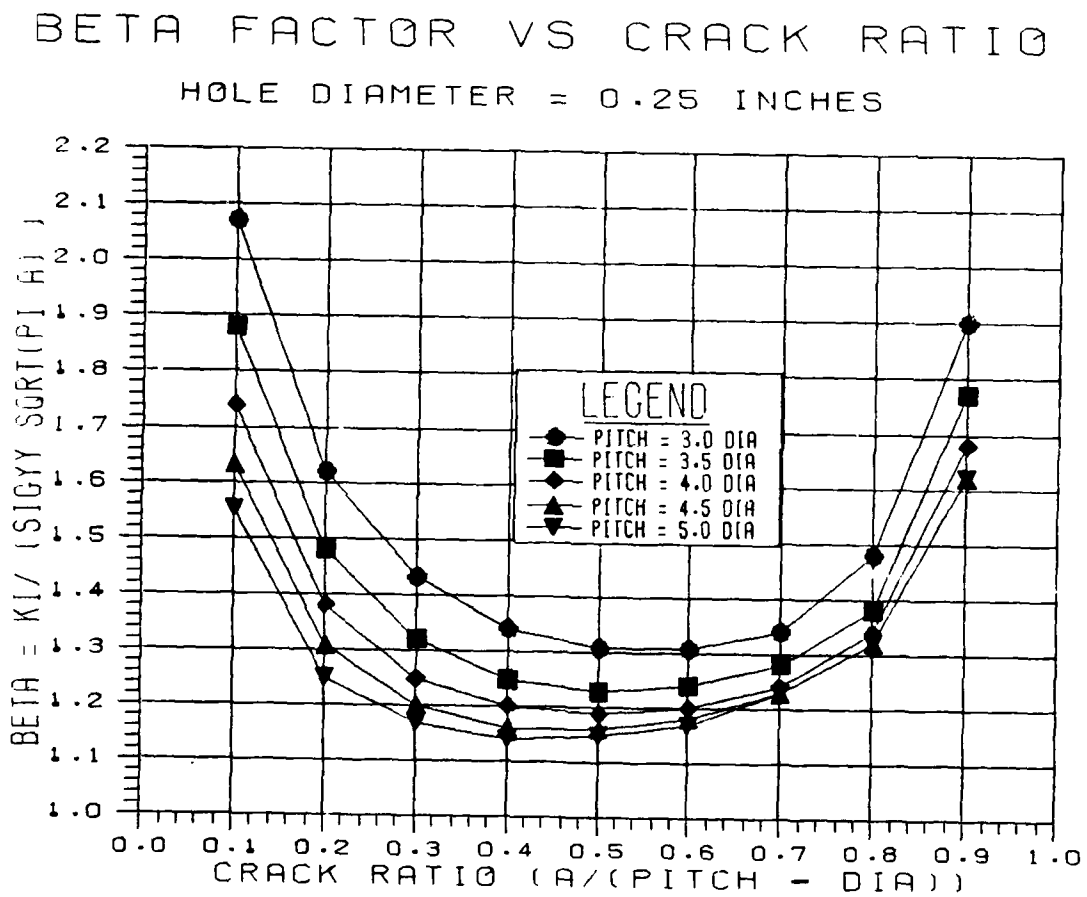

Figure 24. β Factor vs Crack Ratio for Hole Diameter=0.25

compression in the β curves at the location mentioned earlier. It was postulated that this was a "net area" effect relating to the rigid edge distance criteria of the original problem. For a given diameter hole, the pitch was varied as a ratio of the diameter, but the edge distances remained constant at three diameters. Therefore, as the crack ratio grows towards 0.9, the reduction in net area as a percentage of the total original pre-cracked net area, is higher for the higher pitch ratios. The effects of this would be increased as the crack grew in length. To examine this trend, the β factors from Figure 23 were modified to calculate β based on net stress, σ_{net}, instead of far field stress, σ, and then calculate β_{net} as follows

$$\beta_{net} = K_I/(\sigma_{net} (\pi a)^{1/2}) \qquad (47)$$

The results are shown in Figure 25. Both β and β_{net} are plotted against crack ratio. The plot shows that at crack ratios above 0.5, as the β factors based on far field stress began to increase uniformly in value, the β_{net} factors based on net stress cross over as the effects of pitch ratio seem to reverse. It is further postulated by the author, that if the net section effects were subtracted from the final β curves of Figure 23, a family of β curves would thus be created with the same generic trends of Figure 23, but without the collapse of curves at the higher pitch ratios

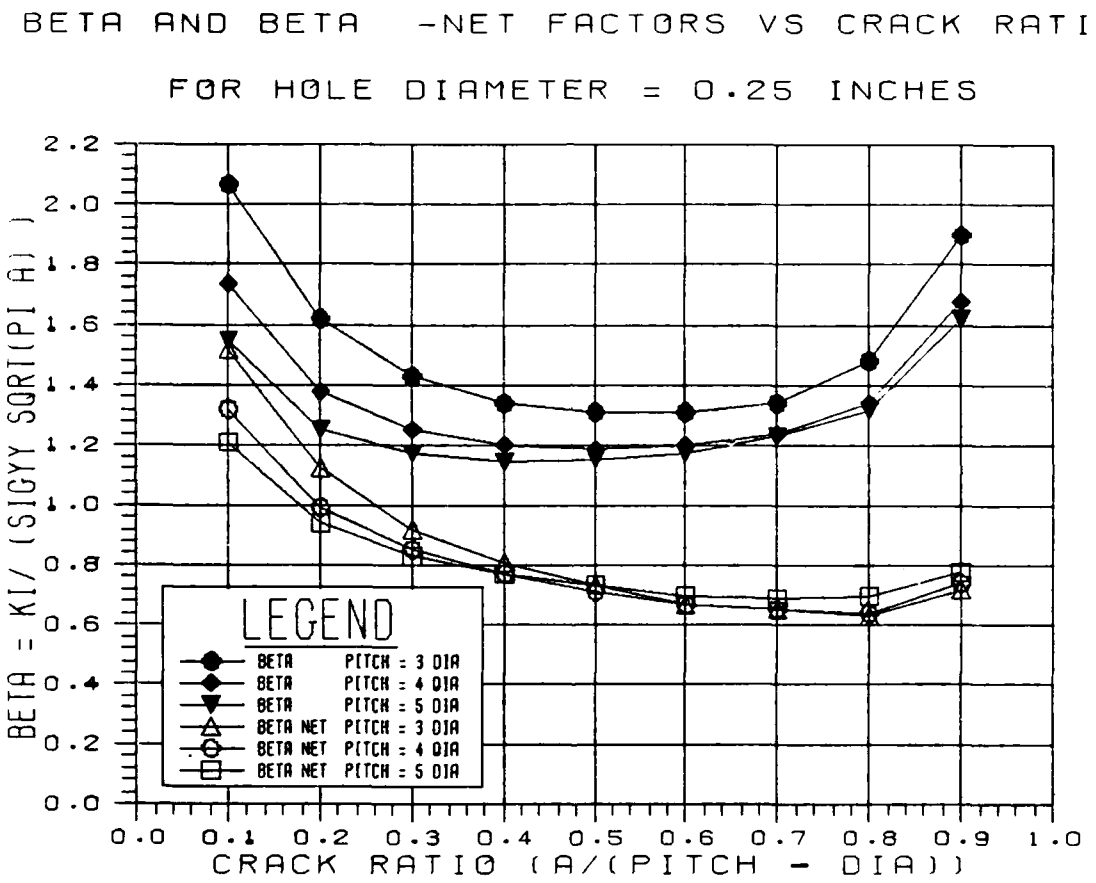

Figure 25. β and β_{net} Factors vs Crack Ratio

above a crack ratio of 0.5 .

It can be seen from Figure 23 that for crack ratios up to 0.5, the effects of the initial hole are dominate, with the influence of the hole decreasing with increased distance from the hole. At a crack ratio of 0.5, the crack begins to approach the second hole and the value of β now increases with the decrease in distance to the second hole. So all of the items of the initial problem can be seen in the final β curves of Figure 23. The first hole is seen in the high initial values of β, with the effects of the hole decreasing with distance. The β value are at a minimum approximately half way between the holes, with the effects of the second hole seen as the β values increasing with the crack tip approaching the second hole. The effects of the edge distances are seen in the "collapse" of the β curves at high pitch and crack ratios. All of this is in addition to the obvious effects of pitch and crack ratio as a function of hole diameter.

Table II. Parametric Study β Factors for Pitch Ratio = 3 Dia

Crack Ratio	$\beta_{dia=0.50}$	$\beta_{dia=0.33}$	$\beta_{dia=0.25}$
.1	2.07	2.07	2.07
.2	1.62	1.62	1.62
.3	1.43	1.43	1.43
.4	1.34	1.34	1.34
.5	1.31	1.31	1.31
.6	1.31	1.31	1.31
.7	1.34	1.35	1.34
.8	1.46	1.46	1.48
.9	1.90	1.90	1.90

Table III. Parametric Study β Factors for Pitch Ratio = 4 Dia

Crack Ratio	$\beta_{dia=0.50}$	$\beta_{dia=0.33}$	$\beta_{dia=0.25}$
.1	1.74	1.74	1.74
.2	1.38	1.37	1.38
.3	1.25	1.25	1.25
.4	1.20	1.20	1.20
.5	1.19	1.19	1.19
.6	1.20	1.20	1.20
.7	1.24	1.25	1.24
.8	1.34	1.35	1.34
.9	1.70	1.73	1.68

Table IV. Parametric Study β Factors for Pitch Ratio = 5 Dia

Crack Ratio	$\beta_{dia=0.50}$	$\beta_{dia=0.33}$	$\beta_{dia=0.25}$
.1	1.55	1.55	1.55
.2	1.26	1.25	1.25
.3	1.17	1.17	1.17
.4	1.14	1.14	1.14
.5	1.15	1.15	1.15
.6	1.18	1.18	1.18
.7	1.23	1.23	1.26
.8	1.32	1.32	1.34
.9	1.58	1.58	1.58

VIII. Parametric Study Application

This section's purpose is to present an example of how the fracture mechanics engineer in the aircraft industry might apply the results of the parametric study undertaken in the last section. The example outlined here is hypothetical and not intended to limit the potential usage of the stress intensity data in the last section.

It will be assumed that there is a requirement for a particular structure, in this case a machined fitting made out of 7075-T6 aluminum plate (with E=10300 KSI, and ν=0.33). The fitting is to have a service life of 500 flight hours. It will be further assumed that the only significant load on the fitting is aircraft pressurization, and therefore the fitting will experience one load cycle per flight. The average flight for this airplane will be one hour.

To establish the Damage Tolerance of this part under current Air Force requirements [7], this analysis will qualify the fitting as being "slow crack growth" structure, and therefore it must be shown that two service lifetimes of slow crack growth exist.

Though fracture mechanics and stress intensity factor calculations are based on theory, fatigue crack growth is empirical. Crack growth for a particular stress cycle is a function of the change in stress intensity and stress ratio (the minimum stress divided by the maximum stress in a cycle)

for a given material. This thesis will not cover the theory of crack growth analysis, nor of material fracture properties. However, it is important for the reader to understand that for a given material, the crack growth increment for a given stress cycle is dependent on the stress intensity at the time of load application.

Many software codes have been written to do fatigue crack growth analysis (CRACKS, CRKGRO, FLAGRO, etc.), and they all share certain traits in common. After input of basic material fracture properties for the material being used, the stress spectrum is input. Then the algorithm to calculate the stress intensity factor throughout the analysis is selected. (The stress intensity factor will vary with the crack length and applied stress) Most crack growth codes have a library of predefined crack stress intensity solutions to choose from. Most codes also allow the user to input a "look-up" table of stress intensity data vs crack length. The look-up data is usually in the form of a β factor, as calculated in the last section. The format of the stress spectrum is usually written as

$$\sigma_{max}, \sigma_{min}, \text{cycles} \qquad (48)$$

where

σ_{max} = maximum stress

σ_{min} = minimum stress

cycles = number of repetitions

The information of equation (48) can be repeated to create layers in a complex stress spectrum. The spectrum applied in this analysis is very simple as it has only one cycle per flight. Stress analysis of the fitting indicated an applied stress of 30 KSI under fully pressurized conditions, with 0 KSI unpressurized. Therefore the stress spectrum for one flight would be

$$\sigma_{max} = 30 \text{ KSI} \qquad (49)$$

$$\sigma_{min} = 0 \text{ KSI}$$

$$\text{cycles} = 1$$

Most engineers attempt to compile a spectrum into a "block" that would represent many flights, and then repeat the block until the service life requirements are met. This analysis defines 100 flights to be a block, therefore one block represents 100 flight hours of life. Two service lives of slow crack growth must be shown before critical crack length is reached. Critical crack length is either loss of a part, or when the crack length grows to a point where the local stress intensity factor for σ_{max} exceeds the material fracture

toughness. (This thesis will also not cover the Air Force residual strength requirements) To achieve two lifetimes of slow crack growth, an assumed initial crack must not grow to critical crack length before 1000 flight hours.

In this example, the fatigue crack growth computer program NASA/FLAGRO [15] was used. This was also the source for the calculations of the Shivakumar solution used in section VII. The built in material fracture data for 7075-T6 aluminum, and a constant spectrum of 0 - 30 KSI was used for all versions of this analysis.

Three approaches were taken in the analysis of the fitting. It was assumed the critical crack location was a through the thickness flaw emerging from a fastener hole, with a geometry as shown in Figure 19. The fitting has 0.25 inch fastener holes with a hole separation (pitch) of four diameters (1.0 inch in this case). The initial flaw sizes are dictated by the Air Force, and vary by type and location. The size is determined by the largest "rogue flaw" that could be induced in the fitting during manufacture, assembly, or service use that could not be detected by routine non-destructive inspections (NDI) with a 90 percent probability of detection, and a 95 percent confidence. It was assumed here that the local NDI was not very good, and that an initial through the thickness crack size of 0.075 inches would be used. This is convenient as this translates into a crack ratio of 0.1 (using the definitions of the previous section).

The fitting was analyzed using three different approaches to the calculation of the stress intensity factor as a function of crack length and applied stresses. The first method used the Bowie solution approach to idealize the fitting as a hole in an infinite plate. The spectrum was applied to the initial flaw and grown to a length of 0.75 inches which represents the length required to "break through" into the second hole. The second method used the Shivakumar solution assuming a row of holes in an infinite plate. This analysis also terminated upon the crack reaching the second hole. The last method involved the β factors derived in the last section. The β factors were placed in a β look-up table as a function of crack length. Stress intensity factors were then calculated for a given crack length, a, and a given applied stress, σ, as follows

$$K_I = \sigma (\pi a)^{1/2} \beta \qquad (50)$$

The results of the three analysis are shown in Figure 26. It can be seen that the Bowie solution method was the least conservative, as it did not consider the second hole, or the tension strip edge effects. The Shivakumar solution method was the second least conservative as it did not consider the finite edge effects. Both the Bowie and Shivakumar methods grew the crack until it reached the second hole. The last method, or "β look-up" table method was the most conservative. The crack did

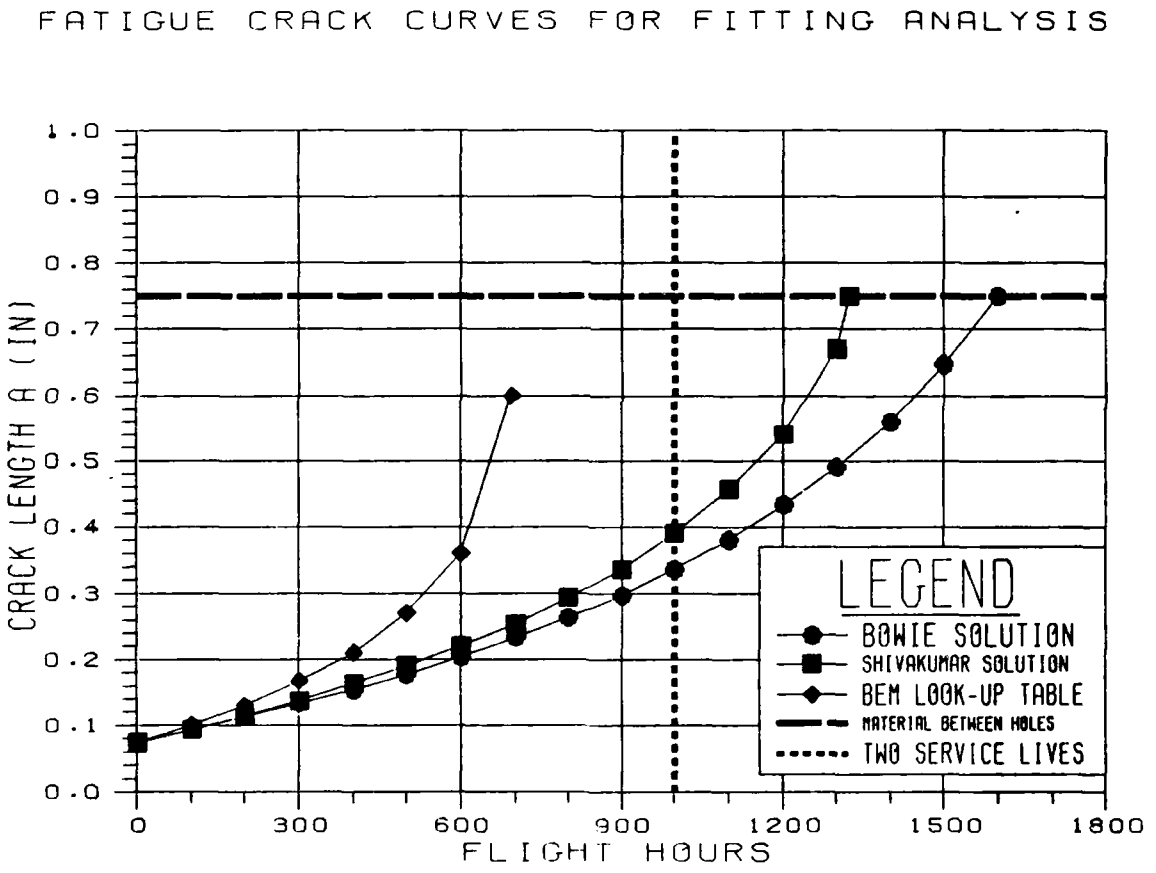

Figure 26. Example Analysis Fatigue Crack Growth Curves

not reach the second hole as the local crack tip stress intensity factor reached the material fracture toughness at a crack length of only 0.66 inches. The β look-up method also was the only one unable to show 1000 hours of slow crack growth, thus not meeting the design requirements.

From this simple example, it can be seen how detailed analysis through the β look-up table method enables an engineer to analyze detailed geometry beyond the scope of the common K_I solutions found in most fatigue crack codes. In this case, it would have been unconservative to ignore the effects of the second hole, and the edge effects. The output from the NASA/FLAGRO program are included in Appendix E.

IX. Conclusions

Application of the Boundary Element Method to structures problems is just beginning to become popular in the aircraft industry. Traditional Finite Element Methods are still the predominate technique used. However, the Finite Element Method is expensive in both manpower and computer costs, and cost saving alternatives are always being sought.

The Fictitious Stress Method, presented in this thesis, is shown to correlate well with both analytical and FEM solutions. The BEM was shown to work well for the parametric study of Section VII. A complicated fracture mechanics problem with no analytical solution was solved for various geometry, with the results displayed as a family of β-curves in Figure 23. These curves in themselves are important as they represent useful Stress Intensity Factor correction factors for the various geometric configurations analyzed in Section VII.

It has been shown herein that BEM is an acceptable method for fracture mechanics analysis and can be used in fatigue crack growth predictions for Air Force Durability and Damage Tolerance Analysis (DADTA). The analysis in Section VIII shows how easily the results of the BEM work in Section VII could be applied to a "real" design problem and prevent unconservative structural life predictions.

One possible source for additional work is in the area of FEM and BEM combined in a single solution. This might prove to be the best of both worlds with a fine grid FEM model near the crack tip, and a coarse BEM definition of the external boundaries of a problem. Additional study should be done to see if the BEM/FEM combined analysis offers advantages in actual applications to each method used separately.

The question of increased efficiency is a more difficult one. Though dramatic reductions in degrees of freedom are shown for comparable accuracy of analysis, final CPU time is not always improved. Since the CPU time is proportional to the square of the Root Mean Square (RMS) number of active columns multiplied by the total degrees of freedom (DOF), the BEM would have a CPU time advantage for smaller problems where the DOF factor would dominate the squared RMS term. This indicates that the BEM is computationally more efficient for problems up to a certain size. Even at problem sizes of 13858 DOF the BEM still has a CPU time advantage of 1.7 (reference Section III).

It should also be noted that the BEM program used in this thesis utilized only single precision accuracy which on the VAX computer provides six significant digits. This helped improve the BEM computer efficiency and still obtain the excellent correlation to the FEM and analytical results documented in this thesis.

It is therefore concluded that for the structural fracture mechanics problems analyzed in this thesis, the BEM accurately derived Stress Intensity Factors for fracture analysis, and produced a minimum computational efficiency improvement of 1.7 over traditional FEM.

Appendix A: Computer Implementation

The source for the computer program used in this study was a FORTRAN program, TWOFS, for the fictitious stress boundary element method published by Crouch and Starfield [4]. The version used in this study was converted to the Microsoft BASIC computer language for ease of implementation on PC class computers. Upon initiation of actual calculations, it was decided to port the program up to a Digital VAX computer for speed purposes, so limited code changes were made to run under VAX BASIC 3.1. Additional small changes were made to facilitate post processing by outputting desired calculations to an external file. The VAX Basic version of TWOFS was labeled TWOFS99. The final work was done on a Digital VAX 8800 running the VMS (V4.7) operating system. The average BEM model consisting of 300 elements (600 by 600 matrix of influence coefficients) took approximately 25 minutes of CPU time. The CPU comparisons made to the MSC/NASTRAN finite element program were done on a Digital VAX 8350 computer as it was the only machine set up to run NASTRAN.

The flow of the program TWOFS99 is identical to the original FORTRAN TWOFS code. The sizes of the matrices were increased to allow larger problems. The TWOFS99 input was modified to allow for the BEM model to be read from a disk

file. This was particularly important as the final tension strip parametric analysis required over one hundred models to be built, run and analyzed. The models were constructed by an independent VAX Basic program, CHOLE, and written to disk in the format required by TWOFS99. Aside from the normal TWOFS output, which was also written to a disk file, a third file was created by TWOFS99 of unlabeled final stress results. A third VAX Basic computer program, TWOFS99_EX, extracted necessary stress data from the post processing file created by TWOFS99 and computed a value for the stress intensity factor based on a regression fit technique. This allowed for a great degree of mechanization in the analysis process.

A. Fictitious Stress Method Program (*TWOFS99*)

The input file for TWOFS99 defines the geometry of the problem, along with the necessary boundary conditions. The program first reads in values for NUMBS, NUMOS, KSYM, PR and E. NUMBS defines the number of straight line segments which will be input. NUMOS defines the number of additional segments to establish data points for displacement and stress calculations within the body to be analyzed. KSYM is a code to take advantage of any lines of symmetry in a model by calculating image elements as mirrored across the line of symmetry so that their effects are included in the final results. KSYM equal to one implies no symmetry exists, which

was used primarily in this study. KSYM equal to two implies symmetry about the y axis at a line x=XSYM. KSYM equal to three implies symmetry about the x axis at a line y=YSYM. And KSYM equal to four implies two axis of symmetry about x=XSYM, y=YSYM. If symmetry is requested, the value of XSYM and, or YSYM is input. PR is the Poison's Ratio and E is the Young's Modulus for the material for the problem. The field stresses are next input as PXX, PYY and PXY. All input must be in consistent units. All input is echoed in the output file.

At line 460 in the code, a loop is entered from 1 to NUMBS. For each iteration of the loop, values for ZNUM, XBEG, YBEG, XEND, YEND, KODE, BVS and BVN are input. XBEG, YBEG, XEND and YEND define the x and y co-ordinates for the beginning and end of the current line segment. ZNUM subdivides the current line segment into that many equal length boundary element segments. BVS and BVN are the boundary conditions for all of the boundary elements defined for the current line segment, in the shear and normal local co-ordinates of the elements respectively. KODE defines if BVS and BVN are displacement or stress boundary conditions. Remember, it is allowable to mix them as indicated in [4]. KODE equal to one means both are stresses, two means both are displacements, three means a shear displacement with a normal stress, and four is a shear stress with a normal displacement. Upon completion of the loop, all input of the

data for the definition of the boundary elements and boundary conditions is completed.

At line 690 in the code, a similar loop is entered from 1 to NUMOS. Here the variables EXTERNL(N,i), i=1 to 4, and NUMMTX(N) are read. The data for the interior points are stored in matrices to facilitate changes made to output formats. In order,the XBEG, YBEG, XEND, YEND, and NUMPD are input and placed in the EXTERNL and NUMMTX arrays. XBEG, YBEG, XEND and YEND are as for the boundary element line segment definitions. NUMPD defines the number of straight equally spaced points between and including XBEG, YBEG, XEND, YEND to be included for displacement and stress calculations after the fictitious stresses are solved for.

Lines 1250 through 2000 make various calls to subroutines to calculate the influence coefficients for all of the boundary elements, and assembles them into a matrix C. Line 2020 calls a Gauss Elimination subroutine to solve for the fictitious stresses which are stored in the matrix P. Line 2100 enters a loop to calculate the unknown boundary conditions at all of the boundary element midpoints. And, finally, line 3060 is a loop to calculate influence coefficients and the resulting stresses and displacements at all of the interior data points.

Line 2920 begins a loop to store all stresses computed at boundary element midpoints, along with the x value of the element midpoint. This data is written to a disk

file for post processing in line 2965. The program TWOFS99 is listed in Appendix B.

B. Boundary Element Generation (CHOLE)

This program was written specifically for the two hole tension strip analysis. The boundary conditions for the study were incorporated into the program. The user inputs a problem title, hole diameter, hole spacing and crack length. The program divides the crack length into boundary elements using the F.R. Harris refinement technique [8], and then creates elements to model the remainder of the tension strip boundary. The final result is a disk file in the format required by TWOFS99 for analysis. The program CHOLE is listed in Appendix D.

C. Stress Intensity Factor Calculation (TWOFS99 EX)

The assumptions used are to calculate the stress intensity factor for a given problem by using the tension stresses, σ, normal to the line of the crack. The value of the stress intensity factor is calculated with the tension stresses with the equation

$$K_I = \sigma (2\pi r)^{1/2} \qquad (42)$$

file for post processing in line 2965. The program TWOFS99 is listed in Appendix B.

B. Boundary Element Generation (CHOLE)

This program was written specifically for the two hole tension strip analysis. The boundary conditions for the study were incorporated into the program. The user inputs a problem title, hole diameter, hole spacing and crack length. The program divides the crack length into boundary elements using the F.R. Harris refinement technique [8], and then creates elements to model the remainder of the tension strip boundary. The final result is a disk file in the format required by TWOFS99 for analysis. The program *CHOLE* is listed in Appendix D.

C. Stress Intensity Factor Calculation (TWOFS99 EX)

The assumptions used are to calculate the stress intensity factor for a given problem by using the tension stresses, σ, normal to the line of the crack. The value of the stress intensity factor is calculated with the tension stresses with the equation

$$K_I = \sigma (2\pi r)^{1/2} \qquad (42)$$

All of the tension strip parametric study results were processed through TWOFS99_EX for K_I calculations, and the results presented in that section of this report. The program TWOFS99_EX is listed in Appendix C.

Appendix B: Computer Program TWOFS99

This appendix contains the listings of the computer program used for the boundary element analysis in this thesis. The boundary element analysis program TWOFS99 was basically extracted from Crouch and Starfield (Reference [4]) with changes to output a post processing file for TWOFS99_EX to do regression analysis for K_I predictions. The source document program was written in FORTRAN, and that was converted into BASIC. Also, the data matrix limits were raised to analyze larger problems. The program TWOFS99 was compiled under VAX BASIC 3.1 .

```
10 REM  BOUNDARY ELEMENT PROGRAM TWOFS 5 OCT 85
20 REM  MODIFIED FOR LARGE MODELS FOR VAX
30   REM
32    DIM C(600,600),B(600),P(600)
40    DIM XM(300),YM(300),A(300),
        COSBET(300),SINBET(300),KOD(300)
50    DIM EXTRNL(300,4),NUMMTX(300),OUTPT(300,10)
60    REM
70    REM PRINT"*****************************************"
80    REM PRINT" "
90    REM PRINT"   BOUNDARY ELEMENT PROGRAM   "
100   REM PRINT" "
110   REM PRINT"*****************************************"
120   REM PRINT" "
130   REM PRINT" "
132 REM INPUT "ENTER INPUT FILE NAME ",QIN$
134 REM INPUT "ENTER OUTPUT FILE  NAME ",QOUT$
136 OPEN "QIN" FOR INPUT AS #1
138 OPEN "QOUT" FOR OUTPUT AS #2
139 OPEN "QMAT" FOR OUTPUT AS #3
140   INPUT #1,TITLE$
150   INPUT #1,NUMBS,NUMOS,KSYM,PR,E
160   IF KSYM=1 THEN GOTO  200
170   IF KSYM=2 THEN GOTO  210
180   IF KSYM=3 THEN GOTO  240
190   IF KSYM=4 THEN GOTO  260
```

```
200   GOTO  300
210   INPUT #1,XSYM
220    GOTO  300
240      INPUT #1,YSYM
250      GOTO  300
260       INPUT #1,XSYM
280      INPUT #1,YSYM
290     REM
300    REM
310      INPUT #1,PXX
320      INPUT #1,PYY
330      INPUT #1,PXY
340     REM
360      CNST=1.0/(4.0*PI*(1.0-PR))
370      COND=(1.0+PR)/E
380      PR1=1.0-2.0*PR
390      PR2=2.0*(1.0-PR)
400      PR3=3.0-4.0*PR
410     REM
415 REM PRINT" "
420    REM PRINT"  DEFINE LOCATIONS, SIZES, ORIENTATIONS AND
             BOUNDARY CONDITIONS "
430   REM PRINT"  OF BOUNDARY ELEMENTS "
435 REM PRINT" "
440     REM
450      NUMBE=0
460      FOR N=1 TO NUMBS
470      INPUT #1,ZNUM,XBEG,YBEG,XEND,YEND,KODE,BVS,BVN
480      XD=(XEND-XBEG)/ZNUM
490      YD=(YEND-YBEG)/ZNUM
500      SW=SQR(XD*XD+YD*YD)
510     REM
520    FOR NE=1 TO ZNUM
530      NUMBE=NUMBE+1
540      M=NUMBE
550      XM(M)=XBEG+.5*(2.0*NE-1.0)*XD
560      YM(M)=YBEG+.5*(2.0*NE-1.0)*YD
570      A(M)=.5*SW
580      SINBET(M)=YD/SW
590      COSBET(M)=XD/SW
600      KOD(M)=KODE
610      MN=2*M
620      MS=MN-1
630      B(MS)=BVS
640      B(MN)=BVN
650 NEXT NE
655 NEXT N
660 REM PRINT" "
670 REM PRINT" INPUT OF EXTERNAL ELEMENTS"
680 REM PRINT" "
690     FOR N=1 TO NUMOS
700 INPUT#1,EXTRNL(N,1),EXTRNL(N,2),
```

```
        EXTRNL(N,3),EXTRNL(N,4),NUMMTX(N)
710     NEXT N
720      PRINT #2,TITLE$
730      PRINT #2, "NUMBER OF STRAIGHT LINE SEGMENTS TO DEFINE
         BOUNDARY ",NUMBS
740      PRINT #2,"NUMBER OF NON BOUNDARY POINTS TO CALCULATE
         RESULTS AT ",NUMOS
750   IF KSYM=1 THEN GOTO  780
760   IF KSYM=2 THEN GOTO  800
770   IF KSYM=3 THEN GOTO  820 ELSE GOTO  840
780     PRINT #2," " \ PRINT #2,"NO SYMMETRY CONDITIONS
         IMPOSED"
790       GOTO  850
800     PRINT #2," " \ PRINT #2,"THE LINE X = XS = ";XSYM;" IS
         A LINE OF SYMMETRY"
810       GOTO  850
820     PRINT #2," " \ PRINT #2,"THE LINE Y = YS = ";YSYM;" IS
         A LINE OF SYMMETRY"
830       GOTO  850
840     PRINT #2," " \ PRINT #2,"THE LINES X = XS = ";XSYM;"
         AND Y = YS = ";YSYM;" ARE LINES OF SYMMETRY"
850    REM
860 PRINT #2," " \ PRINT #2,"POISSON'S RATIO = ";PR
870 PRINT #2," YOUNG'S MODULUS = ";E
880 PRINT #2," " \ PRINT #2,"XX-COMPONENT OF FIELD STRESS =
        ";PXX
890 PRINT #2,"YY-COMPONENT OF FILED STRESS = ";PYY
900 PRINT #2,"XY-COMPONENT OF FIELD STRESS = ";PXY
910 PRINT #2," "
920 PRINT #2,"BOUNDARY ELEMENT DATA" \ PRINT #2," "
930 PRINT #2,"ELEMENT","KODE","X CENTER","Y CENTER"
940 FOR I=1 TO NUMBE
950  PRINT #2,I,KOD(I),XM(I),YM(I)
960 NEXT I
970 PRINT #2," "
980 PRINT #2,"ELEMENT","LENGTH","ANGLE","US OR SIGMA-S","UN
       OR SIGMA-N"
990 FOR M=1 TO NUMBE
1000    MSIZE=2.0*A(M)
1005   IF COSBET(M)=0.0 AND SINBET(M)>0.0 THEN ANGLE=90 \ GOTO
1020
1007   IF COSBET(M)=0.0 AND SINBET(M)<0.0 THEN ANGLE=270 \
         GOTO 1020
1010   ANGLE=180 * ATN(SINBET(M)/COSBET(M))/PI
1015 IF ANGLE<0 THEN ANGLE=ANGLE+180
1020       PRINT #2,M,MSIZE,ANGLE,B(2*M-1),B(2*M)
1030 NEXT M
1040 REM PRINT" "
1050     REM PRINT" ADJUST STRESS BOUNDARY VALUES TO ACCOUNT
         FOR INITIAL STRESSES "
1060 REM PRINT" "
1070     FOR N=1 TO NUMBE
```

```
1080       NN=2*N
1090       NS=NN-1
1100       COSB=COSBET(N)
1110       SINB=SINBET(N)
1120       SIGS=(PYY-PXX)*SINB*COSB+PXY*(COSB*COSB-SINB*SINB)
1130       SIGN=PXX*SINB*SINB-2.0*PXY*SINB*COSB+PYY*COSB*COSB
1140      IF KOD(N)=1 THEN GOTO 1170
1150      IF KOD(N)=2 THEN GOTO 1240
1160     IF KOD(N)=3 THEN GOTO  1200 ELSE GOTO  1230
1170    B(NS)=B(NS)-SIGS
1180       B(NN)=B(NN)-SIGN
1190     GOTO  1240
1200    REM
1210       B(NN)=B(NN)-SIGN
1220       GOTO 1240
1230    B(NS)=B(NS)-SIGS
1240    NEXT N
1250 REM PRINT" "
1260 REM PRINT"COMPUTE INFLUENCE COEFFICIENTS AND SET UP
        SYSTEM OF ALGEBRAIC EQUATIONS"
1270 REM PRINT" "
1280      REM
1290 FOR I=1 TO NUMBE
1295 REM PRINT" " \ REM PRINT" FOR ELEMENT ";I
1300       IN=2*I
1310       IS=IN-1
1320       XI=XM(I)
1330       YI=YM(I)
1340       COSBI=COSBET(I)
1350       SINBI=SINBET(I)
1360       KODE=KOD(I)
1370      REM
1380   FOR J=1 TO NUMBE
1390       JN=2*J
1400       JS=JN-1
1410    REM   CALL INITL
1415   GOSUB 10000
1420       XJ=XM(J)
1430       YJ=YM(J)
1440       COSBJ=COSBET(J)
1450       SINBJ=SINBET(J)
1460       AJ=A(J)
1470   REM       CALL COEFF(XI,YI,XJ,YJ,AJ,COSBJ,SINBJ,+1)
1480 QXI=XI \ QYI=YI \ QXJ=XJ \ QYJ=YJ \ QAJ=AJ \ QCOS=COSBJ
1490 QSIN=SINBJ \ QQ=1
1500   GOSUB 15000
1510 IF KSYM=1 THEN GOTO  1690
1520 IF KSYM=2 THEN GOTO  1550
1530 IF KSYM=3 THEN GOTO  1580 ELSE GOTO  1610
1540      REM
1550   XJ=2.0*XSYM-XM(J)
1560   REM    CALL COEFF(XI,YI,XJ,YJ,AJ,COSBJ,-SINBJ,-1)
```

```
1562  QXI=XI \ QYI=YI \ QXJ=XJ \ QYJ=YJ \ QAJ=AJ \ QCOS=COSBJ
1564  QSIN=-SINBJ \ QQ=-1 \ GOSUB 15000
1570      GOTO 1690
1580   YJ=2.0*YSYM-YM(J)
1590  REM     CALL COEFF(XI,YI,XJ,YJ,AJ,-COSBJ,SINBJ,-1)
1592 QXI=XI \ QYI=YI \ QXJ=XJ \ QYJ=YJ \ QAJ=AJ \ QCOS=-COSBJ
1594 QSIN=SINBJ \ QQ=-1 \ GOSUB 15000
1600      GOTO 1690
1610   XJ=2.0*XSYM-XM(J)
1620   REM    CALL COEFF(XI,YI,XJ,YJ,AJ,COSBJ,-SINBJ,-1)
1622  QXI=XI \ QYI=YI \ QXJ=XJ \ QYJ=YJ \ QAJ=AJ \ QCOS=COSBJ
1624  QSIN=-SINBJ \ QQ=-1 \ GOSUB 15000
1630      XJ=XM(J)
1640      YJ=2.0*YSYM-YM(J)
1650  REM     CALL COEFF(XI,YI,XJ,YJ,AJ,-COSBJ,SINBJ,-1)
1652  QXI=XI \ QYI=YI \ QXJ=XJ \ QYJ=YJ \ QAJ=AJ \
        QCOS=-COSBJ
1654  QSIN=SINBJ \ QQ=-1 \ GOSUB 15000
1660      XJ=2.0*XSYM-XM(J)
1670  REM     CALL COEFF(XI,YI,XJ,YJ,AJ,-COSBJ,-SINBJ,+1)
1672  QXI=XI \ QYI=YI \ QXJ=XJ \ QYJ=YJ \ QAJ=AJ \
        QCOS=-COSBJ
1674  QSIN=-SINBJ \ QQ=1 \ GOSUB 15000
1680     REM
1690   REM
1700   IF KODE=1 THEN GOTO  1740
1710   IF KODE=2 THEN GOTO  1800
1720   IF KODE=3 THEN GOTO  1860 ELSE GOTO  1920
1730     REM
1740 C(IS,JS)=(SYYS-SXXS)*SINBI*COSBI
       +SXYS*(COSBI*COSBI-SINBI*SINBI)
1750     C(IS,JN)=(SYYN-SXXN)*SINBI*COSBI
       +SXYN*(COSBI*COSBI-SINBI*SINBI)
1760     C(IN,JS)=SXXS*SINBI*SINBI
       -2.0*SXYS*SINBI*COSBI+SYYS*COSBI*COSBI
1770     C(IN,JN)=SXXN*SINBI*SINBI
       -2.0*SXYN*SINBI*COSBI+SYYN*COSBI*COSBI
1780      GOTO 1970
1790     REM
1800   C(IS,JS)=UXS*COSBI+UYS*SINBI
1810      C(IS,JN)=UXN*COSBI+UYN*SINBI
1820      C(IN,JS)=-UXS*SINBI+UYS*COSBI
1830      C(IN,JN)=-UXN*SINBI+UYN*COSBI
1840      GOTO 1970
1850     REM
1860    C(IS,JS)=UXS*COSBI+UYS*SINBI
1870      C(IS,JN)=UXN*COSBI+UYN*SINBI
1880     C(IN,JS)=SXXS*SINBI*SINBI
       -2.0*SXYS*SINBI*COSBI+SYYS*COSBI*COSBI
1890     C(IN,JN)=SXXN*SINBI*SINBI
       -2.0*SXYN*SINBI*COSBI+SYYN*COSBI*COSBI
1900      GOTO 1970
```

```
1910      REM
1920   C(IS,JS)=(SYYS-SXXS)*SINBI*COSBI
         +SXYS*(COSBI*COSBI-SINBI*SINBI)
1930      C(IS,JN)=(SYYN-SXXN)*SINBI*COSBI
         +SXYN*(COSBI*COSBI-SINBI*SINBI)
1940       C(IN,JS)=-UXS*SINBI+UYS*COSBI
1950       C(IN,JN)=-UXN*SINBI+UYN*COSBI
1970 NEXT J
1975 NEXT I
1980 REM PRINT" "
1990     REM PRINT"   SOLVE SYSTEM OF ALGEBRAIC EQUATIONS "
2000 REM PRINT" "
2010       N=2*NUMBE
2020   REM       CALL SOLVE(N)
2030   GOSUB 20000
2040 REM PRINT" "
2050     REM PRINT"   COMPUTE BOUNDARY DISPLACEMENTS AND
         STRESSES "
2060 REM PRINT" "
2069 PRINT #2," "
2070 PRINT #2,"  DISPLACEMENTS AND STRESSES AT BOUNDARY
         ELEMENT MIDPOINTS"
2080 PRINT #2," "
2090   PRINT #2,"ELEMENT","UX","UY","US","UN"
2092 PRINT #2,"SIGXX       SIGYY        SIGXY        SIGS
         SIGN         SIGT"
2100   FOR I=1 TO NUMBE
2110       XI=XM(I)
2120       YI=YM(I)
2130       COSBI=COSBET(I)
2140       SINBI=SINBET(I)
2150      REM
2160       UX=0.0
2170       UY=0.0
2180       SIGXX=PXX
2190       SIGYY=PYY
2200       SIGXY=PXY
2210      REM
2220    FOR J=1 TO NUMBE
2230       JN=2*J
2240       JS=JN-1
2250 REM       CALL INITL
2260   GOSUB 10000
2270       XJ=XM(J)
2280       YJ=YM(J)
2290       AJ=A(J)
2300       COSBJ=COSBET(J)
2310       SINBJ=SINBET(J)
2320 REM       CALL COEFF(XI,YI,XJ,YJ,AJ,COSBJ,SINBJ,+1)
2330 QXI=XI \ QYI=YI \ QXJ=XJ \ QYJ=YJ \ QAJ=AJ \ QCOS=COSBJ
2340 QSIN=SINBJ \ QQ=1 \ GOSUB 15000
2350   IF KSYM=1 THEN GOTO  2650
```

```
2360    IF KSYM=2 THEN GOTO  2390
2370   IF KSYM=3 THEN GOTO  2450  ELSE GOTO  2510
2380      REM
2390    XJ=2.0*XSYM-XM(J)
2400 REM       CALL COEFF(XI,YI,XJ,YJ,AJ,COSBJ,-SINBJ,-1)
2410  QXI=XI \ QYI=YI \ QXJ=XJ \ QYJ=YJ \ QAJ=AJ \ QCOS=COSBJ
2420  QSIN=-SINBJ \ QQ=-1 \ GOSUB 15000
2430       GOTO 2650
2440      REM
2450    YJ=2.0*YSYM-YM(J)
2460 REM       CALL COEFF(XI,YI,XJ,YJ,AJ,-COSBJ,SINBJ,-1)
2470  QXI=XI \ QYI=YI \ QXJ=XJ \ QYJ=YJ \ QAJ=AJ \
        QCOS=-COSBJ
2480  QSIN=SINBJ \ QQ=-1 \ QQ=-1 \ GOSUB 15000
2490       GOTO 2650
2500      REM
2510     XJ=2.0*XSYM-XM(J)
2520 REM       CALL COEFF(XI,YI,XJ,YJ,AJ,COSBJ,-SINBJ,-1)
2530 QXI=XI \ QYI=YI \ QXJ=XJ \ QYJ=YJ \ QAJ=AJ \ QCOS=COSBJ
2540 QSIN=-SINBJ \ QQ=-1 \ GOSUB 15000
2550       XJ=XM(J)
2560       YJ=2.0*YSYM-YM(J)
2570 REM       CALL COEFF(XI,YI,XJ,YJ,AJ,-COSBJ,SINBJ,-1)
2580 QXI=XI \ QYI=YI \ QXJ=XJ \ QYJ=YJ \ QAJ=AJ \ QCOS=-COSBJ
2590 QSIN=SINBJ \ QQ=-1 \ GOSUB 15000
2600       XJ=2.0*XSYM-XM(J)
2610 REM       CALL COEFF(XI,YI,XJ,YJ,AJ,-COSBJ,-SINBJ,+1)
2620  QXI=XI \ QYI=YI \ QXJ=XJ \ QYJ=YJ \ QAJ=AJ \
        QCOS=-COSBJ
2630 QSIN=-SINBJ \ QQ=1 \ GOSUB 15000
2640      REM
2650     REM
2660      REM
2670       UX=UX+UXS*P(JS)+UXN*P(JN)
2680       UY=UY+UYS*P(JS)+UYN*P(JN)
2690       SIGXX=SIGXX+SXXS*P(JS)+SXXN*P(JN)
2700       SIGYY=SIGYY+SYYS*P(JS)+SYYN*P(JN)
2710       SIGXY=SIGXY+SXYS*P(JS)+SXYN*P(JN)
2720      REM
2730  NEXT J
2740      REM
2750       US=UX*COSBI+UY*SINBI
2760       UN=-1.0*UX*SINBI+UY*COSBI
2770      SIGS=(SIGYY-SIGXX)*SINBI*COSBI
         +SIGXY*(COSBI*COSBI-SINBI*SINBI)
2780      SIGN=SIGXX*SINBI*SINBI
         -2.0*SIGXY*SINBI*COSBI+SIGYY*COSBI*COSBI
2790      SIGT=SIGXX*COSBI*COSBI
         +2.0*SIGXY*SINBI*COSBI+SIGYY*SINBI*SINBI
2800      REM
2810  OUTPT(I,1)=UX
2820  OUTPT(I,2)=UY
```

```
2830 OUTPT(I,3)=US
2840 OUTPT(I,4)=UN
2850 OUTPT(I,5)=SIGXX
2860 OUTPT(I,6)=SIGYY
2870 OUTPT(I,7)=SIGXY
2880 OUTPT(I,8)=SIGS
2890 OUTPT(I,9)=SIGN
2900 OUTPT(I,10)=SIGT
2905 REM PRINT"OUTPUT FOR ELEMENT ";I;" COMPLETE"
2910  NEXT I
2912 A$="#.###^^^^    " \ A$=A$+A$+A$+A$+A$+A$
2920 FOR I=1 TO NUMBE
2930  PRINT #2,I,OUTPT(I,1),OUTPT(I,2),OUTPT(I,3),OUTPT(I,4)
2935 PRINT #2 USING A$;OUTPT(I,5),OUTPT(I,6),OUTPT(I,7),
       OUTPT(I,8),OUTPT(I,9),OUTPT(I,10)
2936 PRINT #2, " "
2940 NEXT I
2950 REM  THIS IS THE BEM ELEMENT DISP-STRESS MATRIX OUTPT TO
       FILE
2960 MAT PRINT #3 , OUTPT
2965 MAT PRINT #3 , XM   \ CLOSE #3
2990 REM PRINT" "
3000 REM PRINT"   COMPUTE DISPLACEMENTS AND STRESSES AT
       SPECIFIED POINTS IN THE BODY"
3010 REM PRINT" "
3020       IF NUMOS <= 0 THEN GOTO  3910
3030   PRINT #2," " \ PRINT #2," "
3040  PRINT #2," DISPLACEMENTS AND STRESSES AT SPECIFIED
       POINTS IN THE BODY"
3042 PRINT #2," " \ PRINT #2,"POINT","X COORD","Y
       COORD","UX","UY"
3045 PRINT #2,"   ","SIGXX","SIGYY","SIGXY" \ PRINT #2," "
3050        NPOINT=0
3060  FOR N=1 TO NUMOS
3070       XBEG=EXTRNL(N,1)
3080       YBEG=EXTRNL(N,2)
3090       XEND=EXTRNL(N,3)
3100       YEND=EXTRNL(N,4)
3110       NUMPB=NUMMTX(N)
3120       NUMP=NUMPB+1
3130       DELX=(XEND-XBEG)/NUMP
3140       DELY=(YEND-YBEG)/NUMP
3150       IF NUMPB > 0 THEN NUMP=NUMP+1
3160       IF (DELX^2+DELY^2) = 0 THEN NUMP=1
3170      REM
3180  FOR NI=1 TO NUMP
3190       XP=XBEG+(NI-1)*DELX
3200       YP=YBEG+(NI-1)*DELY
3210      REM
3220       UX=0.0
3230       UY=0.0
3240       SIGXX=PXX
```

```
3250       SIGYY=PYY
3260       SIGXY=PXY
3270      REM
3280 FOR J=1 TO NUMBE
3290       JN=2*J
3300       JS=JN-1
3310  REM       CALL INITL
3320 GOSUP 10000
3330       XJ=XM(J)
3340       YJ=YM(J)
3350       AJ=A(J)
3360      REM
3370       IF SQR((XP-XJ)^2+(YP-YJ)^2) < (2.0*AJ) THEN GOTO
3880
3380      REM
3390       COSBJ=COSBET(J)
3400       SINBJ=SINBET(J)
3410  REM       CALL COEFF(XP,YP,XJ,YJ,AJ,COSBJ,SINBJ,+1)
3420  QXI=XP \ QYI=YP \ QXJ=XJ \ QYJ=YJ \ QAJ=AJ \ QCOS=COSBJ
3430  QSIN=SINBJ \ QQ=1 \ GOSUB 15000
3440  REM       GOTO (840,810,820,830),KSYM
3450 IF KSYM=1 THEN GOTO  3750
3460 IF KSYM=2 THEN GOTO  3490
3470 IF KSYM=3 THEN GOTO  3550 ELSE GOTO  3610
3480      REM
3490    XJ=2.0*XSYM-XM(J)
3500 REM       CALL COEFF(XP,YP,XJ,YJ,AJ,COSBJ,-SINBJ,-1)
3510 QXI=XP \ QYI=YP \ QXJ=XJ \ QYJ=YJ \ QAJ=AJ \ QCOS=COSBJ
3520 QSIN=-SINBJ \ QQ=-1 \ GOSUB 15000
3530       GOTO 3750
3540      REM
3550     YJ=2.0*XSYM-YM(J)
3560 REM       CALL COEFF(XP,YP,XJ,YJ,AJ,-COSBJ,SINBJ,-1)
3570 QXI=XP \ QYI=YP \ QXJ=XJ \ QYJ=YJ \ QAJ=AJ \ QCOS=-COSBJ
3580 QSIN=SINBJ \ QQ=-1 \ GOSUB 15000
3590       GOTO 3750
3600      REM
3610     XJ=2.0*XSYM-XM(J)
3620 REM       CALL COEFF(XP,YP,XJ,YJ,AJ,COSBJ,-SINBJ,-1)
3630 QXI=XP \ QYI=YP \ QXJ=XJ \ QYJ=YJ \ QAJ=AJ \ QCOS=COSBJ
3640 QSIN=-SINBJ \ QQ=-1 \ GOSUB 15000
3650       XJ=XM(J)
3660       YJ=2.0*YSYM-YM(J)
3670 REM      CALL COEFF(XP,YP,XJ,YJ,AJ,-COSBJ,SINBJ,-1)
3680 QXI=XP \ QYI=YP \ QXJ=XJ \ QYJ=YJ \ QAJ=AJ \ QCOS=-COSBJ
3690 QSIN=SINBJ \ QQ=-1 \ GOSUB 15000
3700       XJ=2.0*XSYM-XM(J)
3710 REM       CALL COEFF(XP,YP,XJ,YJ,AJ,-COSBJ,-SINBJ,+1)
3720 QXI=XP \ QYI=YP \ QXJ=XJ \ QYJ=YJ \ QAJ=AJ \ QCOS=-COSBJ
3730 QSIN=-SINBJ \ QQ=1 \ GOSUB 15000
3740      REM
3750     REM
```

```
3760      REM
3770       UX=UX+UXS*P(JS)+UXN*P(JN)
3780       UY=UY+UYS*P(JS)+UYN*P(JN)
3790       SIGXX=SIGXX+SXXS*P(JS)+SXXN*P(JN)
3800       SIGYY=SIGYY+SYYS*P(JS)+SYYN*P(JN)
3810       SIGXY=SIGXY+SXYS*P(JS)+SXYN*P(JN)
3820      REM
3830     NEXT J
3840      REM
3850       NPOINT=NPOINT+1
3860       PRINT #2,NPOINT,XP,YP,UX,UY \  PRINT #2,"
         ",SIGXX,SIGYY,SIGXY
3870      REM
3880    NEXT NI
3890    NEXT N
3900      REM
3910    REM
3920      REM
4000     GOTO 25000
10000    REM       SUBROUTINE INITL
10010     REM
10020       SXXS=0.0
10030       SXXN=0.0
10040       SYYS=0.0
10050       SYYN=0.0
10060       SXYS=0.0
10070       SXYS=0.0
10080       SXYN=0.0
10090      REM
10100       UXS=0.0
10110       UXN=0.0
10120       UYS=0.0
10130       UYN=0.0
10140      REM
10150       RETURN
15000 REM       SUBROUTINE COEFF(X,Y,CX,CY,A,COSB,SINB,MSYM)
15010     REM
15020    X=QXI \ Y=QYI \ CX=QXJ \ CY=QYJ \ A=QAJ \ COSB=QCOS
15030    SINB=QSIN \ MSYM=QQ
15040      REM
15050       COS2B=COSB*COSB-SINB*SINB
15060       SIN2B=2.0*SINB*COSB
15070      REM
15080       XB=(X-CX)*COSB+(Y-CY)*SINB
15090       YB=-1.0*(X-CX)*SINB+(Y-CY)*COSB
15100      REM
15110       R1S=(XB-A)*(XB-A)+YB*YB
15120       R2S=(XB+A)*(XB+A)+YB*YB
15130       FL1=.5*LOG(R1S)
15140       FL2=.5*LOG(R2S)
15150       FB2=CNST*(FL1-FL2)
15160       IF YB <> 0  GOTO  15200
```

```
15170       FB3=0
15180       IF ABS(XB) <A THEN FB3=CNST*PI
15190       GOTO  15210
15200      FB3=-CNST*(ATN((XB+A)/YB)-ATN((XB-A)/YB))
15210     FB1=YB*FB3+CNST*((XB-A)*FL1-(XB+A)*FL2)
15220       FB4=CNST*(YB/R1S-YB/R2S)
15230       FB5=CNST*((XB-A)/R1S-(XB+A)/R2S)
15240      REM
15250       UXPS=COND*(PR3*COSB*FB1+YB*(SINB*FB2+COSB*FB3))
15260       UXPN=COND*(-PR3*SINB*FB1-YB*(COSB*FB2-SINB*FB3))
15270       UYPS=COND*(PR3*SINB*FB1-YB*(COSB*FB2-SINB*FB3))
15280       UYPN=COND*(PR3*COSB*FB1-YB*(SINB*FB2+COSB*FB3))
15290      REM
15300      SXXPS=FB2+PR2*(COS2B*FB2-SIN2B*FB3)
          +YB*(COS2B*FB4+SIN2B*FB5)
15310      SXXPN=FB3-PR1*(SIN2B*FB2+COS2B*FB3)
          +YB*(SIN2B*FB4-COS2B*FB5)
15320      SYYPS=FB2-PR2*(COS2B*FB2-SIN2B*FB3)
          -YB*(COS2B*FB4+SIN2B*FB5)
15330      SYYPN=FB3+PR1*(SIN2B*FB2+COS2B*FB3)
          -YB*(SIN2B*FB4-COS2B*FB5)
15340      SXYPS=PR2*(SIN2B*FB2+COS2B*FB3)
          +YB*(SIN2B*FB4-COS2B*FB5)
15350      SXYPN=PR1*(COS2B*FB2-SIN2B*FB3)
          -YB*(COS2B*FB4+SIN2B*FB5)
15360      REM
15370       UXS=UXS+MSYM*UXPS
15380       UXN=UXN+UXPN
15390       UYS=UYS+MSYM*UYPS
15400       UYN=UYN+UYPN
15410      REM
15420       SXXS=SXXS+MSYM*SXXPS
15430       SXXN=SXXN+SXXPN
15440       SYYS=SYYS+MSYM*SYYPS
15450       SYYN=SYYN+SYYPN
15460       SXYS=SXYS+MSYM*SXYPS
15470       SXYN=SXYN+SXYPN
15480      REM
15490       RETURN
20000 REM       SUBROUTINE SOLVE(N)
20010      REM
20020       NB=N-1
20030   FOR J=1 TO NB
20040       L=J+1
20050   FOR JJ=L TO N
20060       XM=C(JJ,J)/C(J,J)
20070    FOR I=J TO N
20080     C(JJ,I)=C(JJ,I)-C(J,I)*XM
20090          NEXT I
20100    B(JJ)=B(JJ)-B(J)*XM
20110          NEXT JJ
20120          NEXT J
```

```
20130      REM
20140       P(N)=B(N)/C(N,N)
20150    FOR J=1 TO NB
20160       JJ=N-J
20170       L=JJ+1
20180       SUM=0.0
20190   FOR I=L TO N
20200     SUM=SUM+C(JJ,I)*P(I)
20210       NEXT I
20220     P(JJ)=(B(JJ)-SUM)/C(JJ,JJ)
20230       NEXT J
20240       RETURN
25000 REM PRINT"END OF PROCESSING"
25300   CLOSE #1
25400   CLOSE #2
25401   END
```

Appendix C: Computer Program TWOFS99_EX

This appendix contains the listing for the program TWOFS99_EX. This program used the stress versus x location output from TWOFS99 and computed the stress intensity factor asa function of distance, r, from the crack tip. The equation used was

$$K_I = \mathrm{Lim}_{r \to 0} \left[\sigma_{yy} \, (2\pi r)^{1/2} \right] \qquad (43)$$

The distribution of K_I vs r was only taken as valid from a distance five to ten percent of the crack length away from the crack tip. The K_I data was then fit through linear regression analysis against r^2. The rational for selecting r^2 over an r distribution is explained in the main body of the text. The program inputs the name of the source file, the crack length, the hole diameter, and hole pitch. The data that fit in the acceptable distances from the crack tip are printed with calculated K_I values, and the final regression fit for K_I at r=0 is printed. All K_I values used to create the β factors in the parametric tension strip study were calulated by this program.

The program is written in VAX BASIC 3.1 and run on a VAX 8800.

```
1 DIM OUTPT(300,10), XM(300),X(300),SIGYY(300),R(300),K(300)
10 PRINT " PROGRAM TWOFS99_EX" \ PRINT " "
20 REM    TO EXTRACT DATA FROM OUTPT FILES
30 INPUT  "ENTER OUTPT FILE NAME ROOT ";QIN$
31 INPUT "ENTER PITCH: ";PITCH
35 INPUT "ENTER CRACK LENGTH A : ";A
36 INPUT "ENTER HOLE DIA: ";DIA
37 PRINT "INPUT FILE ROOT: ";QIN$
38 PRINT "CRACK LENGTH A :";A \ PRINT "HOLE DIAMETER :";DIA
39 PRINT "PITCH= ";PITCH
40 QOUT$ = QIN$ + ".OUTPT_EX"
42 QIN$ = QIN$ + ".OUTPT"
50 OPEN QIN$ FOR INPUT AS #1
55 OPEN QOUT$ FOR OUTPUT AS #2
56 PRINT #2," PROGRAM TWOFS99_EX" \ PRINT #2," "
57 PRINT #2," INPUT FILE : ";QIN$
58 PRINT #2," OUTPUT FILE : ";QOUT$
59 PRINT #2," " \ PRINT #2," CRACK LENGTH = ";A
60 PRINT #2,"HOLE DIAMETER :";DIA \ PRINT #2,"PITCH = ";PITCH
      \PRINT #2," "
61 FOR I=1 TO 300
62 FOR J=1 TO 10
64 INPUT #1, OUTPT(I,J)
66 NEXT J
68 NEXT I
70 FOR I=1 TO 300
72 INPUT #1, XM(I)
74 NEXT I
76 XMIN = DIA/2 + A + 0.05*A \ XMAX = XMIN + 0.05*A
78  REM  CHECK FOR LONG CRACK PROBLEM
80 IF XMAX < PITCH-(DIA/2) THEN GOTO 83
81 XMAX = PITCH-(DIA/2)   \ XMIN =XMAX - ( XMAX - DIA/2 -
      A)/2
82 PRINT#2,"LARGE CRACK WARNING"
83 PRINT #2,"XMIN (5% A) = ";XMIN \ PRINT #2,"XMAX (10% A) =
      ";XMAX
85 KOUNT=0.0
88 PRINT #2," " \ PRINT #2," "
89 PRINT #2,"ELEMENT","X DIM","TIP RAD","TIP RAD ^2","SIGMA
      YY","KI"
90 FOR I = 2 TO 100
91 REM  CHECK BEM 2 TO 100
92 REM  CHECK FOR 5% < X < 10% OF A
94 IF XM(I) > XMAX OR XM(I) < XMIN THEN GOTO 180
100 KOUNT=KOUNT + 1
110  X(I) = XM(I) \ SIGYY(I) = OUTPT(I,6)/1000
120 R(I) = X(I) - A - DIA/2.0
125 R2= R(I)^2
130 K(I) = SIGYY(I) * ( 2 * PI * R(I) )^0.5
140 SUMR = SUMR + R2
150 SUMR2 = SUMR2 + R2^2
160 SUMRK = SUMRK + R2*K(I)
```

```
170 SUMK = SUMK + K(I)
175 PRINT #2, I, XM(I), R(I),R(I)^2, SIGYY(I), K(I)
180 NEXT I
200 B = (KOUNT * SUMRK - SUMR*SUMK)/(KOUNT *SUMR2-(SUMR)^2)
210 KICFIT = (SUMK - B*SUMR)/KOUNT
215 BETA = KICFIT / ( 46 * SQR( PI * A) )
220 PRINT #2 ,"-----------------------------------------"
230 PRINT #2 ,"  "
240 PRINT #2 ," KI (REGRESSION FIT R=0.0) = ";KICFIT
245 PRINT #2 ,"      BASED ON R SQUARED "
250 PRINT #2," "
255 PRINT #2,"     BETA (SIG=46) = ";BETA
260 PRINT #2, "-----------------------------------------"
```

Appendix D: Computer Program CHOLE

This appendix contains the listing for the program CHOLE. This program is a model generator for the tension strip parametric study of section VII. The input to the program is hole diameter, pitch, and crack length. The program divides the crack into segments with the F.R. Harris refinement technique [8]. The final model as output is in a format required for TWOFS99 to read in.

All of the models used in the tension strip parametric study were created with CHOLE. CHOLE is a VAX BASIC 3.1 program run on a VAX 8800.

```
20 PRINT "BEM  HOLE WITH CRACK MODEL GENERATOR - QUAD FINITE
      BOUND"
22 print "      GRADUATED CRACK ELEMENTS 3-3-3-25 RULE "
30 PRINT " "
35 INPUT"ENTER NAME OF OUTPUT FILE : ";O$
36 OPEN O$ FOR OUTPUT AS #1
40 INPUT"ENTER HOLE DIAMETER";DIA
50 INPUT"ENTER DISTANCE BETWEEN HOLE CENTERS ";PITCH
60 INPUT"ENTER LENGTH OF CRACK ";A
70 PRINT #1," TWO HOLES S=46 D=";DIA;" P=";PITCH;" A=";A
80 SXX=0.0 \ SYY=46000. \ SXY=0.0
115 RAD = DIA/2.0
120 CIRCUM= 2 * 3.14159 * RAD
130 REM   DIVIDE CRACK BY 20 TO GET ELEMENT LENGTH
140 ELEN = A/12
150 REM CALCULATE HOW MANY ELEMENTS IN HALF CIRCLE (HOLE)
160 CEL =( CIRCUM/ ELEN )/2.0
170 CEL = INT( CEL) + 1  \ IF CEL < 20 THEN CEL=20
175 REM  4 FOR CRACK 4 FOR PRECRACK 1 FOR INBETWEEN
176 REM  2 CLOSE HORIZON 2 SIDES 1 TOP 1 SPC
185 ELTOT = 2 * CEL + 4 + 4 + 1 + 2 + 2 + 1 + 1
187 IF RAD + A = PITCH/2 THEN ELTOT=ELTOT-1
190 PRINT #1, ELTOT;",0,1,.3,10.3E6"
220 PRINT #1,"0.0"
230 PRINT #1,"0.0"
240 PRINT #1,"0.0"
242 T$ = "1,0,0" \ C$=","
```

```
244  REM   THIS IS THE NON CRACK MATERIAL BETWEEN HOLES
245 IF PITCH >  2 * ( A + RAD) THEN GOTO 270
247 LTEMP = PITCH - RAD - RAD - A
248 X1=PITCH - RAD   \ X2 = A + RAD + 0.5 * LTEMP
249 PRINT #1, "15,"; X1 ; C$ ; Y1 ; C$ ; X2 ; C$ ; Y2 ; C$
      ;"4,0,0"
250 X1=X2 \ X2 = A + RAD + 0.25 * LTEMP
251 PRINT #1, "15,"; X1 ; C$ ; Y1 ; C$ ; X2 ; C$ ; Y2 ; C$
      ;"4,0,0"
252 X1=X2 \ X2 = A + RAD + 0.125 * LTEMP
253 PRINT #1, "15,"; X1 ; C$ ; Y1 ; C$ ; X2 ; C$ ; Y2 ; C$
      ;"4,0,0"
254 X1=X2 \ X2 = A + RAD
255 PRINT #1, "15,"; X1 ; C$ ; Y1 ; C$ ; X2 ; C$ ; Y2 ; C$
      ;"4,0,0"
256 X1=X2 \ X2 = A + RAD - 0.125 * LTEMP
257 PRINT #1, "25,"; X1 ; C$ ; Y1 ; C$ ; X2 ; C$ ; Y2 ; C$ ;
      T$
258 X1=X2 \ X2 = A + RAD - 0.25 * LTEMP
259 PRINT #1, "3,"; X1 ; C$ ; Y1 ; C$ ; X2 ; C$ ; Y2 ; C$ ;
      T$
260 X1=X2 \ X2 = A + RAD-  0.5 * LTEMP
261 PRINT #1, "3,"; X1 ; C$ ; Y1 ; C$ ; X2 ; C$ ; Y2 ; C$ ;
      T$
262 X1=X2 \ X2 = A+ RAD - LTEMP
263 PRINT #1, "3,"; X1 ; C$ ; Y1 ; C$ ; X2 ; C$ ; Y2 ; C$ ;
      T$
264 IF A+RAD = PITCH/2 THEN GOTO 290
265 LTEMP = X2 - RAD \ LTEMP2 = (X1 - X2)/3
266 LTOT = INT(LTEMP/LTEMP2) + 1
267 X1=X2  \ X2 = RAD \ Y2 = 0. \ Y1 = 0.
268 PRINT #1,LTOT ;","; X1 ; C$ ; Y1 ; C$ ; X2 ; C$ ; Y2 ; C$
      ;"1,0,0"
269 GOTO 290
270 LTEMP = PITCH-RAD -RAD -A -A
271 LTOT = INT (LTEMP/A) +1
272 X1 = PITCH-RAD \ Y1 = 0.0 \ X2 = X1 - LTEMP \ Y2 = Y1
273 PRINT #1,LTOT ;","; X1 ; C$ ; Y1 ; C$ ; X2 ; C$ ; Y2 ; C$
      ;"4,0,0"
274 X1=X2 \ X2 = A + RAD + 0.5 * A
275 PRINT #1, "3,"; X1 ; C$ ; Y1 ; C$ ; X2 ; C$ ; Y2 ; C$
      ;"4,0,0"
276 X1=X2 \ X2 = A + RAD + 0.25 * A
277 PRINT #1, "3,"; X1 ; C$ ; Y1 ; C$ ; X2 ; C$ ; Y2 ; C$
      ;"4,0,0"
278 X1=X2 \ X2 = A + RAD + 0.125 * A
279 PRINT #1, "3,"; X1 ; C$ ; Y1 ; C$ ; X2 ; C$ ; Y2 ; C$
      ;"4,0,0"
280 X1=X2 \ X2 = A + RAD
281 PRINT #1, "25,"; X1 ; C$ ; Y1 ; C$ ; X2 ; C$ ; Y2 ; C$
      ;"4,0,0"
282 X1=X2 \ X2 = A + RAD - 0.125 * A
```

```
283 PRINT #1, "25,"; X1 ; C$ ; Y1 ; C$ ; X2 ; C$ ; Y2 ; C$ ;
        T$
284 X1=X2 \ X2 = A + RAD - 0.25 * A
285 PRINT #1, "3,"; X1 ; C$ ; Y1 ; C$ ; X2 ; C$ ; Y2 ; C$ ;
        T$
286 X1=X2 \ X2 = A + RAD-  0.5 * A
287 PRINT #1, "3,"; X1 ; C$ ; Y1 ; C$ ; X2 ; C$ ; Y2 ; C$ ;
        T$
288 X1=X2 \ X2 = RAD
289 PRINT #1, "3,"; X1 ; C$ ; Y1 ; C$ ; X2 ; C$ ; Y2 ; C$ ;
        T$
290 REM THIS IS THE HOLE CALCULATION SECTION
291 ANGLE = 3.14159 \ DELA = ANGLE/ CEL \ ANGLE=0.0
310 FOR I=1 TO CEL
320 X1 = X2 \ Y1 = Y2
330 ANGLE = ANGLE + DELA
340 X2 = RAD * COS( ANGLE)
350 Y2 = RAD * SIN( ANGLE)
400 PRINT #1,"1," ; X1 ; C$ ; Y1 ; C$ ; X2 ; C$ ; Y2 ; C$ ;
        T$
420 NEXT I
600 REM THIS IS THE SECOND HOLE
605 ANGLE = 3.14159 \ DELA = ANGLE/ CEL \ ANGLE=0.0
607 X2 =  RAD + PITCH\ Y2 = 0.0 \ C$=","
610 FOR I=1 TO CEL
620 X1 = X2 \ Y1 = Y2
630 ANGLE = ANGLE + DELA
640 X2 = RAD * COS( ANGLE)  + PITCH
650 Y2 = RAD * SIN( ANGLE)
660 PRINT #1,"1," ; X1 ; C$ ; Y1 ; C$ ; X2 ; C$ ; Y2 ; C$ ;
        T$
720 NEXT I
721 REM   THIS IS 3-D ON LEFT OF LEFT HOLE
722 DIST=3*DIA \X1 = -RAD \ X2 = X1 - DIST \ Y1=0.0 \ Y2=0.0
728 PRINT #1,"10," ; X1 ; C$; Y1 ; C$; X2; C$; Y2; C$;
        "4,0,0"
732 REM   THIS IS 3-D ON RIGHT OF RIGHT HOLE
734 X1 = PITCH + RAD +DIST \ X2 = X1 - DIST \ Y1=0.0 \ Y2=0.0
738 PRINT #1,"10," ; X1 ; C$; Y1 ; C$; X2; C$; Y2; C$;
        "4,0,0"
750 REM  THIS IS THE FINITE (3-DIA) BOUNDARY
752 REM  L SIDE
754 X1 = -RAD - DIST \ X2 = X1
756 Y2 = DIST + RAD   \ Y1 = 0.0
758 PRINT #1,"10," ; X1 ; C$; Y1 ; C$; X2; C$; Y2; C$; "1,
        0,";SXX
759 REM   TOP
760 DIST = 3 * DIA
765 X1 = -RAD - DIST \ X2 = RAD +  PITCH + DIST
770 Y1 = DIST + RAD   \ Y2 = Y1
775 PRINT #1,"40," ; X1 ; C$; Y1 ; C$; X2; C$; Y2; C$; "1,
        0,";SYY
```

```
780 REM  R SIDE
782 X1 = X2
784 Y1 = DIST + RAD   \ Y2 = 0.1
785 PRINT #1,"10," ; X1 ; C$; Y1 ; C$; X2; C$; Y2; C$; "1,
      0,";SXX
790 REM  THIS IS THE SPC
800 Y1=Y2 \ Y2 = 0.0
815 PRINT #1,"1," ; X1 ; C$; Y1 ; C$; X2; C$; Y2; C$; "2,
      0,0"
900 PRINT "END OF PROCESSING"
910 CLOSE #1
1000 END
```

Appendix E: Fitting NASA/FLAGRO Crack Growth Output

This appendix contains the output from the NASA/FLAGRO analysis of section VIII. All three of the analysis used the same materials and stress spectrums.

A. Bowie Solution Analysis

FATIGUE CRACK GROWTH ANALYSIS

(computed: NASA/FLAGRO, 1986 Aug version, 1987 Jul rev.)
U.S. customary units [inches, ksi, ksi sqrt(in)]

PROBLEM TITLE

TEST OF BOWIE SOLUTION ANALYSIS

GEOMETRY

MODEL: TC03-Through crack from hole in plate.

Plate Thickness, t = 0.2500
" Width, W = 100.0000
Hole Diameter, D = 0.2500
Distance of Hole Center to Edge, B = 50.0000

FLAW SIZE:

a (init.) = 0.7500E-01

MATERIAL

MATL 1: 7075-T6 AL, L-T

Material Properties:

Matl: No.	YS	Kle	Klc	Ak	Bk	Thk	Kc	KIscc
1	65.0	42.0	27.0	0.75	1.25	0.250	54.9	

Matl: No.	Crack Growth Eqn Constants (closure) C	n	p	q	DKo	Co	d	DK1	Alpha	Smax/SIGo
1	0.275D-07	2.836	0.50	0.50	2.50	1.00	1.00	5.74	1.75	0.30

TEST OF BOWIE SOLUTION ANALYSIS
MODEL: TC03

FATIGUE SPECTRUM STRESS TABLE

STEP	MAT	NUMBER OF FATIGUE CYCLES	S0 (ksi) t1	S0 (ksi) t2	S1 (ksi) t1	S1 (ksi) t2
1	1	100	0.00	30.00	0.00	0.00

Environmental Crack Growth Check for Sustained Stresses
(Kmax less than KIscc): NOT SET

TEST OF BOWIE SOLUTION ANALYSIS
MODEL: TC03

ANALYSIS RESULTS:

Block Step	Final Flaw Size a	K max a-tip
1	0.092832	23.873066
2	0.111912	24.298998
3	0.132318	24.740814
4	0.154225	25.221426
5	0.177883	25.756659
6	0.203603	26.360479
7	0.231775	26.993177
8	0.262879	27.740626
9	0.297515	28.528124
10	0.336449	29.429157
11	0.380675	30.424570
12	0.431521	31.576437
13	0.490817	32.815969
14	0.561179	34.270541
15	0.646548	35.996892
16	0.753263	38.005786
17	0.892600	40.549542
18	1.088274	43.766852
19	1.412186	48.761760

FINAL RESULTS:
Unstable crack growth, max stress intensity exceeds critical value:
K max = 55.00 K cr = 54.94
at Cycle No. 56. of Load Step No. 1 of Block No. 20
Crack Size a = 1.87187

B. Shivakumar Solution Analysis

FATIGUE CRACK GROWTH ANALYSIS

(computed: NASA/FLAGRO, 1986 Aug version, 1987 Jul rev.)
U.S. customary units [inches, ksi, ksi sqrt(in)]

PROBLEM TITLE

TEST OF SHIVAKUMAR SOLUTION ANALYSIS

GEOMETRY

MODEL: TC05-Through crack from hole in row of holes.

Plate Thickness, t = 0.2500
Hole Diameter, D = 0.2500
Distance between Holes, H = 1.0000
Ratio of Hole Diameter to Edge Distance, D/B = 0.0000
(Ratio of 0.0 denotes a very large edge distance)

FLAW SIZE:

a (init.) = 0.7500E-01

MATERIAL

MATL 1: 7075-T6 AL, L-T

Material Properties:

Matl: No.	YS	Kle	Klc	Ak	Bk	Thk	Kc	KIscc
1	65.0	42.0	27.0	0.75	1.25	0.250	54.9	

Matl: No.	Crack Growth Eqn Constants (closure) C	n	p	q	DKo	Co	d	DK1	Alpha	Smax/SIGo
1	0.275D-07	2.836	0.50	0.50	2.50	1.00	1.00	5.74	1.75	0.30

TEST OF SHIVAKUMAR SOLUTION ANALYSIS
MODEL: TC05

FATIGUE SPECTRUM STRESS TABLE

SAWTOOTH 0 - 30 KSI

S T E P	M: A: T: L:	NUMBER OF FATIGUE CYCLES	S0 (ksi) t1	S0 (ksi) t2	S1 (ksi) t1	S1 (ksi) t2	S2 (ksi) t1	S2 (ksi) t2
1:	1:	100	0.00:	30.00:	0.00:	0.00:	0.00:	0.00:

Environmental Crack Growth Check for Sustained Stresses
(Kmax less than KIscc): NOT SET

TEST OF SHIVAKUMAR SOLUTION ANALYSIS
MODEL: TC05

ANALYSIS RESULTS:

ADVISORY: Estimated Net Section Stress > Yield Strength.
at Cycle No. 0. of Load Step No. 1 of Block No. 1
Crack Size a = 0.750000E-01

Block Step	Final Flaw Size a	K max a-tip
1	0.094329	24.414055
2	0.115210	24.922510
3	0.137799	25.448033
4	0.162406	26.050727
5	0.189473	26.739437
6	0.219583	27.535714
7	0.253507	28.430209
8	0.292277	29.476453
9	0.337329	30.668877
10	0.390770	32.098262
11	0.456008	33.810283
12	0.539788	36.204720
13	0.668205	42.025305

FINAL RESULTS:
Unstable crack growth, max stress intensity exceeds critical value:
K max = 56.32 K cr = 54.94
at Cycle No. 24. of Load Step No. 1 of Block No. 14
Crack Size a = 0.747562

C. β Look-Up Table Analysis

FATIGUE CRACK GROWTH ANALYSIS

(computed: NASA/FLAGRO, 1986 Aug version, 1987 Jul rev.)
U.S. customary units [inches, ksi, ksi sqrt(in)]

PROBLEM TITLE

TEST OF BOUNDARY ELEMENT LOOK UP TABLE ANALYSIS

GEOMETRY

MODEL: DT01-One-dimensional data table for through crack.

Plate Thickness, t = 0.2500

a/D	F0
0.1000	1.7400
0.2000	1.3800
0.3000	1.2500
0.4000	1.2000
0.5000	1.1900
0.6000	1.2000
0.7000	1.2400
0.8000	1.3400
0.9000	1.6800

where
S0 : TENSION STRESS

FLAW SIZE:

a (init.) = 0.7500E-01

MATERIAL

MATL 1: 7075-T6 AL, L-T

Material Properties:

Matl: No.	YS	Kle	Klc	Ak	Bk	Thk	Kc	KIscc
1	65.0	42.0	27.0	0.75	1.25	0.250	54.9	

Matl: No.	Crack Growth Eqn Constants (closure) C	n	p	q	DKo	Co	d	DK1	Alpha	Smax/SIGo
1	0.275D-07	2.836	0.50	0.50	2.50	1.00	1.00	5.74	1.75	0.30

TEST OF BOUNDARY ELEMENT LOOK UP TABLE ANALYSIS
MODEL: DT01

FATIGUE SPECTRUM INPUT TABLE

SAWTOOTH 0 - 30 KSI

[Note: Stress = Input Value * Stress Factor]
Stress Factor SF0: 1.00

S : M:	NUMBER	: S0	:
T : A:	OF	:	:
E : T:	FATIGUE	:	:
P : L:	CYCLES	: t1 :	t2 :
1: 1:	100	: 0.00:	30.00:

Environmental Crack Growth Check for Sustained Stresses
(Kmax less than KIscc): NOT SET

TEST OF BOUNDARY ELEMENT LOOK UP TABLE ANALYSIS
MODEL: DT01

ANALYSIS RESULTS:

Block Step	Final Flaw Size a	K max a-tip
1	0.100650	26.642060
2	0.131098	27.751991
3	0.166947	29.046889
4	0.211160	30.923850
5	0.270492	33.563043
6	0.361315	38.080432

FINAL RESULTS:
Unstable crack growth, max stress intensity exceeds critical value:
K max = 55.11 K cr = 54.94
at Cycle No. 95. of Load Step No. 1 of Block No. 7
Crack Size a = 0.599436

Appendix F: Comparison of Regression Fit Analysis

This appendix shows examples of linear regression fits for large and small crack ratios, for both r (distance from crack tip) and r^2. As was explained in the main text of this thesis, there is insignificant differences for the values of K_I predicted for small crack ratio problems from linear regression fits of K_I vs r or r^2. Figures 27 and 28 show the plots of K_I vs r and r^2 respectively for a small crack ratio problem (crack ratio = 0.1) from the tension strip parametric study of section VII. This data is for hole diameter equal to 0.25 inches and pitch equal to four diameters. Both plots indicate a value of K_I at r=0 of approximately 39 KSI(in)$^{1/2}$. However, Figures 29 and 30 show the same plots for a crack ratio of 0.9 (same diameter hole and pitch). While the r^2 regression fit will indicate a K_I value of 112.7 KSI(in)$^{1/2}$, the r fit data will not even predict a positive value of K_I. It is hypothesized that the indicated values of K_I are not linear in r, and the portion of the K_I vs r curve plotted in Figure 29 is quadratic in r. Therefore a linear regression fit is inadequate for the large crack ratios, and was not used for the parametric study of section VII.

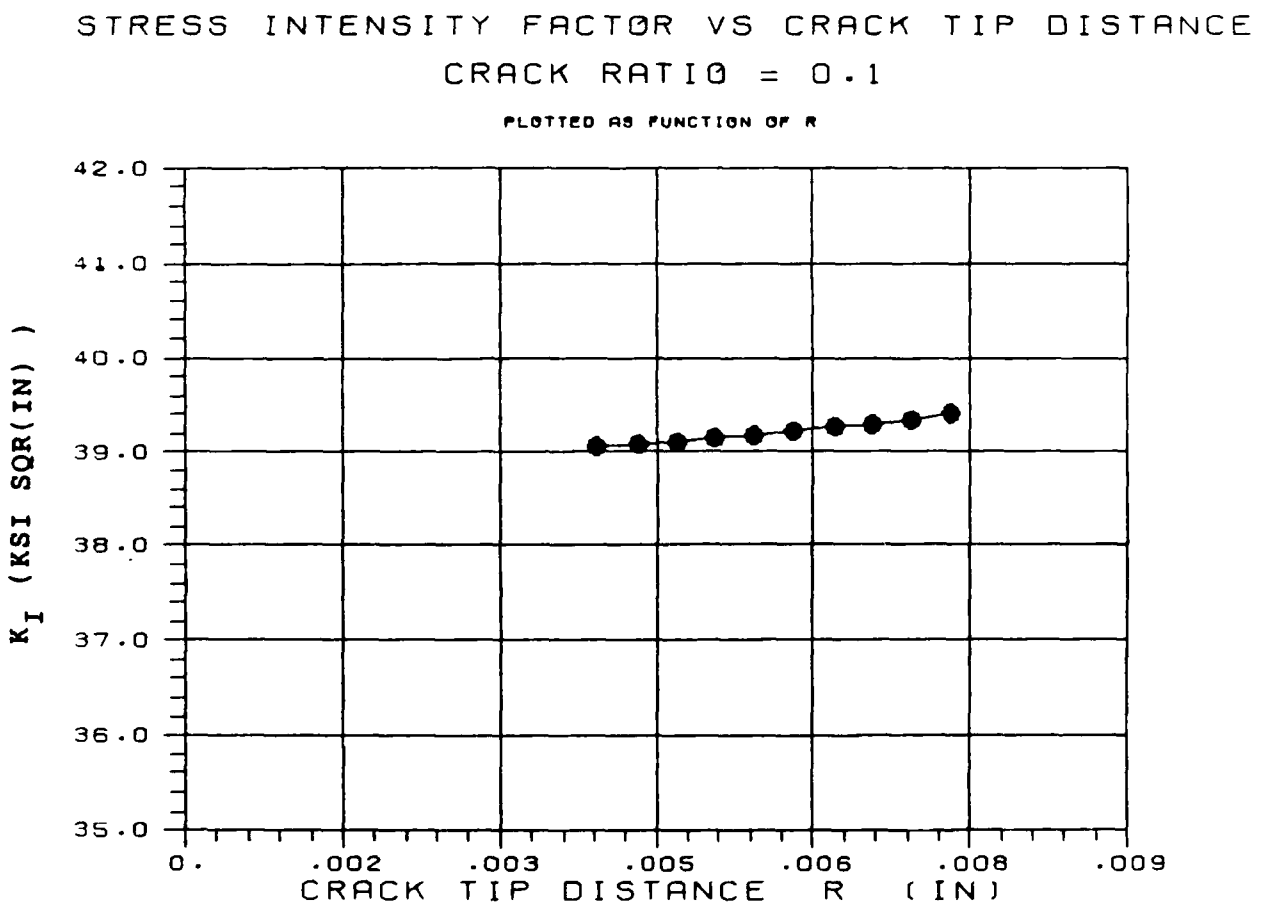

Figure 27. Stress Intensity Factor Vs Radius (Crack Ratio=0.1)

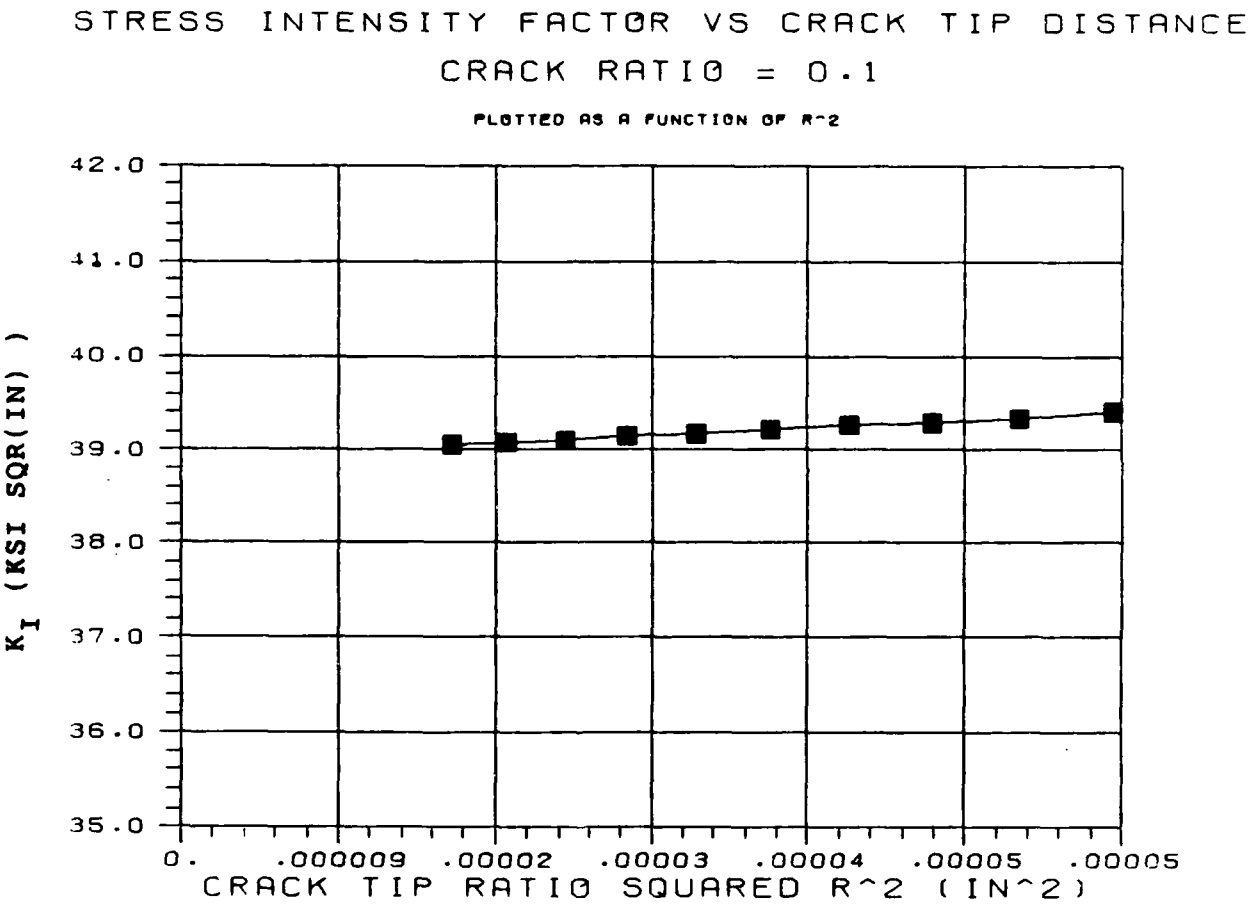

Figure 28. Stress Intensity Factor Vs Radius^2 (Crack Ratio=0.1)

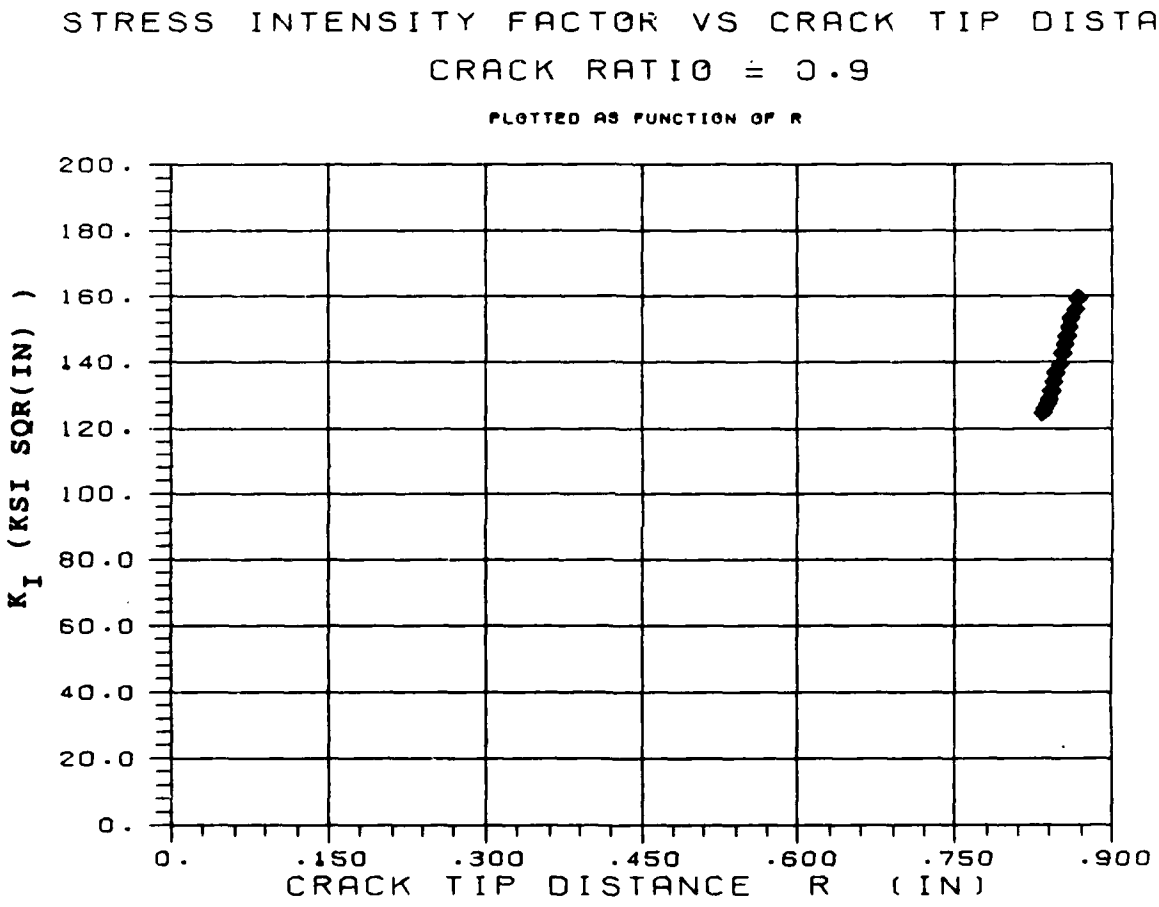

Figure 29. Stress Intensity Factor Vs Radius (Crack Ratio=0.9)

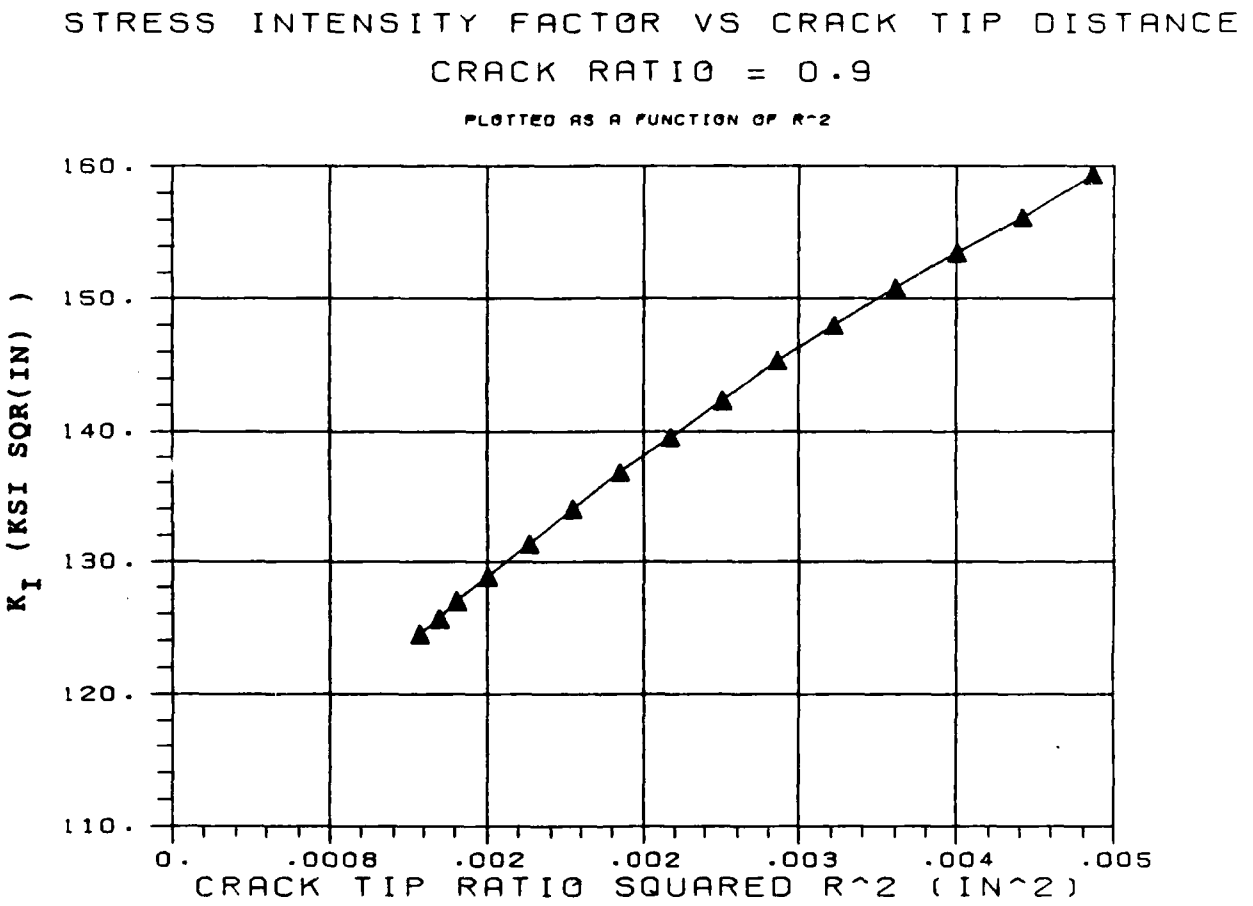

Figure 30. Stress Intensity Factor Vs Radius^2 (Crack Ratio=0.9)

Bibliography

1. Air Force Wright Aeronautical Laboratories. USAF Damage Tolerant Design Handbook: Guidelines for the Analysis and Design of Damage Tolerant Aircraft Structures. AFWAL-TR-82-3073. Wright-Patterson Air Force Base: Flight Dynamics Laboratory, Air Force Wright Aeronautical Laboratories, May 1984.

2. Babuska, I Szabo, B. and Katz, I. N. "The p-Version of the Finite Element Method", SIAM Journal of Numerical Analysis, Vol 18, 515-545, (1981).

3. Broek, David. Elementary Engineering Fracture Mechanics (Third Edition). The Hague: Martinus Nijhoff Publishers, 1982.

4. Crouch, S. L. and Starfield, A. M. Boundary Element Methods in Solid Mechanics. London: George Allen and Unwin Ltd., 1983.

5. Department of the Air Force, Airplane Damage Tolerance Requirements, Military Specification MIL-A-83444, 2 July 1974.

6. Department of the Air Force. Aircraft Structural Integrity Program, Airplane Requirements. Military Standard MIL-STD-1530A, 11 December1975.

7. Department of the Air Force, General Specifications for Aircraft Structures. Military Specification MIL-A-87221, 28 February 1985.

8. Harris, F. R. Two-Dimensional Elastic Analysis by the Boundary Element Method. MS thesis, AFIT/GA/AA/86D-6. School of Engineering, Air Force Institute of Technology (AU), Wright-Patterson AFB OH, December 1986.

9. Jaswon, M. A. "Integral Equation Methods in Potential Theory I", Proceedings of the Royal Society., Ser. A 275 (1963).

10. Jaswon, M. A. and Porter, A. R., "An Integral Equation Solution of the Torsion Problem",Proceedings of the Royal Society., Ser. A 273 (1963).

11. Lincoln, John W., Damage Tolerance - USAF Experience. Report to ASD/ENF. ASD/ENFS, Wright Patterson AFB, August 1985.

12. Mackerle, J. and Andersson, T. "Boundary Element Software in Engineering", Advanced Engineering Software, 6:66-102 (1983).

13. MSC/NASTRAN Handbook for Linear Analysis. MSC/NASTRAN version 64 Handbook for Linear Analysis. The MacNiel-Schwendler Corporation, Los Angeles, CA, August 1985.

14. MSC/NASTRAN Users Manual. MSC/NASTRAN version 65C Users Manual. The MacNiel-Schwendler Corporation, Los Angeles, CA, August 1987.

15. National Aeronautics and Space Administration. Fatigue Crack Growth Program "NASA/FLAGRO". JSC-22267. Houston: Johnson Space Flight Center, August 1986

16. Negaard, Gordon R. The History of the Aircraft Structural Integrity Program. Aerospace Structures Information and Analysis Center (ASIAC) Report No. 680.1B, 1980.

17. Rizzo, F. J. "An Integral Equation Approach to Boundary Value Problems in Classical Elastostatics", Quarterly of Applied Mathematics 25, 213-228 1967.

18. Rizzo, F. J. and Shippy, D. J. "An Advanced Boundary Integral Equation Method for 3D Thermoelasticity", International Journal for Numerical Methods in Engineering, 10 301-318 (1977).

19. Shivakumar, V. , Foreman, R. G. and Rosencranz, R. "Green's Function Solution and Applications for Cracks Emanating from a Circular Hole in an Infinite Sheet",Res Mechanica, Vol 9, 87-104, (1983).

20. Snyder, M. D. and Cruse, S. L. "Boundary-Integral Equation Analysis of Cracked Anisotropic Plates", International Journal of Fracture, 11: 315-328 (1975).

21. Solkolnikoff, I. S. Mathematical Theory of Elasticity (Second Edition). New York: McGraw-Hill Book Company, 1956.

22. Symm, G. T. "Integral Equation Methods in Potential Theory II", Proceedings of the Royal Society., Ser. A 275 (1963).

23. Szabo, B. A. , PROBE: Theoretical Manual, Noetic Technologies, St. Louis, MO, (1985).

24. Timoshenko, S. P. and Goodier, J. N. Theory of Elasticity (Third Edition). New York: McGraw-Hill Book Company, 1970.

25. Two Hole Tension Strip with Large Crack Stress Intensity Factor Analysis. PROBE sample problem. Noetic Technologies, St. Louis, MO, (undated)

Vita

Timothy C. Kelley [redacted] in 1977 [redacted] attended the University of Maryland from which he received his Bachelor of Science in Aerospace Engineering in May 1982. Upon graduation and commissioning through the R.O.T.C. program, he was stationed at Wright-Patterson AFB, Ohio. At WPAFB, he was assigned to the Aeronautical Systems Division and served as an aircraft static strength engineer. While serving at ASD he took all the courses required for the Master of Science degree as a part-time student. He separated from the Air Force in 1986 and is currently working as a static, durability and damage tolerance engineer at E-Systems Inc., Greenville, Texas.

UNCLASSIFIED
SECURITY CLASSIFICATION OF THIS PAGE

REPORT DOCUMENTATION PAGE

Form Approved
OMB No. 0704-0188

1a. REPORT SECURITY CLASSIFICATION UNCLASSIFIED	1b. RESTRICTIVE MARKINGS
2a. SECURITY CLASSIFICATION AUTHORITY	3. DISTRIBUTION/AVAILABILITY OF REPORT Approved for public release; distribution unlimited
2b. DECLASSIFICATION/DOWNGRADING SCHEDULE	
4. PERFORMING ORGANIZATION REPORT NUMBER(S) AFIT/GAE/AA/88S-1	5. MONITORING ORGANIZATION REPORT NUMBER(S)
6a. NAME OF PERFORMING ORGANIZATION School of Engineering 6b. OFFICE SYMBOL (If applicable) AFIT/ENY	7a. NAME OF MONITORING ORGANIZATION
6c. ADDRESS (City, State, and ZIP Code) Air Force Institute of Technology Wright-Patterson AFB, OH 45433	7b. ADDRESS (City, State, and ZIP Code)
8a. NAME OF FUNDING/SPONSORING ORGANIZATION 8b. OFFICE SYMBOL (If applicable)	9. PROCUREMENT INSTRUMENT IDENTIFICATION NUMBER
8c. ADDRESS (City, State, and ZIP Code)	10. SOURCE OF FUNDING NUMBERS PROGRAM ELEMENT NO. / PROJECT NO. / TASK NO / WORK UNIT ACCESSION NO.
11. TITLE (Include Security Classification) See Box 19	
12. PERSONAL AUTHOR(S) Timothy C. Kelley, B.S.	
13a. TYPE OF REPORT MS Thesis 13b. TIME COVERED FROM _____ TO _____ 14. DATE OF REPORT (Year, Month, Day) 1988 September 15. PAGE COUNT 131	
16. SUPPLEMENTARY NOTATION	

17. COSATI CODES			18. SUBJECT TERMS (Continue on reverse if necessary and identify by block number)
FIELD	GROUP	SUB-GROUP	
20	11		Boundary Elements, Fracture, Crack
12	01		

19. ABSTRACT (Continue on reverse if necessary and identify by block number)

Title: Application of the Boundary Element Method to Fatigue Crack Growth Analysis

Thesis Chairman: Anthony N. Palazotto
Professor of Aeronautics and Astronautics

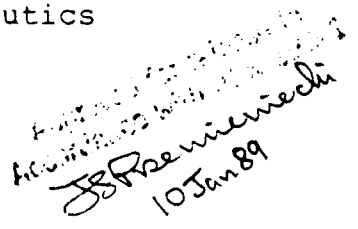

20. DISTRIBUTION/AVAILABILITY OF ABSTRACT ☒ UNCLASSIFIED/UNLIMITED ☐ SAME AS RPT ☐ DTIC USERS	21. ABSTRACT SECURITY CLASSIFICATION UNCLASSIFIED
22a. NAME OF RESPONSIBLE INDIVIDUAL Anthony N. Palazotto	22b. TELEPHONE (Include Area Code) 513-255-2998 22c. OFFICE SYMBOL AFIT/ENY

DD Form 1473, JUN 86 *Previous editions are obsolete.*

SECURITY CLASSIFICATION OF THIS PAGE
UNCLASSIFIED

This investigation analyzes a crack emanating from one hole, and approaching a second hole, in a two hole tension strip with finite boundaries using the Boundary Element Method. The study included the effects of varying the hole diameter, hole separation and the length of crack. The final results were plotted as a function of the geometric correction factor β, which can be presented as a family of curves. An example damage tolerance analysis is presented with the β curves being incorporated into a β look-up table as used in the NASA/FLAGRO fatigue crack growth program. This technique is acceptable in most fatigue crack growth programs now used in the aircraft industry to ensure aircraft structural integrity.

Several classic fracture mechanics problems are analyzed, and computational efficiency as compared to conventional finite element techniques is investigated. Agreement with analytic solutions as well as other numerical methods (finite element) is excellent. The computation efficiency was shown to an improvement over existing methods. Keywords:

Fata. Cracking (Fracturing); (Sounds)

Theses.